BIDGE Publications

Innovative Approaches in Civil Engineering, and Management
Watershed-Based Water Resources

Editor: Doç. Dr. Atila KUMBASAROĞLU

ISBN: XXX

Page Layout: Gözde YÜCEL
1st Edition:
Publication Date: 25.12.2023
BIDGE Publications

Certificate No: 71374

www.bidgeyayinlari.com.tr - bidgeyayinlari@gmail.com

Krc Bilişim Ticaret ve Organizasyon Ltd. Şti.
Güzeltepe Mahallesi Abidin Daver Sokak Sefer Apartmanı No: 7/9 Çankaya /
Ankara

Preface

Thanks to the Structural, Mechanical, Hydraulic, Geotechnical and Transportation science fields within the scope of Civil Engineering, sustainable innovative developments in construction and/or infrastructure/superstructure technology are supported by basic scientific achievements and multi-criteria decision-making theories. In Civil Engineering, it has always been the aim to review the state-of-the-art through theoretical/parametric or experimental methods applied/developed to support construction selection processes in terms of more innovative evaluations.

Watershed-based water resources management and sustainability assessment models are constantly being developed to evaluate the sustainability of water resources at the watershed scale in the context of the river basin. Many criteria can be used for the developed models, including economic efficiency, social equity, environmental conservation, maintenance capacity, etc.

Within the scope of this book, innovative issues such as Features of Siirt Masonry CAS Houses, Runoff SCS Models Discharge Estimation: Application on Various Sized Catchments In Pakistan, The Mathematical Analysis of Non-Homogeneous Horizontal Flow Model for Salinization in the Gediz Delta (Izmir), Development of Empirical Equations to Predict the Strength Properties of Rocks with Non-Destructive Test Techniques, Evaluation of Oak and Pine Wood Ashes in Gypsum-Based Mixtures, and Influence of Drill-Holes on Molded Column-Like Test Samples' Surface Displacements: Digital Image Correlation Analyses were mentioned.

We would like to thank all the authors who contributed to the arrangement and publication of the book, especially **BIDGE PUBLICATIONS**.

Editor

Doç. Dr. Atila KUMBASAROĞLU

Contents

CHAPTER I

Runoff SCS Models Discharge Estimation: Application on Various Sized Catchments In Pakistan

Sajid MAHMOOD
Zeyneb KILIÇ
Zafer ASLAN
Aliasghar IRAJPOOR
Gümüş FUNDA GÖKÇE

1. Introduction

Runoff represents the response of a catchment to precipitation causing stream flow. The precipitation occurs quantitatively and its distribution over Asia is 286 mm per year [1]. The transformation of the rainfall into runoff is a complex process. Under changing climate conditions, estimation of rainfall amounts is important for flood predictions and attracts the attention of researchers [2-4]. Several methods and models are available to predict the direct runoff from rainstorms. Primarily there are three sources of irrigation water in Pakistan, namely, surface water (canal water), ground water and rainfall. Rainfall is neither sufficient nor reliable. Practically whole of the Pakistan lies in arid to semi-arid zone. The annual rainfalls over the lndus Basin varies form 5 to14 inches in plains and above 20 inches in the northern areas. On overall basis, about 9 MAF net rainfall is estimated to reach the irrigation system for crop use annually. The rainfall zones can be roughly described as under. The most popular among available methods are Rational Method, Cook's Method, Harmon model, Singh-Dickinson (S-D) model and Soil Conservation Service (SCS) - Curve Number (CN) method. The SCS-CN method is commonly used all over the world for computing the runoff volume from a given rainfall event on small agricultural watersheds [5-7]. It is based on empirical procedure and developed after field investigations of more than 20 years. Although the SCS method popularity exists because of simplicity in selecting parameters according to physical characteristics of watershed easily.

Although it was originally developed for design of soil conservation works, but now extensively adopted for urbanized and forested watersheds. Using the volumetric concept of soil water air, Mishra and Singh (2002) further improved the existing SCS Method and described the curve number as the percent degree of saturation of the watershed [8]. The latest treatise of Mishra and Singh (2003) describes the SCS-CN concept as one of the fundamental concepts of hydrology to extend its applications to several watershed areas [9]. The method has now been equally applied to watersheds which are hydrologically homogeneous and exhibit the weighted CN greater than 40. Research studies indicated it to be the best method to convert rainfall to rainfall excess or direct surface runoff [10,11]. But still its validity needs to be tested for its adaptation [12].

In this research, it is aimed to determine the runoff estimation capabilities under different sized catchments using SCS and modified SCS-CN methods, for testing its applicability and validity under local Pakistan conditions. Three different sized catchments (Soan River, Ling River, Darmalak Dam) is estimated by using SCS method and modified SCS method with three variants i.e. (λ=0, a=1), (λ=0.2, a=1), (λ=0, a=0.5). However out of three different approaches of Modified SCS Method, each with different variants overestimated but modified SCS-CN method with variant (λ=0.2, a=1) is nearer to observed runoff in all cases. The results get with the modified SCS-CN method show larger variations, so it is not recommended under local conditions, thus the validity of the modified SCS-CN method is doubtful. However, it is suggested that the parameters should need to redefine and re-test before its adaptation at local scale. So, it may be recommended that SCS method be preferred on the modified SCS method in different-sized catchments i.e. Soan River, Ling River and Darmalak dam and its suitability is more significant for small sized catchments.

2. Material and Method

2.1. Research Area

The catchments selected for the study were of Soan River near Chirah, Ling River near Kahuta and Darmalak Dam near Kohat. All of these were used for testing the validity of the method in Runoff estimation for different sized catchments in order to suggest the best one under local conditions. Rainfall data used in this research, was taken from reports of the surface water hydrology project office. Catchment area for the basins were determined from the topo sheets of the Survey of Pakistan.

Soan River near Chirah: The outlet of the catchment is located at latitude 33^{0}, 39^{0}, and longitude 73^{0} 18^{0}, on Rawalpindi-Lethar Road bridge which is one mile Northwest of Chirah, 12 miles upstream from Ling River at Kahuta and 14 miles East of Rawalpindi. The catchment area, about 126 square miles is located between latitude 73^{0} -18^{0} to 73^{0} -32^{0} N and longitude 33^{0} -39^{0} to 33^{0} – 53 E. The catchment area elevation varied from about 7500ft to about 2200 MSL. The river is monsoon fed with some minor contribution due to snowmelt.

Ling River at Kahuta: It is located at latitude 33^{0} -36, and longitude 73^{0}-22 on Sihla Azad Pattan road bridge ¾ miles west of Kahuta and 18 miles east of Rawalpindi. The catchment area about

56 square miles is located between latitude 73^0-22 to 73^0-34 N and longitude 33^0-36, to 33^0 -45, E. The catchment area generally consists of hills varying in elevation from about 6000ft to about 2500ft above MSL. Catchment is forested in the upstream area and rolling plains with sparse vegetation at lower end. Ling river is fed stream with minor contribution from snow melt.

Darmalak Dam at Kohat: The Darmalak Dam is proposed on Maram Zai Toi. Dam site approximately 15 miles south of Kohat & Village Darmalak approximately 1 km in west of Dam site. Northings and Eastings of dam are 1021030 m, 3044996 m. Maram Zai Toi, generally carries run-off produced by rainfall only. The proposed Dam is meant basically to store floodwater for irrigation purposes. The catchment area of the Maram Zai Toi, upto the proposed dam site is 41.48 Sq. Miles. The hydrological conditions of the area are poor and run-off potential is high. The point of maximum elevation in the catchment area is 1312.47 m and at proposed dam site nullah bed is 513 m. Toi bed slope is 169.12 ft per miles or 3.2%. The length of main channel is 15.51 miles. There is no snow melt run-off in the area.

2.2. Theoretical Consideration of SCS Models

SCS-CN Method

The method consisted of three variables used in estimating runoff. The variables are rainfall, antecedent moisture condition, and the hydrologic soil-cover complex [13]. Mathematically it can be described by the following equation;

$$\frac{(P-Q)}{S} = \frac{Q}{P} \tag{1}$$

where; Q is the direct runoff (inch); P is the total rainfall (inch); and S is the potential maximum retention (difference between P and Q) (inch).

(P–Q) / S is visualized as the ratio of actual to potential difference between P and Q and Q/P is visualized as the ratio of actual to potential runoff. By simplifying equation, it can be written as;

$$Q = \frac{P^2}{(P+S)} \tag{2}$$

Equation (2) is more clear form of SCS-CN method used under the conditions, where there is a possibility of runoff due to rainfall.

For the condition that Q = 0 for P greater than zero, use of an initial abstraction $I_{a,}$ is required. With the condition that I_a (I_a is equal to the rainfall that occurs before runoff starts) cannot be greater than P. The equation 1 can be written as;

$$\frac{(P-I_a)-Q}{S} = \frac{Q}{(P-I_a)} \tag{3}$$

Solving it for Q, it become as;

$$Q = \frac{(P-I_a)^2}{(P-I_a+S)} \tag{4}$$

Research conducted so far in the application of the above equation for various sized watersheds in different parts of the world gives I_a a common value 0.2S. Substituting (0.2S) for I_a in equation (4), the value of Q can be determined as;

$$Q = \frac{(P-I_a)^2}{(P+0.8S)} \tag{5}$$

Modified SCS-CN Method

Mishira and Singh (2003) modified the popular SCS-CN equation by introducing two more parameter ‘a’ and redefining the term I_a. Field studies indicated that the modified model with ‘a’ = 0.5 and λ = 0 performs significantly better than the existing SCS-CN method [13]. So, the modified form of the general SCS-CN method so developed can be described as:

$$Q = \frac{(P-I_a)^2}{a(P-I_a)+S} \quad (6)$$

To solve above equation we have,

$$I_a = \lambda S \quad (7)$$

$$S = \frac{1000}{CN} - 10 \quad (8)$$

2.3. Hydro-Meteorological Data

Soan River near Chirah: Observed flow data is available by Surface Water Hydrology Project (SWHP). Data is available from April 1960 to date. Records available are gauge height, river discharge and suspended sediment from April 1960 to date. Gauge height, river discharge suspended sediment and quality of water record from May 1962 to-date by SWHP, Lahore. Average discharge was 167 cusecs (15 year, 1975) equivalent to 121,000 acre-feet per year or 18.07 inches. The highest discharge was observed as 96200 cusecs on August 20, 1975 and the gauge height was 22.35 ft. The lowest daily-observed discharge recorded was zero cusecs on many days in June 1963, 1970, 1974.

Ling River near Kahuta: Data is based on observed flows by SWHP, WAPDA. Data is available from August 1962 to June 1971. Records available are gauge Height, river discharge, suspended sediment from Jan.1962 to June 1971with SWHP, WASID, WAPDA, Lahore .The site was closed by SWHP office in June 1971. Average Discharge was 64 cusecs (9 years, 1962-70) equivalent to 46,060 acre-feet per year or 15.4. The highest discharge was observed as 39,800 cusecs on August 31, 1970 and the gauge height was 19.00 ft .The lowest daily-observed discharge recorded was zero cusecs on many days in June 1966.

Darmalak Dam near Kohat observed: Flow data is available by Surface Water Hydrology project (SWHP), WAPDA.Data is available from 1970 to date. Records available are gauge height, river discharge and suspended sediment from April 1970 to date. Average discharge was 10020 Acres-ft (35 year, 2004) equivalent to

4.53 inches. The lowest daily-observed discharge recorded was zero on many days in June exc.

2.4. Rainfall Data

Three rain gauges at Palanderi, Kallar and Rawal Dam are located near the Soan and Ling Rivers catchment areas. All these are recording rain gauges and being maintain by SWHP office. Rain gauges stations are shown in Table 1. Daily rainfall data observed at these rain gauges for the period 1960-78 was used for the present study and brief detailed is given below.

Palanderi Rainfall: Data is available on the daily basis as well as on hourly basis from 1962 to date. The site is situated at about 24 miles from Soan River near Chirah about 20 miles from Ling River and about 50 miles from Sil River near Chirah. Palandri rainfall station is located at latitude 33^0 43’ and longitude 73^0 41’ at an elevation of 4600 ft MSL.

Kallar Rainfall: Data is available on daily basis as well as on hourly basis from 1960 to date. This station is situated about 15 miles from Soan River, about 10 miles from Ling River and about 30 miles from Sil River near chirah. Kallar rainfall station is located at latitude 33^0 25’ and longitude 73^0 22’ at an elevation of 1700 ft MSL.

Rawal Dam: Rainfall data is available on daily basis as well as hourly basis from 1963 to 1980. The station is about 10 miles from Soan River about 15 miles from Ling River and about 20 miles from Sil River near chirah. Rawal Dam rain gauge Station is located at latitude33^0 40’ and longitude 73^0 07’ at an elevation of 1700 ft MSL.

Rainfall data of Kohat: No gauge data is available for the proposed dam site. Rainfall data of Kohat have been adopted for the proposed dam site because it is very near and almost at same elevation as that of catchment of dam. Daily rainfall data for Kohat have been collected from meteorological partment for period of 1970-2004. Kohat is located 15.63 miles in North East direction of dam site. Elevation at gauge site is 1650ft. Mean monthly rainfall for

Kohat varies from 0.34 inches to 4.77 inches while mean annual rainfall for corresponding period is 21.48 inches. Annual normal isohytel maps for period of 1931 to 1960 have been collected from metrological department Lahore. It clearly indicates that proposed dam site lies between 20 to 30 inches rainfall contour.

2.5. Soil Data

The soils of the area are generally very shallow with exposed bedrocks. Soil types and land use of the research area is available from Soil Survey of Pakistan. The maps of 1:250,000 scales are available. Types of soil and land use for the study area are estimated with the help of maps mentioned about and topo maps provided by Survey of Pakistan. Topo maps are also available on 1: 250,000 scales. Land use description, treatment and hydrologic conditions for the study area are determined with the help of maps available from Soil Survey of Pakistan. A, B, C and D are the soil types specified by Soil Conservation Service.

2.6. Analysis with Reference to Gauge Site

In order to avoid erroneous conclusion, it is important to make proper interpretation of rainfall data. It cannot be accepted at face value. For example, a mean annual rainfall value for a station is of little use if the gauge site has been changed significantly during the period for which the average is computed. Rain gauges located nearer to the proposed study areas, are Palandri, Kallar and Rawal Dam.

Thiessen Polygon Method was used to estimate the average rainfall for the catchments under study. Thiessen-Mean Method: In this method the rainfall recorded at each station is given a weight age on the basis of an area closest to the station. The procedure of determining the weighting area is as follows: consider a catchment area as containing three rain gauges stations. The catchment area is drawn to scale and the positions of the three stations marked on it.

Stations 1 to 3 are joined to form a network of triangles. Perpendicular bisectors for each of the sides of the triangle are drawn. These bisectors form a polygon around each station. The boundary of the catchment, if it cuts the bisectors is taken as the outer limit of the polygon.

Thus for station 1, the bounding polygon is let abcd. These bounding polygons are calling thiessen polygon. The areas of these three thissen polygons are determined with planimeter. P_1, P_2, P_3 are the rainfall magnitudes recorded by the stations 1,2,3 respectively, and A_1, A_2, A_3 are the respective areas of the thiessen polygons, then the average rainfall over the catchment P is given by

$$P = \frac{(P_1A_1+P_2A_2+P_3A_3)}{(A_1+A_2+A_3)} \tag{9}$$

Once the weight age factors are determined, the calculation of P is relatively easy for a fixed network of station. Percentage area covered by each rain gauge and average rainfall datas of stations are as in Table 1-4.

Table 1. *Rainfall data (percentage) collected from different catchments*

Darmalak Dam Catchment Rainfall	100% of Kohat
Ling River Catchment Rainfall	21% of Kallar, 67% of Palandri an 12% of Rawal Dam.
Soan River Catchment Rainfall	52% of Palandri and 48% of Rawa Dam.

Table 2. *Average Monthly Rainfall for Darmalak Dam Catchment Rainfall in inches*

Darmal k Dam	Jan	Feb	Mar	Apr	May	Jun	Jul	Aug	Sep	Oct	Nov	Dec	Annu
	1.04	1.66	2.74	1.99	1.44	1.05	3.07	4.77	1.76	0.96	0.34	0.66	21.48

Table 3. *Average Rainfall Data (1963 to 1978) For the Selected Stations Site*

Rainfa Statio	Jan	Feb	Mar	Apr	May	Jun	Jul	Aug	Sep	Oct	Nov	Dec	Annu
Kallar (K)	1.52	2.69	2.31	1.87	1.17	2.37	8.90	11.2	3.43	0.83	0.50	0.98	37.76
Paland i (P)	3.96	5.06	4.00	3.91	2.34	3.75	12.1	11.2	4.02	1.74	0.95	2.03	55.15
Rawal (R)	2.12	3.00	3.06	2.40	1.57	3.13	10.4	14.0	5.02	1.30	0.72	1.27	48.04

Table 4. *Estimation of Average Monthly Rainfall for Ling & Soan River Catchments*

	Jan	Feb	Mar	Apr	May	Jun	Jul	Aug	Sep	Oct	Nov	Dec	Annu
Ling River Rainfall 0.21(K)+0.67(P +0.12(R)	3.23	4.32	3.53	3.30	2.00	3.38	11.2	11.5	4.02	1.49	0.83	1.72	50.65
Soan River Rainfall 0.52(P)+0.48(R	3.08	4.07	3.55	3.19	1.97	3.45	11.3	12.5	4.50	1.53	0.84	1.66	51.74

* 21% of Kallar + 67% of Palandari + 12% of Rawal prepared for Ling River
* 52 % of Palandri + 48% of Rawal prepared for Soan River

2.7. River Flow Data Analysis

As already discussed, the discharge data of Soan River, Ling River and Darmalak Dam are available on daily basis. For each discharge station three years data was analyzed. Three years were selected according to dry average and wet conditions of the corresponding rainfall stations. After the dry, average and wet years selected, their discharge data was analyzed. Hydrographs developed and base flow was separated from the total runoff to check the variability of runoff estimates using SCS and modified SCS methods [2,3].

This method is applied on dry, average and wet rainfall years. Dry, average and wet rainfall years are taken to check the variability of the method for extreme conditions**.**

2.8. Runoff Estimation by SCS Methods

In this method curve numbers are estimated using soil data, vegetation cover, Hydrological conditions and land use [14]. Based on the soil type, vegetation covers and lands the curve number is determined. For the estimation of CN soil group classification and cover complex classification is needed.

Soil group classification is made as explained above. Cover complex classification depends on land uses, which are subdivided by treatment or practice, such as contoured or straight row; this separation reflects the different hydrologic runoff potential that is associated with variation in land use treatment. It is separated with three classes poor, fair and good.

These curve number are for AMC I, F AMC II and AMC III curve numbers are estimated using Table 5. Once the curve numbers are determined, the runoff is estimated as follows;

- Antecedent rainfall is estimated using the procedure proposed by SCS;
- Curve number used to estimate runoff is according to AMC rainfall;
- The maximum relation S is estimated using the equation.

$$S = \frac{1000}{CN} - 10 \tag{10}$$

After estimating S for the given rainfall P, the runoff Q is estimated using equation:

$$Q = {(P - 0.2\,S)}\Big/{(P - 0.8\,S)} \tag{11}$$

where, *Q* is the runoff in inches; P is the antecedent rainfall; and *S* is the maximum relation.

In this procedure antecedent moisture conditions (AMC) are considered. Soil Conservation Service developed three antecedent soil moisture conditions labeled as I, II and III.

The soil conditions for each AMC is as follows:

Condition I: Soil are dry but not to a wilting point. Satisfactory cultivation has taken place.

Condition II: Average condition

Condition III: Heavy rainfall or light rainfall and low temperatures have occurred within the last 5 days, saturated soil.

Table 5. *Using estimated curve numbers for AMC I, F AMC II and AMC III*

AMC	Total 5- day antecedent: rainfall (inches)	
	Dormant Season	Growing Season
I	Less than 0.5	Less than 1.4
II	0.5 to 1.1	1.4 to 2.1
III	Over 1.1	Over 2.1

Using Curve Number as Soil Cover Complex Procedure for Selected Catchments are seen in Table 6.

Table 6. *Using curve number as soil cover complex procedure for selected catchments*

Land use Description/Treatment/ Hydrologic condition		**Hydrological Soil Group**					
		A	B	C	D	CN	% age area
Soan River Near Chirah							
Row Crops, Contoured and Terraced	Poor %	66	74	80 95	82 2	80	58
Pasture or Range Contoured	fair %	25	59	75 77	83	64	3
Wood for Forest Land	fair %	36	60	73	79 100	79	7
Forest Land	good	25	55	70 80	77 20	71	32
Weighted Curve Number = 77							
Ling River Near Kahuta							
Row Crops, Contoured and Terraced	poor	66	74	80	82		
	%	-	13	67	20	80	70
Wood or Forest Land	fair	36	60	73	79		
	%	-	44	12	44	70	20
Forest Land	good	25	55	70	77		
	%	-	23	77	-	67	10
Weighted Curve Number = 77							
Darmalak Dam Near Kohat							
Row Crops, Straight Row	poor	72	81	88	91		
	%	-	30	70	-	86	22
	Gravel	76	85	89	91		
	%	-	30	70	-	88	78
Weighted Curve Numbe r= 88							

The CN values obtained from above Table 6 are for soil moisture conditions 11. If either of the soil condition 1 or 11 are to be used, the CN can be adjusted using the following Table 7 given below:

Table 7. *Curve number estimation for different antecedent soil moisture conditions*

CN for AMC.11 condition	Corresponding CN for Conditions	
	1	**111**
100	100	100
95	87	99
90	78	98
85	70	97
80	63	94
75	57	91
70	51	87
65	45	83
60	40	79
55	35	75
50	31	70
45	27	65
40	23	60
35	19	55
30	15	50
25	12	45
20	9	39
15	7	23
10	4	26
5	2	17
0	0	0

3. Results and Discussion

The purpose of the study is to estimate the runoff for various sized catchments using SCS and Modified SCS methods and to determine the variability in runoff estimation for different sized catchments. The Soil Conservation Services method consisted of three variables in estimating runoff that are rainfall, antecedent moisture condition, and the hydrologic soil-cover complex [10].

Mishira and Singh (2003) modified the popular SCS-CN equation by introduction two parameter ‘a’ and ‘λ’ that performs significantly better. A spreadsheet model was developed for different rainfall data to compute the direct runoff. Parameters such as precipitation, (P), Potentional maximum retention, (S) and Initial abstraction (I_a) are used to compute runoff (Q) in spread sheet model of SCS Method. But two parameters λ and ‘a’ with three variants 0.2,0,0 and 1,1,0.5 are used respectively along with parameter mentioned above for the calculation of runoff in Modified SCS Method to refine the results of SCS Method.

3.1. Runoff Estimation at Selected Sites

3.1.1. Soan River

Runoff Estimation Using SCS and Modified SCS Methods

Table 8 gives the direct runoff of Soan River rainfall data estimated on the basis average monthly from 1963-1978 using both existing and Modified SCS Methods.

Table 8. *Direct runoff of Soan River rainfall by using SCS and Modified SCS methods average rainfall data in inches from (1963-1978)*

Average Month	**Precipitation P (Inches)**	**Calculated Q SCS Method**	**Calculated Q Modified SCS Method**		
			$\lambda=0$, a=	$\lambda=0.2$, a=1	$\lambda=0$, a=0.5
Jan	3.08	1.125	1.561	1.125	2.092
Feb	4.07	1.869	2.350	1.869	3.302
Mar	3.55	1.466	1.926	1.466	2.644
Apr	3.23	1.236	1.681	1.236	2.271
May	1.97	0.433	0.785	0.433	0.979
Jun	3.47	1.407	1.863	1.407	2.548

Jul	11.32	8.387	8.957	8.387	14.820
Aug	12.59	9.598	10.172	9.598	17.070
Sep	4.50	2.212	2.706	2.212	3.868
Oct	1.53	0.220	0.515	0.220	0.620
Nov	0.84	0.018	0.185	0.018	0.208
Dec	1.84	0.366	0.703	0.366	0.869

Above Table 8 illustrate calculated runoff Q of Soan River by using SCS Method and Modified SCS Method (with different values of variant ‘a’ and λ). Detail of the parameters Precipitation, (P), Potentional maximum retention,(S) and Initial abstraction (I_a) calculated on average monthly basis.

Precipitation, (P) on average monthly basis found to be 0.84 inches minimum for the November and maximum in August as 12.59 inches. Potentional maximum retention, (S) which is calculated by using SCS equation is 2.987.Initial abstraction I_a is also calculated and found to be 0.597. Finally runoff, (Q) is also computed by using equation (3) for all the months of different years (averagely). The results indicate that runoff occurred maximum (9.598) and (8.387) inches for the August & July respectively. But it indicates that precipitation is maximum through the year.

Modified SCS method for runoff estimation is applied on the observed data of Soan River with different values of variants λ and ‘a’ which are described below.

Table 8 presents the estimated direct runoff by applying equation (3) of Modified SCS Method with variant λ=0, a=1 by using rainfall data of Soan River. Average rainfall data is taken for 16 years (1963-1978). Precipitation, (P) is calculated on average monthly basis which is observed minimum for the month of November that is 0.84 inches and maximum for the month of August which is 12.59 inches. Potential maximum retention, (S) is 2.987. Initial abstraction I_a is also calculated which 0 is. Finally runoff, (Q) is also calculated for all months of different years (averagely), which was maximum 10.172 and 8.957 inches for the months of August and July respectively.

By applying λ=0.2 and a=1, the direct runoff of Soan River is presented in Table 8. The rainfall data used for applying Modified SCS Method was taken for same number of years [15]. In Modified SCS Method, similarly the two parameter ‘a’ and λ are introduced for capturing better estimation of direct runoff. Precipitation, (P) is also average monthly basis calculated which is minimum (0.84) inches for the month of November and maximum (12.59) inches for the august. It means that maximum average precipitation in inches is measured in the august. Potential maximum retention, (S) is calculated by using SCS equation is 2.987. Initial abstraction I_a is 0.597. Finally runoff, (Q) is also computed for all months of different years (averagely), which maximum was observed 9.598 and 8.387 inches for the august & july respectively where precipitation is maximum through the year. These runoff results are same as that of SCS method. In Modified SCS Method, two parameter λ and ’a’ are introduced with values 0, 0.5 respectively to produce significantly better results than the existing one. Precipitation, (P) is taken on average monthly basis and observed minimum for the month of November i.e., 0.84 inches and maximum for the august, which is 12.59 inches. Potential maximum retention, (S) is calculated by using SCS equation was found to be 2.987 Initial abstraction I_a is 0. Finally runoff, (Q) is estimated for all months of different years (averagely). Results from the present study indicate that it was found maximum 17.070 and 14.820 inches for the august & July respectively, similarly precipitation is maximum through the year. By the rainfall data of Soan River it is clarify that runoff is observed maximum during the June, July, August, September. It is due to the rainy season which is started in the mid of June and goes up to the mid of September in Pakistan.

SCS and Modified SCS Methods are used for the calculation of runoff by using the observed data of Soan River. In the Modified SCS Method two parameters **λ** and **‘**a’ with three variants 0.2, 0 and 1,1,0.5 are used respectively. The calculated runoff is same as it was calculated by using existing SCS Method with variant of λ =0.2**,** ‘a’=1. Finally it is found the comparatively good result of calculated runoff with SCS Method. Similarly monthly runoff estimation of Soan River by using SCS and Modified SCS Methods with two variants λ and ‘a’ having different values. When the results of both Methods are compared then it is found SCS Method give comparatively good results.

Comparison of Runoff using SCS Method

Table 9 presents the comparison of observed runoff and calculated runoff of Soan River for the years 1963 & 1964 by using SCS method. The maximum difference is observed 7.34 inches in the august for year 1963 and the maximum difference is 11.64 inches in the month of July for year 1964. The minimum difference is observed during the october & december for the year 1963 and 1964 respectively.

Table 9. *Comparison of observed runoff and calculated runoff of Soan River for the years 1963 & 1964 by using SCS Method*

Year	**1963**			**1964**		
Month	Observed	Calculated	Difference	Observed	Calculated	Difference
Jan	0.09	0.15	-0.06	1.89	6.06	-4.17
Feb	0.52	0.27	0.25	0.52	0.12	0.4
Mar	1.05	2.24	-1.19	0.23	0.2	0.03
Apr	0.26	1.74	-1.48	0.34	1.46	-1.12
May	0.17	0.52	-0.35	0.14	0.25	-0.11
Jun	0.06	0.6	-0.54	0.08	0.01	0.07
Jul	6.45	7	-0.55	5.5	17.14	-11.64
Aug	4.63	11.97	-7.34	5.93	8.4	-2.47
Sep	3.2	3.83	-0.63	3.85	3.21	0.64
Oct	0.12	0.06	0.06	0.39	0.15	0.24
Nov	0.11	0.41	-0.3	0.15	0.07	0.08
Dec	0.08	0.51	-0.43	0.14	0.08	0.06

Comparison of Runoff using Modified SCS Method

Comparison of observed runoff and calculated runoff of Soan River for the years 1963 & 1964 by using Modified SCS Method (When λ=0, a=0.5) is shown in Table 10. The maximum difference is observed 16.91 inches in august for year 1963 and the maximum difference is 25.94 inches in the july for year 1964.

Table 10. *Comparison of observed runoff and calculated runoff of Soan River for the years 1963 & 1964 by using Modified SCS Method With (λ=0, a=0.5)*

Year	**1963**			**1964**		
Month	Observed	Calculated	Difference	Observed	Calculated	Difference
Jan	0.09	0	0.09	1.89	10.56	-8.67
Feb	0.52	0.71	-0.19	0.52	0.43	0.09
Mar	1.05	3.91	-2.86	0.23	0.59	-0.36
Apr	0.26	3.1	-2.84	0.34	2.63	-2.29
May	0.17	1.11	-0.94	0.14	0.67	-0.53
Jun	0.06	1.24	-1.18	0.08	0.06	0.02
Jul	6.45	12.27	-5.82	5.5	31.44	-25.94
Aug	4.63	21.54	-16.91	5.93	14.85	-8.92
Sep	3.2	6.61	-3.41	3.85	5.56	-1.71
Oct	0.12	0.01	0.11	0.39	0	0.39
Nov	0.11	0.94	-0.83	0.15	0.01	0.14
Dec	0.08	1.1	-1.02	0.14	0.36	-0.22

Comparison of Rainfall Runoff

It is clear from the Figures 1-3 that the runoff results by SCS Method are comparatively closer to observed runoff than modified SCS method [15]. Modified SCS Method overestimate the runoff from rainfall and the difference increase between observed and computed runoff at higher precipitation value than at lower precipitation.

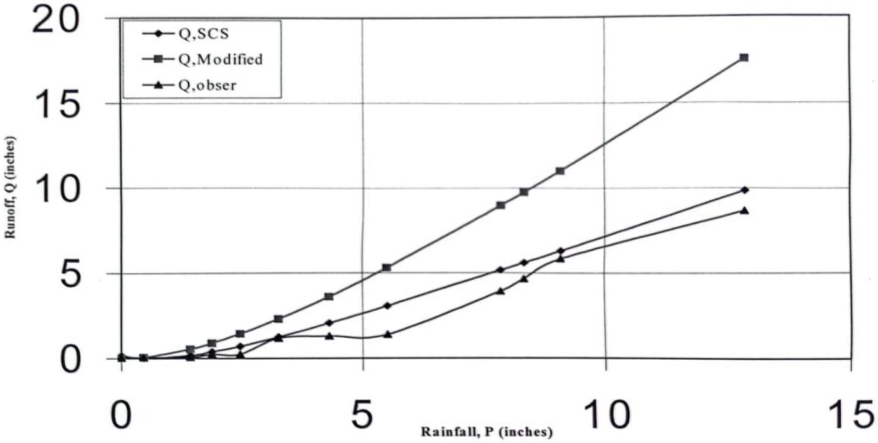

Figure 1. Comparison between the existing SCS method and modified SCS method on the rainfall-runoff Data of Soan River

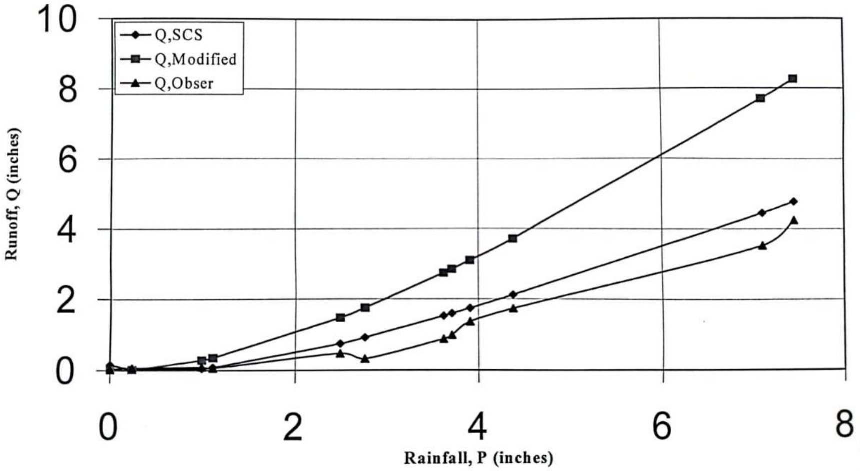

***Figure 2.** Comparison between the Existing SCS Method and Modified SCS Method on Dry Year Rainfall Runoff Data of 1969 of Soan river*

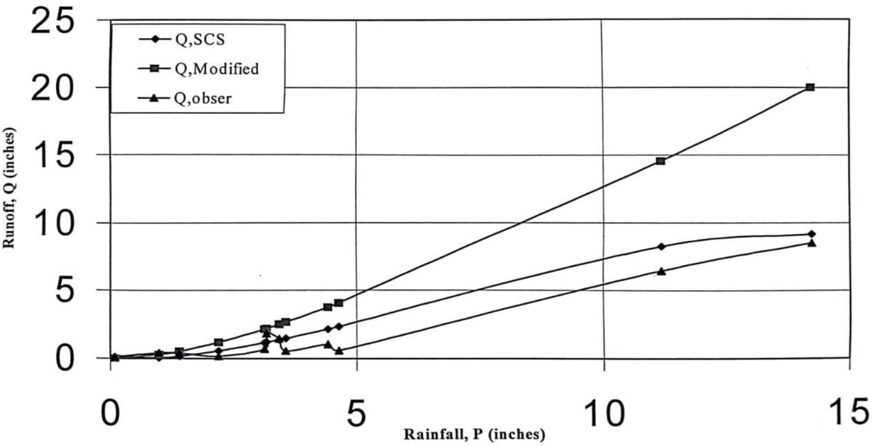

Figure 3. *Comparison between the Existing SCS Method and Modified SCS Method on Dry Year Rainfall Runoff Data of 1969 of Soan river*

Three Years are selected from historical record according to Dry, Average, and Wet conditions for the collected data of Soan River and their graphs are plotted in figures 3.1, 3.2 and 3.3 respectively. In these figures runoff computed by Modified SCS Method did not fall closed to observe runoff but the results obtained by the calculation of SCS Method are comparatively closer to observed one as compared to Modified SCS Method.

3.1.2. Ling River

Runoff Estimation Using SCS and Modified SCS Methods

Table 11 indicates direct runoff of Ling River rainfall for average rainfall data is taken from 1963-1978. Calculated runoff Q of Ling River shown in Table 11 with the application of SCS Method and Modified SCS Method (with different values of variant λ and 'a'). Parameters Precipitation, (P), Potential maximum retention, (S) and Initial abstraction (Ia).

Average monthly precipitation, (P) is minimum for the november (0.83 inches) and maximum for the august (11.58 inches).It is observed that maximum average precipitation in inches is measured in the august. Potentional maximum retention, (S) is 2.98 calculated by using equation (3.8), while Initial abstraction Ia is 0.60. Runoff, (Q) is also calculated for all months of different years (averagely), which was maximum 8.64 and 8.33 inches for august and july respectively where precipitation is maximum through the year due to the rainy season.

Table 11. *Direct Runoff of Ling River Rainfall by using SCS and Modified SCS Methods Average Rainfall Data in Inches from (1963-1978)*

Average Month	**Precipitation P (Inches)**	**Calculated Q SCS Method**	**Calculated Q Modified SCS Method**		
			λ=0, a=1	λ=0.2, a=1	λ=0, a=0.5
Jan	3.23	1.24	1.68	1.24	2.27
Feb	4.32	2.07	2.56	2.07	3.63
Mar	3.53	1.46	1.91	1.46	2.63
Apr	3.3	1.29	1.73	1.29	2.35
May	2	0.45	0.80	0.45	1.01
Jun	3.38	1.34	1.80	1.34	2.45
Jul	11.25	8.33	8.89	8.33	14.71
Aug	11.58	8.64	9.21	8.64	15.29
Sep	4.02	1.83	2.31	1.83	3.24
Oct	1.49	0.21	0.50	0.21	0.60
Nov	0.83	0.02	0.18	0.02	0.20
Dec	1.72	0.31	0.63	0.31	0.77

Runoff estimated for Modified SCS Method by using average rainfall data of Ling River with different values of λ and ‘a’ which are given below.

In Table 11, direct runoff is computed by applying modified SCS Method with $\lambda = 0$ & $a = 1$ for ling river. Precipitation, (P) is observed minimum for the november (0.83 inches) and maximum for the august (11.58 inches). The maximum average precipitation is obtained in the month of August. Potentional maximum retention, (S) calculated by using SCS equation is 2.98. Initial abstraction Ia is also calculated 0. Finally runoff, (Q) is computed for all months of different years (averagely), which was got maximum 9.21 and 8.89 inches for the months of August and July respectively where precipitation is maximum through the year.

Table 11 presents the calculated direct runoff for Ling River rainfall data by using modified SCS method with parameters (λ=0.2, a=1) the average rainfall data taken in inches for 16 years (1963-1978). Precipitation, (P) is calculated average monthly basis which is observed minimum (0.83 times) for the month of November and maximum (11.58 inches) for the month of August. Potentional maximum retention, (S) calculated by using SCS equation is 2.98. Initial abstraction Ia is 0.60. The runoff, (Q) is obtained (averagely), maximum 8.64 and 8.33 inches for the august & july, respectively. Due to high precipitation these two months give maximum value of runoff.

Modified SCS Method with values of (λ=0, a=0.5) is applied on data and express in Table 11 for Ling River for years 1963 to 1978. Precipitation, (P) on average monthly basis calculated and observed which is minimum for the month of November (0.83 inches) and maximum for the month of August (11.58 inches). It means that maximum average precipitation is measured in the month of August. Potentional maximum retention, (S) computed by using SCS equation is 2.98. The calculated initial abstraction Ia is 0. Finally runoff, (Q) is gained maximum 15.29 and 14.71 inches for the months of August and July respectively; similarly it was found that precipitation is also maximum for same months.

The calculated data of Ling River is shown in the Table 11 by using two methods SCS Method and Modified SCS Method. In Modified SCS Method two parameters λ and ‘a’ with three variants (λ=0.2, a=1), (λ=0, a=1) and (λ=0, a=0.5) are used. SCS Method gives the comparatively better results as compared to Modified SCS Method.

Monthly data Ling River is calculated for direct runoff by using two methods i.e. SCS Method and Modified SCS Method. After computed the runoff of both Methods it was found that SCS Method gave good results.

Comparison of Runoff using SCS Method

Table 12. *Comparison of observed Runoff and calculated Runoff of Ling River for the years 1963 & 1964 by using SCS Method*

Year	**1963**			**1964**		
Month	**Observed**	**Calculated**	**Difference**	**Observed**	**Calculated**	**Difference**
Jan	**0.07**	**0.15**	**-0.08**	**2.06**	**6.27**	**-4.21**
Feb	**0.34**	**0.75**	**-0.41**	**0.5**	**0.11**	**0.39**
Mar	**0.41**	**2.38**	**-1.97**	**0.21**	**0.18**	**0.03**
Apr	**0.31**	**1.97**	**-1.66**	**0.37**	**1.22**	**-0.85**
May	**0.1**	**0.54**	**-0.44**	**0.15**	**0.24**	**-0.09**
Jun	**0.08**	**0.81**	**-0.73**	**0.01**	**0.01**	**0**
Jul	**5.98**	**4.86**	**1.12**	**6.62**	**17.52**	**-11.90**
Aug	**8.07**	**7.57**	**0.50**	**6.48**	**7.26**	**-0.78**
Sep	**2.58**	**2.65**	**-0.07**	**2.49**	**2.5**	**-0.01**
Oct	**0.15**	**0.05**	**0.1**	**0.18**	**0.15**	**0.03**
Nov	**0.21**	**0.44**	**-0.23**	**0.07**	**0.04**	**0.03**
Dec	**0.18**	**0.44**	**-0.26**	**0.16**	**0.21**	**-0.05**

Table 12 gives the comparison of observed runoff and calculated runoff of Ling River for the years 1963 &1964 by using SCS Method. The maximum difference was (1.12) inches and (11.90) inches in the month of July for year 1963 & 1964 respectively.

Comparison of Runoff using Modified SCS Method

Table 13. *Comparison of observed Runoff and calculated Runoff of Ling River for the years 1963 & 1964 by using Modified SCS Method with (λ=0, a=0.5)*

Year	**1963**			**1964**		
Month	Observed	Calculated	Difference	Observed	Calculated	Difference
Jan	0.07	0	0.07	2.06	10.95	-8.89
Feb	0.34	1.5	-1.16	0.5	0.43	0.07
Mar	0.41	4.14	-3.73	0.21	0.55	-0.34
Apr	0.31	3.47	-3.16	0.37	2.25	-1.88
May	0.1	1.16	-1.06	0.15	0.66	-0.51
Jun	0.08	1.58	-1.5	0.01	0.07	-0.06
Jul	5.98	8.42	-2.44	6.62	32.16	-25.54
Aug	8.07	13.31	-5.24	6.48	12.76	-6.28
Sep	2.58	4.6	-2.02	2.49	4.35	-1.86
Oct	0.15	0.02	0.13	0.18	0	0.18
Nov	0.21	1	-0.79	0.07	0.02	0.05
Dec	0.18	0.99	-0.81	0.16	0.6	-0.44

Table 13, illustrated the comparison of observed runoff and calculated runoff of Ling River for the 1963 & 1964 by using Modified SCS Method (When λ=0, a=0.5).

The maximum difference is observed 5.24 inches in the month of August for year 1963 and the maximum difference 25.54 inches in the month of July for year 1964.The minimum difference is observed during the months of January and February for the years 1963 and 1964 respectively.

Comparison of Rainfall Runoff

Figure 4 is clarify that SCS Method give close results as compare to the Modified SCS Method. Modified SCS Method overestimate the runoff and the difference increase between observed and computed runoff at higher precipitation value than at lower precipitation. SCS Method gives comparatively good results of runoff after processing the rainfall data [16].

According to dry, average, and wet conditions for the collected data of Ling River, three years are selected from historical record (Figures 5-7). In figures 5-7 the curves generated by runoff obtained by SCS Method lies comparatively closer to the runoff curves of observed data. Runoff generated by Modified SCS Method is very high as compare to observed runoff data.

DarMalak Dam

Runoff Estimation Using SCS and Modified SCS Methods

Average rainfall data of Darmalak Dam in Table 14 is calculated by using SCS Method and Modified SCS Method the data taken for years (1970-2004).

Table 14. *Direct Runoff of Damalak Dam Rainfall by using SCS and Modified SCS Methods Average Rainfall Data in Inches from (1970-2004)*

Average Mo	**Precipitation P (Inches)**	**Calculated Q SCS Method**	**Calculated Q Modified SCS Method**		
			$\lambda=0$, $a=1$	$\lambda=0.2$, $a=1$	$\lambda=0$, $a=0.5$
Jan	1.04	0.28	0.45	0.28	0.58
Feb	1.66	0.70	0.91	0.70	1.26
Mar	2.74	1.59	1.83	1.59	2.57
Apr	1.99	0.96	1.18	0.96	1.68
May	1.44	0.54	0.74	0.54	1.00
Jun	1.05	0.28	0.46	0.28	0.58
Jul	3.07	1.88	2.13	1.88	3.26
Aug	4.77	3.45	3.71	3.45	6.08
Sep	1.76	0.78	0.99	0.78	1.38
Oct	0.96	0.23	0.40	0.23	0.50
Nov	0.34	0.00	0.07	0.00	0.08
Dec	0.66	0.09	0.22	0.09	0.26

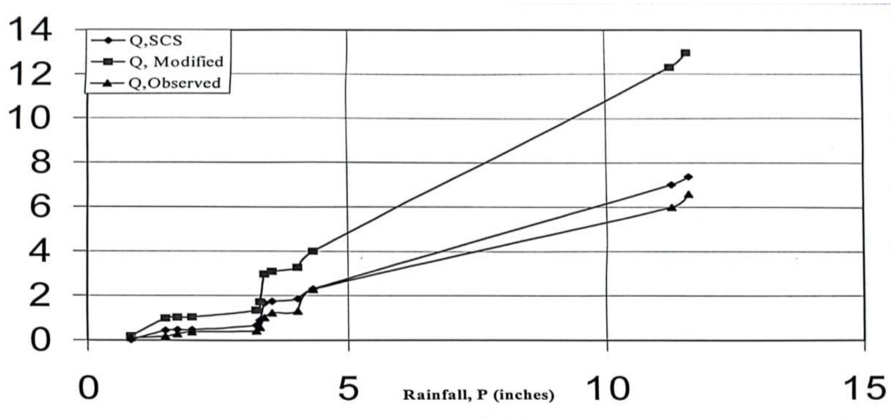

Figure 4. *Comparison between the Existing SCS Method and Modified SCS Method on Rainfall Runoff Data of Ling River*

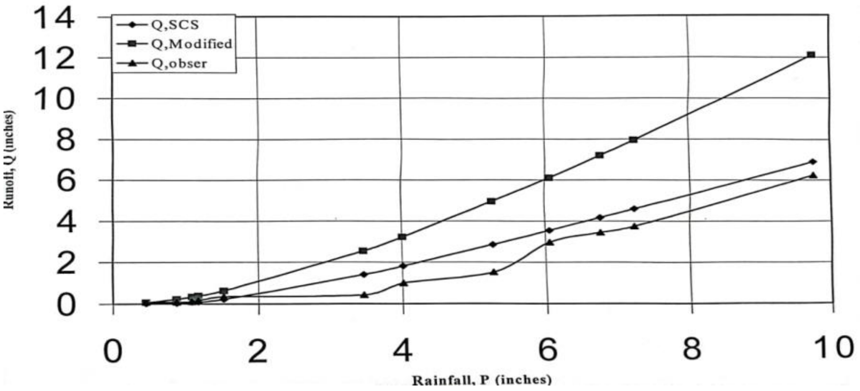

Figure 5. *Comparison between the Existing SCS Method and Modified SCS Method on Dry Year Rainfall Runoff Data of 1969 of Ling River*

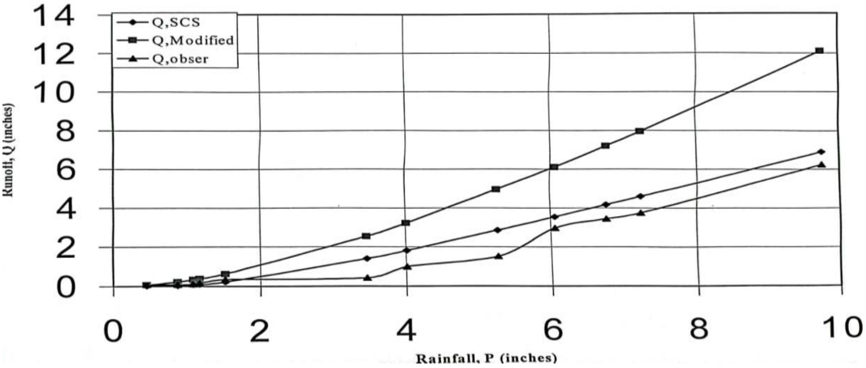

Figure 6. *Comparison between the Existing SCS Method and Modified SCS Method on Average Year Rainfall Runoff Data of 1965 of Ling River*

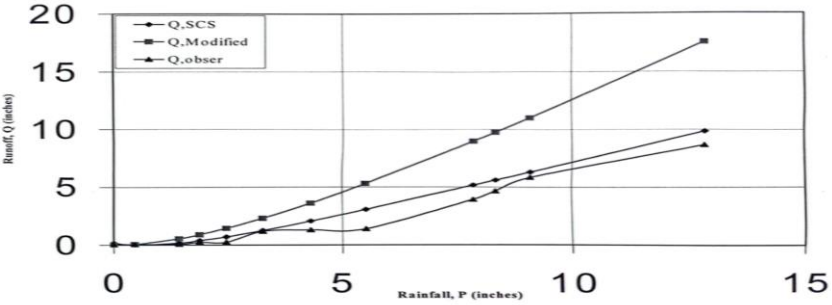

Figure 7. *Comparison between the Existing SCS Method and Modified SCS Method on Wet Year Rainfall Runoff Data of 1967 of Ling River*

By applying two methods SCS and Modified SCS (with different values of variant λ and ‘a’) in table 14 calculated runoff Q is computed while detail of parameters Precipitation, (P). Precipitation, (P) is on average monthly basis calculated and observed minimum for the november (0.34 inches) and maximum for the august (4.77 inches). It means that maximum average precipitation is measured in august. Potentional maximum retention, (S) estimated by using SCS equation is 1.36. Ia (initial abstraction) is calculated 0.27. Finally runoff, (Q) is computed for all months of different years (averagely) and the results indicate that the runoff occurred maximum (3.45) and (1.88) inches for the august & july respectively, where precipitation is maximum.

Table 14 shows the direct runoff of Darmalak Dam by using Modified SCS Method with values of λ=0 and a=1 for average rainfall data taken in Inches for years (1970-2004). Precipitation, (P) is calculated on average monthly basis and observed minimum for november (0.34 inches) and maximum for the month of August (4.77 inches). It means that maximum average precipitation is measured in august. Potentional maximum retention, (S) is calculated by using SCS equation that is 1.36. Initial abstraction Ia is calculated as 0. Table 7 shows that maximum 3.71 and 2.13 inches for august & July respectively, similarly it was found that precipitation was maximum for these months. In Table 14, Modified SCS Method is used for parameters λ=0.2 and a=1for the 35 years (1970-2004) rainfall data of Darmalak Dam. Precipitation, (P) obtained minimum for november (0.34 inches) and maximum for august (4.77 inches). Table 4.7 clearly shows that maximum average precipitation is measured in the month of August. Potentional maximum retention, (S) which is calculated by using SCS equation is 1.36. Initial abstraction Ia is also found 0.27. Finally runoff, (Q) is observed maximum 3.45 and 1.88 inches for august & july, respectively while precipitation is also maximum for these months. Table 14 presents the computed runoff of Darmalak Dam by applying modified SCS Method with variant λ=0,a=0.5). Precipitation, (P) is observed minimum for the month of November (0.34) inches and maximum for the month of August (4.77) inches. Potentional maximum retention, (S) calculated by using SCS equation is 1.36. Initial abstraction Ia is also calculated 0. Runoff computed maximum 6.08 and 3.26 inches for the august & july, respectively.

Rainfall data of Darmalak dam is processed by using SCS and Modified SCS Methods by taking two parameters λ and ‘a’ with the values 0.2, 0, 0 and 1, 1, 0.5 respectively. When λ =0.2 and ‘a’=1 is used then it was found that calculated runoff is same as it was calculated by using existing SCS Method. Finally it is found comparatively better result of computed runoff with SCS Method. After calculated direct runoff of Darmalak Dam on the monthly rainfall data from 1970-2004 by using SCS Method and Modified SCS Method. It was found that the calculated results for each month of every year give better result with existing SCS Method.

Comparison of Runoff using SCS Method

Comparison of observed Runoff and calculated Runoff of Darmalk Dam for the years 1970 & 1971 by using SCS Method is presented in Table 15.

***Table 15**. Comparison of observed Runoff and calculated Runoff of Darmalak Dam for the years 1970 & 1971 by using SCS Method*

Year	**1970**			**1971**		
Month	Observed	Calculated	Difference	Observed	Calculated	Difference
Jan	0.00	0.08	-0.08	0.00	0.01	-0.01
Feb	0.00	0.6	-0.60	0.00	0.35	-0.35
Mar	0.00	1.41	-1.41	0.00	0.16	-0.16
Apr	0.00	0.21	-0.21	0.54	2.4	-1.86
May	0.00	0.33	-0.33	0.00	0.15	-0.15
Jun	0.00	0.27	-0.27	0.00	1.21	-1.21
Jul	0.40	1.52	-1.12	0.83	1.86	-1.03
Aug	0.77	3.52	-2.75	1.52	0.7	0.82
Sep	0.00	0.48	-0.48	0.00	0.14	-0.14
Oct	0.00	0.07	-0.07	0.00	0.01	-0.01
Nov	0.00	0.07	-0.07	0.00	0.06	-0.06
Dec	0.00	0	0.00	0.00	0.02	-0.02

The above table shows the comparison of observed runoff and calculated runoff of Darmalk Dam for the years 1970 & 1971 by using SCS Method. The maximum difference (2.75) inches is observed in the month of August for year 1970 and the same value is (1.86) inches in the month of April for year 1971. The minimum difference is 0.07 in the month of November for the year 1970 and 0.01 for the month October for the year 1971.

Comparison of Runoff using Modified SCS Method

Table 16. *Comparison of observed Runoff and calculated Runoff of Darmalak Dam for the Years 1970 & 1971 by using Modified SCS Method with (λ=0, a=0.5)*

Year	**1970**			**1971**		
Month	Observed	Calculated	Difference	Observed	Calculated	Difference
Jan	0.07	0	0.07	2.06	10.95	-8.89
Feb	0.34	1.5	-1.16	0.5	0.43	0.07
Mar	0.41	4.14	-3.73	0.21	0.55	-0.34
Apr	0.31	3.47	-3.16	0.37	2.25	-1.88
May	0.1	1.16	-1.06	0.15	0.66	-0.51
Jun	0.08	1.58	-1.5	0.01	0.07	-0.06
Jul	5.98	8.42	-2.44	6.62	32.16	-25.54
Aug	8.07	13.31	-5.24	6.48	12.76	-6.28
Sep	2.58	4.6	-2.02	2.49	4.35	-1.86
Oct	0.15	0.02	0.13	0.18	0	0.18
Nov	0.21	1	-0.79	0.07	0.02	0.05
Dec	0.18	0.99	-0.81	0.16	0.6	-0.44

Table 16 describes the comparison of observed runoff and calculated runoff of Darmalak Dam for the Years 1970 & 1971 by using Modified SCS Method (When λ=0, a=0.5). The maximum difference is observed 5.43 inches in the august for year 1970 and the maximum difference 3.63 inches in the April for year 1971.

Comparison of Rainfall Runoff

SCS Method curve lies in closer region to observed runoff curve as compare to Modified SCS Method. Among the different years, three years are selected according to dry, average, and wet conditions for the collected data of Darmalak Dam. Three graphs for dry, average and wet years are plotted in figures 8, and wet seasons of Soan and Ling Rivers 9, 10, 11 respectively. Figures 8-11 give same trends as shown by the graphs of average.

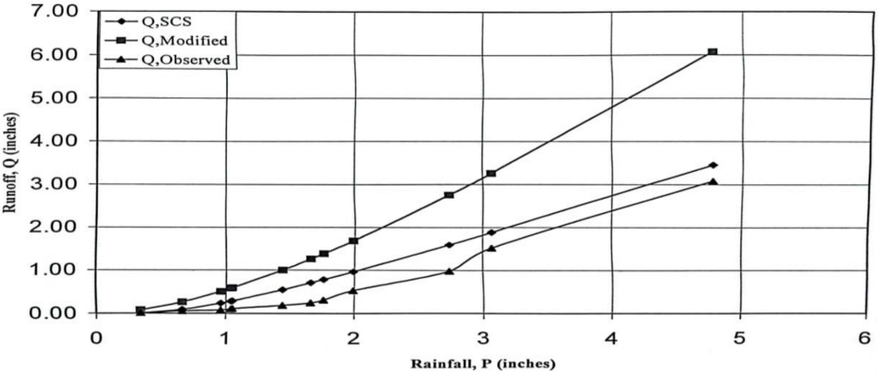

Figure 8. *Comparison between the Existing SCS Method and Modified SCS Method on Rainfall Runoff Data of Darmalak Dam*

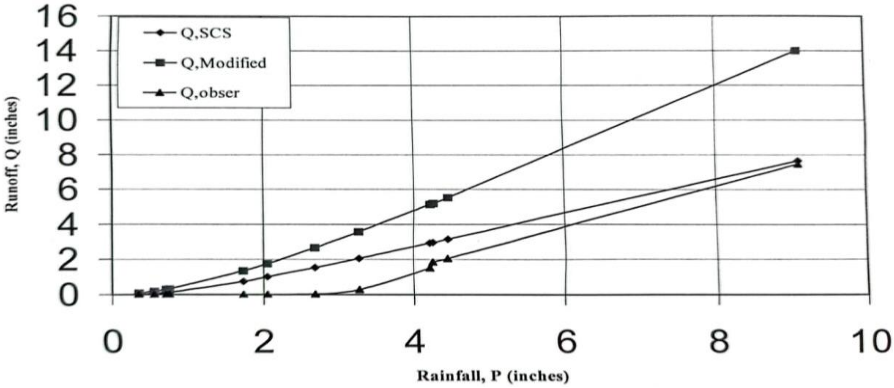

Figure 9. *Comparison between the Existing SCS Method and Modified SCS Method on Dry Year Rainfall Runoff Data of 1992 of Darmalak Dam*

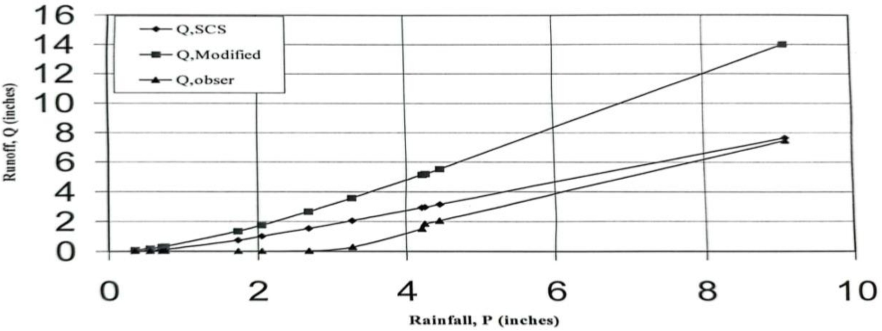

Figure 10. *Comparison between the Existing SCS Method and Modified SCS Method on Average Year Rainfall Runoff Data of 2002 of Darmalak Dam*

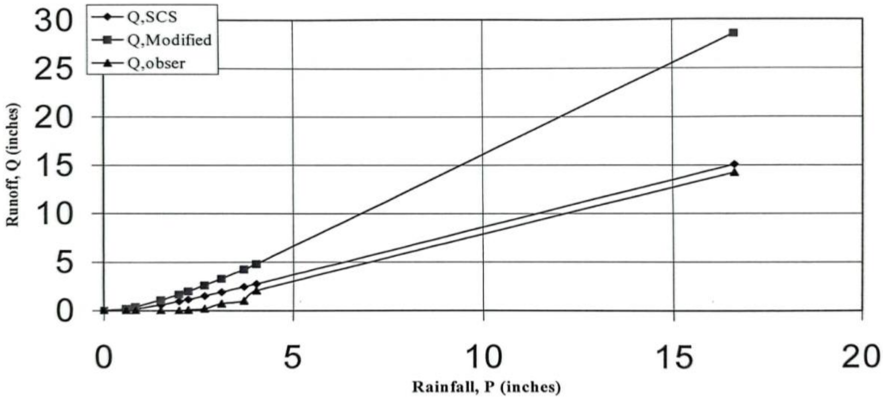

Figure 11. *Comparison between the Existing SCS Method and Modified SCS Method on Wet Year Rainfall Runoff Data of 1976 of Darmalak Dam*

Conclusions

The runoff generated by SCS and Modified SCS Methods after computing the CN for each of three catchments namely Soan River, Ling River and Darmalak Dam and comparing it with observed record of each one indicate that the results are not exactly matching with the observed runoff record. This difference between observed runoff and computed runoff is may be because of the fact that either these methods not usable in the said catchments or because of the possibility of data error. Still the results of SCS Methods are comparatively better than modified SCS Method for each of the catchment and the runoff results are fairly better at low precipitation value than at high Precipitation value, moreover the Modified SCS Method overestimates the runoff on high rate. The Soan River, Ling River and Darmalak Dam Catchments with catchment areas of 126, 56 and 41.48 sq. miles receive annual rainfall of 51.97, 50.65 and 21.48 inches, which produce the average runoff 21.67, 15.37 and 4.53 inches per annum respectively [17]. The annual overall water losses of Soan River, Ling River and Darmalak Dam have been calculated and found to be 30 (for years 1963-1978), 32.13 (for years 1963-1978) and 16.95 (for years 1970-2004) inches per annum respectively. The resulted runoff generated from rainfall shows that existing SCS Method perform significantly better than the modified SCS method in each of the three catchments studied. The maximum variability between observed and computed runoff by SCS and Modified SCS methods found in the month of July and August because of fluctuating rainfall and variability in antecedent storm conditions. It has been observed that modified SCS Method largely varied from the observed runoff and found to overestimates the runoff in all selected catchments. Modified SCS-CN Method used with three set of variants i.e. ($\lambda = 0$, $a = 1$), ($\lambda = 0.2$, $a = 1$) and ($\lambda = 0$, $a = 0.5$) as recommended by Mishira and Singh (1999) were used for runoff generation and found comparatively better with variant $\lambda = 0.2$, $a = 1$ in each of Soan, Ling and Darmalak catchments. But their acceptability cannot be recommended in any case. Thus the validity of Modified SCS Method is doubt and need improvement. The difference between observed and computed runoff by SCS and Modified SCS Methods increase with increase of precipitation value [18]. The results obtained by using SCS Method found to be comparatively better for the Darmalak Dam than other catchments i.e. indicating its suitability for smaller sized catchment for smaller sized catchment.

SCS Method is preferred on Modified SCS Method for Soan River, Ling River and Darmalak Dam because SCS Method is giving better results than Modified SCS Method. Modified SCS Method is not recommended for usage in runoff generation for each of these three catchments and need further modification. Other runoff estimation methods should be tested for these catchments for runoff generation and these results should be compared with SCS method to ascertain best possible technique for these catchments [19]. The SCS and Modified SCS Methods should be tested on other varied size catchment with different hydrological regime to further assess their application ability and results reliability in local catchments of Pakistan

Ackonowledgment

Authors of this study highly ackowledge and salute to Late Engr. M. Kaleem Arshad for his valuabale contribution made as a part of his master work under the supervision of Dr. Sajid Mahmood. Contribution made by the Turkish (especially Dr. Zeyneb Kılıç) and Irani authors in finalizing this study. High appreciation and has been acknowleged by placing their names as co-authors in this article.

Thanks to Tubitak Bideb 2221 Programme 2022/4, to support Dr. Sajid Mahmood (in scope of programme stayed in Adıyaman city for 14 days) and Dr. Zeyneb Kılıç

References

[1] Lvovitch, M.L. (1972). Water Balance, In Report of Symposium of IASH-UNESCO, No. 92, UNESCO, France.

[2] Korkmaz, M. (2022). Statistical Trend Analysis of Long-Term Rainfall in Ayvalık. International Journal of Technology and Emerging Sciences, 2 (4), 34-39.

[3] Korkmaz, M. (2022). Flood Recurrence Calculation and Flood Risk Assessment in Rivers. El-Cezeri, (2), 532-541.

[4] Mishra, S., Tyagi, JV., Singh, VP., Singh, R. (2006). SCS-CN-based modeling of sediment yield. Journal of Hydrology. 324, (1-4), 301-322.

[5] Amatya, DM., Walega, A., Callahan, TJ., Morrison, A., Vulava, V., Hitchcock, DR., Williams, M., Epps, T. (2022). Storm event analysis of four forested catchments on the Atlantic coastal plain using a modified SCS-CN rainfall-runoff model. Journal of Hydrology, 608, 127772.

[6] Walega, A., Amatya, DM., Caldwell, P., Marion, D. (2020). Journal of Hydrology : Regional Studies Assessment of storm direct runoff and peak flow rates using improved SCS-CN models for selected forested watersheds in the Southeastern United States. Journal of Hydrology,Regional Studies, 27, 100645.

[7] Bank W. (2010). Application of GIS-based SCS-CN method in. Water Science and Engineering, 3(1): 1–13.

[8] Mishra, SK, Singh, VP. (2002). SCS-CN method: part-1: Derivation of SCS-CN based models. Acta Geophysica Polonica, 50, (3), 457-477.

[9] Mishra, SK., Singh, VP. (2003). Soil Conservation Services Curve Number (SCS-CN) Methodology. Kluwer Academic Publishers, Dordrecht, The Netherland.

[10] McCuen, RH. (1982). A Guide to Hydrology Analysis Using SCS Methods. Prentice Hall Lne. Englewood Cliffs, 1982, New Jersey.

[11] Ponce, VM. (1989). Engineering Hydrology: Principles and Practices. Prenticr Hall, Englewood Cliffs, New Jersey 07632.

[12] Rauf Ramooz. (1994). Reliability of Runoff Estimates Using Soil Conservation Service Method. MSc thesis in Engineering Hydrology, CEWRE, Lahore.

[13] Authors, T. (2020). Impacts of substrate moisture, 635–647.

[14] Sharma, D., Kumar, V. (2002). Application of SCS model with GIS data base for estimation of runoff in an arid watershed. Journal of Soil and Water Conservation, 30, (2), 141-145.

[15] Hjelmfelt, AT. (1980a) Curve Number Procedure as Infiltration Method. Journal of Hydraulic Division, Vol. No. 6, 1107-1111.

[16] Hawkins, RH. (1980). Infiltration and Curve Numbers: Some Pragmatic and Theoretic Relationships, Proceeding of Symposium on Watershed Management, 925-937.

[17] Hawkins, RH. (1978). Runoff Curve Number Relationships with Varying Site Moisture. Journal of Irrigation and Drainage Division, (National Eng Hand Book, Section 4, Hydrology) 389-398.

[18] Hjelmfelt, AT. (1980b). Empirical Investigation of Curve Number Technique, Journal of Hydraulic Division. 106, 1471-1476.

[19] Kumar, A., Kanga, S., Kumar, A., Kumar, S., Bojan, Đ. (2021). HydroResearch Surface runoff estimation of Sind river basin using integrated SCS-CN and GIS techniques. HydroRes, 4, 61–74.

CHAPTER II

The Mathematical Analysis of Non-Homogeneous Horizontal Flow Model for Salinization in the Gediz Delta (Izmir)

Muhammet Ensar YİĞİT[1]
Ecem TUNCER UYSAL[2]

Introduction

Water stands out as the quintessential and universally essential fluid, serving as a fundamental requirement for humanity. The preservation, utilization, and sustainable management of these invaluable resources represent the core mission of water resources engineering. Water is a resource that not only meets the demands of societies but also contributes significantly to maintaining the harmony of ecosystems. Consequently, extensive research is

---

[1] Doctor, Manisa Celal Bayar University, Civil Eng. Dept., ensar.yigit@cbu.edu.tr Orcid: 0000-0003-0161-7144

[2] Research Assist., Manisa Celal Bayar University, Civil Eng. Dept., ecem.tuncerӕcbu.edu.tr Orcid: 0000-0001-5246-776X

dedicated to the scrutiny of fluid dynamics and their intricate flow characteristics. The quality and accessibility of water are contingent on variables such as salinity, particularly at the junctures where it converges with the sea. The examples of interactions between river and sea can be seen in Figure 1. This underscores the imperative need for the development of mathematical models to scrutinize the properties of fluids, thereby ensuring the efficient management and utilization of these indispensable assets.

a) Filyos River / Zonguldak / Türkiye

(Batı Karadeniz Turizm Master Planı, 2023).

b) Gediz River / İzmir / Türkiye

(Wonder, 2023).

.

c) Sakarya River / Karasu / Türkiye

d) Melet River / Ordu / Türkiye

(Karasu Kaymakamlığı, 2023   (Deniz Haber Ajansı, 2023).

***Figure 1**. Examples of rivers that flow into the sea.*

When high-velocity rivers flow into the sea, they create a stratification with freshwater remaining on top and saltwater below, and the rapid current prevents salinity from increasing along the riverbed. In contrast, in rivers where the seawater's current velocity is relatively low, a phenomenon of mixing occurs along the riverbed, resulting in the salinization of freshwater. This mixing process bears critical importance for its environmental impacts and its implications for the sustainable management of water resources. This type of mixing can lead to the salinization of freshwater sources, an elevation in the salinity levels of groundwater, and reduced agricultural yields in irrigation areas. Additionally, this interaction can exert significant effects on soil salinity and ecosystems, as depicted in Figure 2.

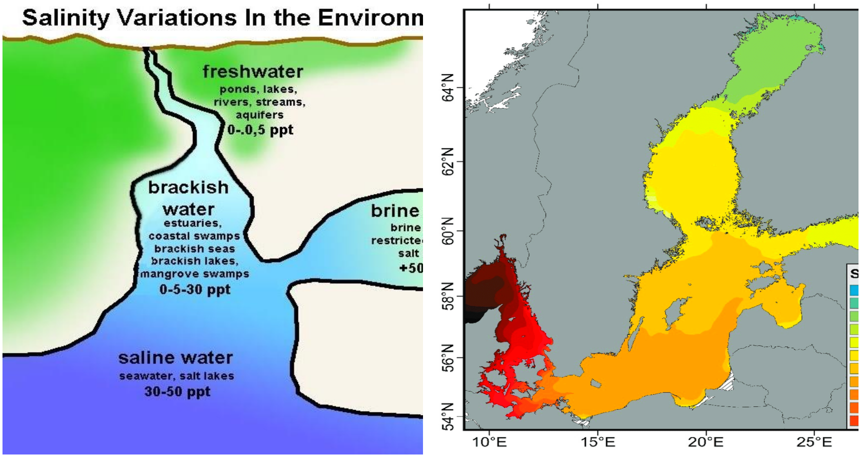

a) Salinity variations in the environment (Hutchison, 2018).

b) The Salinity gradient in the Baltic Sea (Lehmann et. al., 2002).

Figure 2. River-Seawater Contamination.

Understanding and managing these complex interactions are essential for preserving both the quality of our water resources and the health of ecosystems. Effective conservation measures and sustainable agricultural practices play a vital role in mitigating the consequences of the processes.

The discharge of freshwater into the sea carries substantial environmental significance, as it instigates a critical interplay between ecosystems. The amalgamation of freshwater with seawater induces modifications in water salinity, potentially leading to alterations in water quality within the mixing zone. Therefore, research endeavours concentrating on the environmental ramifications of the interaction between seawater and freshwater hold great import for the sustainable management of freshwater resources and the preservation of ecosystems.

Literature Review

Analysing the composition of a fluid and understanding its movement is of great importance. The mixture of fresh and saltwater, especially in coastal areas where freshwater sources merge with seawater, is a complex phenomenon that can have environmental and hydrological implications. These mixtures can lead to changes in salinity levels, significantly affecting water availability, environmental impacts, and water quality. Inhomogeneous fluids exhibit irregular distribution of the fluid. Furthermore, different phase flow systems may experience changes in flow distribution efficiency, capacity, and pressure drop. A study by Somay et al. (2015) suggests that the mixture of seawater and freshwater can have environmental and hydrological impacts, particularly in coastal regions where freshwater resources intermingle with seawater. This mixture can significantly influence changes in salinity, which, in turn, have a decisive impact on water resource availability, environmental effects, and water quality.

The study by Arslan et al. (2011) examines the use of environmental isotopes in situations where traditional methods are insufficient to identify seawater intrusion. They emphasize that seawater intrusion can lead to salinization of groundwater, reduced productivity in irrigation areas, and increased salinity and sodium content in soils. Therefore, they investigate the utility of environmental isotopes to contribute to research on the sustainability of freshwater resources and environmental balance. (Li et. al., 2012) explained the process of calculating salinity changes in the Coastal Modelling System (CMS) using the Surface-water Modelling System (SMS). CMS is a 2D model for coastal and inlet applications. The document highlights the importance of salinity changes in coastal zones and estuaries, affecting various aspects of water dynamics, and discusses the interaction between CMS-Flow and CMS-Wave models in coastal modelling. (Berger et. al., 2019) explained the threat of salinization to freshwater biodiversity and highlights the scarcity of ecological influence investigations in this context with reviewing field observations related to the effects of salinity on various ecosystem processes.

(Çetin et. al., 2009) examined the increasing global population and industrialization, emphasizing how these factors lead to a rising demand for freshwater resources and challenges in achieving equitable and sustainable water allocation and highlights the critical role of water as a vital resource for sustainable development, as recognized by the United Nations. The importance of monitoring the quantity and quality of water resources is investigated and focused on the Gediz Basin as an example where water quality observation studies are conducted. (NSW,2003) examined The Hunter River Salinity Trading Scheme benefits the entire community by enabling controlled discharges of excess water, fostering collaboration among diverse interests, and ensuring ongoing economic development while protecting the region's natural resources to effectively protect water quality in the Hunter River. (Krogh et. al., 2013) aimed to restrict saline water discharges from industry into the Hunter River by regulating discharges during high-flow periods. The regulation emphasizes the need for continuous monitoring to assess environmental impacts. (Matsoukis, 2021) aimed to understand the vulnerability of river deltas by examining salinity distribution. The research revealed a negative exponential relationship between salinity and river discharge and showed that lower stream orders are associated with higher salinity. (Han and McCreary Jr, 2001) used a model to investigate the factors affecting salinity distributions in the Indian Ocean. The study reveals that the inclusion of river inflow into the Bay of Bengal significantly improves salinity values in the upper three layers, especially in certain regions of the Bay and along the coasts of India. Additionally, the Indonesian Throughflow lowers salinities in all layers, particularly in the southern tropical ocean.

(Qiao et. al., 2018) utilized the MIKE 21 hydrodynamic and salinity model to examine the hydrodynamic characteristics and salinity transport processes in the Pink Beach wetlands of the Liao River estuary. The study finds that wetland vegetation has a limited effect on water depth and salinity in this specific wetland area. Additionally, the research explores how salinity conditions can be favourable for specific vegetation growth in the Pink Beach wetlands and provides valuable insights for related studies in other wetland systems. (Wang et. al., 2021) studied to understand differentiate between marine and terrestrial sedimentary environments in clastic sediments, an experiment involving artificial deltaic sediments with varying salinity conditions was conducted. (Nyadjro et. al., 2022) investigated the seasonal variability of sea surface salinity (SSS) in the northwestern Gulf of Guinea (NWGoG) using data from the Soil Moisture Active Passive (SMAP) satellite. The results indicate that SMAP is well-suited for regional studies in this area, effectively reproducing observed SSS features. The study reveals three significant SSS patterns: a basin-wide increase in salinity during boreal summer, a basin-wide decrease in salinity during winter, and a meridionally oriented frontal system in other seasons. Freshwater flux, zonal circulation, and upwelling are identified as major factors contributing to the seasonal SSS variability. (Chen et. al., 2023) focuses on the seasonal variation in mixed layer salinity (MLS) in the northern South China Sea (NSCS). Using an eddy-resolving circulation model, the research examines the essential physical functions contributing to the seasonal MLS cycle.

Situation Analysis

In this study, the interaction between freshwater and saltwater at the point where the Gediz River discharges into the Izmir Gulf is investigated using a mathematical model (Figure 3). The temporal variation of salinity along a 14.38 km stretch, from point 4 where the river meets the sea to point 2, as shown in Figure 4, is examined under non-homogeneous horizontal flow conditions.

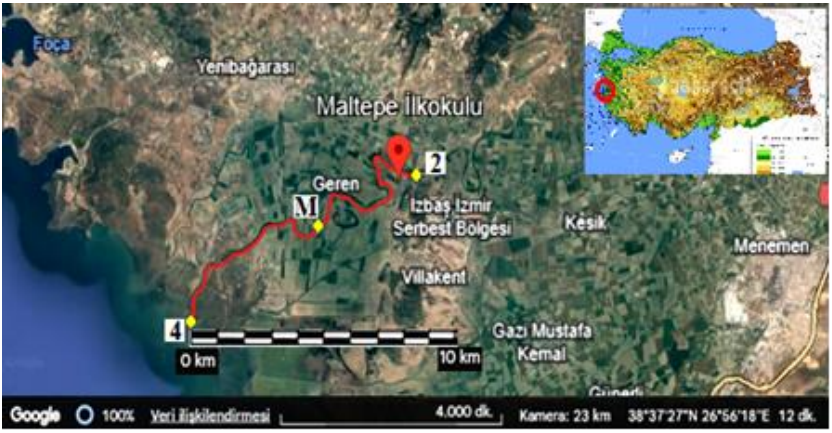

Figure 3. *Satellite View of Gediz Delta/Türkiye (Google Earth, 2023).*

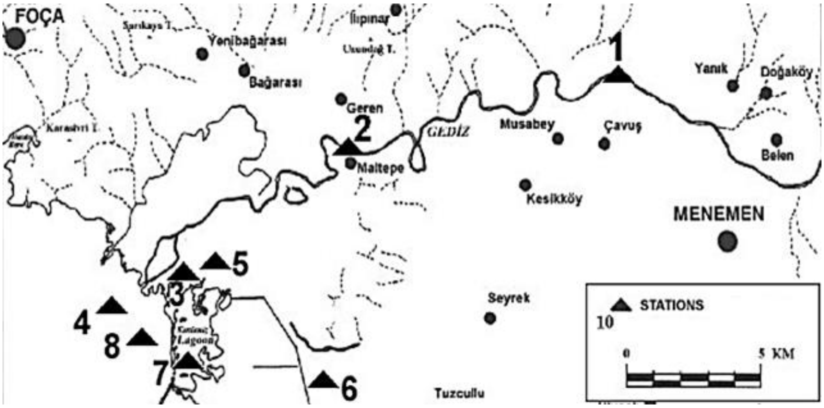

***Figure 4**. Data stations for Gediz Delta/Türkiye (Taşdemir et. al., 2009).*

(Taşdemir et al., 2009) reported the salinity levels measured at station 2 as shown in Table 1. These measurements revealed a maximum salinity of 1.76‰. At point 4, where the river meets the sea, the maximum salinity was recorded at 36.3‰ as provided in the same table. The temporal evolution of this interaction was mathematically observed, and the results section presented this evolution graphically. Consequently, these graphical representations have aided in enhancing the comprehension of the dynamics between saltwater and freshwater within the riverbed.

***Table 1.** In the Gediz Delta, values of temperature and salinity at stations (Taşdemir et al., 2009).*

No	**Temperature (ºC)**			**Salinity (‰)**		
	Min	**Max**	**Avg**	**Min**	**Max**	**Avg**
1	12.00	26.00	18.16	0.56	0.60	0.58
2	12.00	28.00	19.16	0.56	1.76	0.78
3	16.00	28.00	20.83	0.58	12.87	9.07
4	12.50	27.00	19.58	0.59	36.30	14.08
5	15.00	28.00	21.50	5.57	16.08	9.82
6	15.00	29.00	21.75	3.14	16.67	7.35
7	12.00	26.00	19.25	23.99	38.15	30.21
8	15.00	27.00	19.91	23.99	38.10	30.57

(Shaba et al., 2011) provided the values for longitudinal dispersity coefficient in Table 2. These values tend to be higher at the downstream sections where the river flows into the sea and lower in the upstream sections of the river. Furthermore, in the research, there are different dispersity coefficient values for low and high flows.

Table 2. *Overview of the calculated longitudinal dispersion coefficient across various estuaries (Shaha, et al 2011).*

Source	**Estuary**	**Dispersion coefficient (m^2/s)**
West and Williams (1972)	Ems estuary	50–300
Prandle (1981)	A group of six	50–500
Van de Kreeke (1990)	Volkerak estuary	150–325
Vallino and Hopkinson	Parker River estuary	670 (near mouth)
de Swart et al. (1997)	Ems estuary	200–1200
Lewis and Uncles (2003)	Tees-Severn estuary	100-212
Austin (2004)	Chesapeake Bay	200–1000, with a mean 650
Banas et al. (2004)	Willapa bay	20 (upstream) – 710 (near the mouth)

In the study, validation of the mathematical model through real-world data is examined. Within the comprehensive research of various scenarios containing of river and sea water, analysis is covered with critical variables such as salinity, fluctuations, flow velocity and environmental parameters.

Methodology

This section offers a comprehensive explanation of the mathematical model that controls the discharge of freshwater into the sea and the subsequent mixing process. The model has been carefully crafted to provide a quantitative evaluation of the way interactions between river and seawater change over time. This study engages in a thorough mathematical exploration of the complex interplay between two distinct fluids distinguished by varying salt concentrations and densities, all within the framework of uneven horizontal flow conditions. The primary objective of this research is to meticulously examine the phenomena related to the diffusion and shifts in fluid density as they occur during their circulation.

Mathematical Model

Mathematical model is the crudest approximation for the description of circulation with density variations due to advection and diffusion in a coastal domain of very shallow water connected to the open sea (an infinite domain of constant density) and receiving freshwater outflow from a land-based source. It is assumed that due to several physical reasons vertical mixing is complete and that only horizontal density differences drive or regulate the circulation.

The general form of the one-dimensional mathematical model for the depth varying circulation is written in the unknowns u(x, z, t), ζ(x, t), ρ (x, t), S(x, t). Where q is the inflowing discharge, ρ_0 is fresh water of density (Koutitas, 1988).

$$\frac{\partial u}{\partial t} + u\frac{\partial u}{\partial x} = -g\frac{\partial \zeta}{\partial x} + g\frac{z}{\rho}\frac{\partial \rho}{\partial x} + \frac{\partial}{\partial z}\left(v\frac{\partial u}{\partial z}\right) \qquad 1$$

$$\frac{\partial \zeta}{\partial x} + \frac{\partial (Uh)}{\partial x} = q \qquad \left(U = \frac{1}{h}\int_{-h}^{0} udz\right) \qquad 2$$

$$\rho = \rho_0(1 + \alpha S) \qquad 3$$

$$\frac{\partial S}{\partial t} + \frac{\partial (SU)}{\partial x} = \frac{\partial}{\partial x}\left(R\frac{\partial S}{\partial x}\right) \qquad 4$$

These equations are examined to clarify the mixing and transformation of two different fluids in situations involving non-uniform horizontal flow. The aim of this research is to enhance understanding of fluid circulation mechanisms and potential practical uses.

Finite Differences Expansion

The boundary conditions completing Equation (1, 3) are. $u|_{z=-h} = 0$, $\frac{\partial u}{\partial z}\Big|_{z=-h} = 0$ with respect to velocity and $\frac{\partial s}{\partial x} = 0$ on no-flow coastal boundaries, S=given constant on an open sea or river boundary with respect to salinity. The parameters v_v, and R (vertical eddy viscosity and horizontal mass dispersity) are also unknown magnitudes. A sensitivity analysis shows that their values influence the solutions substantially (Koutitas, 1988).

$$O[V_V] = O[U].O[h].0{,}1 \qquad 5$$

$$O[R] = O[U].O[S].O(\Delta x\ /\ \Delta s) \qquad 6$$

Where $\Delta x/\Delta s$ a measure of horizontal salinity gradient. A substantial simplification is introduced by integration of Equation (1) over the depth and its expression in terms of the depth mean velocity.

$$\frac{\partial U}{\partial t} + U\frac{\partial U}{\partial x} = -g\frac{\partial \zeta}{\partial x} + \frac{gh}{2}\frac{\partial ln\rho}{\partial x} - \frac{kU}{h} \qquad 7$$

The bed friction term can be in linear form or a classical quadratic one. The model consisting of Equations (2, 3, 4, 7) can describe the formulation of density induced currents and the density field and their continuous interaction in the case of horizontal density variations only. These density currents can be induced by the inflow of fresh water into initially stagnant salt water or by the joining of a freshwater body with the sea. The problem of the difference in the order of magnitude of the time scales in the formation of the hydrodynamic and density magnitudes can be resolved using implicit finite differences for Equation (7) permitting the increase in a common Δt step used for both Equation (7) and (4). The numerical solution of the depth averaged horizontally stratified fluid model presented here is based on the explicit finite difference scheme using the staggered grid illustrated in Figure 5. The velocity values are computed at the cross-sections (nodes) while the water depth, surface elevation and salinity-density values refer to the reaches between successive nodes.

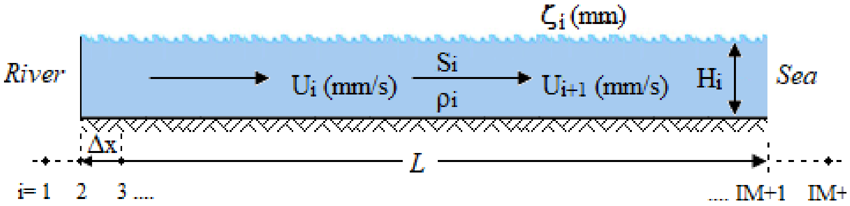

Figure 5. *1-D density current due to horizontal density gradients. Domain morphology and discretisation (Koutitas, 1988).*

The finite difference approximations of the model's equations are:

<u>Continuity Equation</u>

$$\frac{\zeta_i^{n+1}-\zeta_i^{n}}{\Delta t}=\frac{1}{2\Delta x}\left((h_{i+1}+h_i)U_{i+1}^{n}-(h_i+h_{i-1})U_i^{n}\right) \tag{8}$$

Equilibrium Equation

$$\frac{U_i^{n+1}-U_i^n}{\Delta t} = -\frac{U_i^n}{2\Delta x}((U_{i+1}^n - U_i^n) - \frac{g}{\Delta x}(\zeta_i^n - \zeta_{i-1}^n) - \frac{g(h_i - h_{i-1})}{4\Delta x}(ln\rho_i^n - ln\rho_{i-1}^n) - \frac{2kU_i^n}{h_i - h_{i-1}} \qquad 9$$

Salt Conservation

$$\frac{S_i^{n+1}-S_i^n}{\Delta t} = -\frac{1}{g\Delta x}[(S_{i+1}^n - S_i^n)U_{i+1}^n - (S_i^n - S_{i-1}^n)U_i^n] + \frac{R}{\Delta x^2}(S_{i+1}^n - 2S_i^n + S_{i-1}^n) \qquad 10$$

State Equation

$$\rho_i^n = \rho_0(1+\alpha S_i^{n+1}) \qquad 11$$

Where, Δt, Δx: time and position increment interval, t: time, α: linear ρ-S ratio coefficient, k: bed friction coefficient (m/s), R: horizontal mass dispersity (m^2/s), ζ: surface water level change (m), U: river flow velocity (mm/s), S: salinity ratio, ρ: water density, L: length of the interaction zone, H: river water depth (m) (Koutitas, 1988).

The process is structured within a computer program, focusing on a confined region (with no flow conditions upstream and downstream, represented as $\partial S/\partial x = 0$, $U= 0$). In this setup, an initial density distribution triggers a circulation pattern, which, as mixing progresses, gradually approaches a new equilibrium state. This equilibrium is reached as the fluid becomes uniform, and the initial motion experiences frictional decay. With minor adjustments to the program, various boundary conditions can be applied to model different types of density-induced flows.

Material Properties

In Table 3, the offshore salinity rate is given as $S_{4, max}$ = 36.3‰ for point 4. The length of the studied region (L) is divided into 14 equal parts, resulting 15 examination points (IM). Consequently, each segment length (Δx) is measured as 1027 meters. The time increment rate is taken as $\Delta t = \Delta x/10$. Horizontal mass dispersity is taken R=80 (m^2/s) (Shaba et. al., 2011). $\zeta_{(t, 1)} = \zeta_{(t, 2)}$ and $\zeta_{(t, IM+1)} = \zeta_{(t, IM+2)}$ are determined as the boundary conditions for water surface change. The remaining parameters are taken from (Koutitas, 1988).

Table 3. *The values of the variables used in the model (Koutitas, 1988; Taşdemir et. al., 2009; Shaba et. al., 2011).*

L **(m)**	H_0 **(m)**	***K*** **(m/s)**	***R*** **(m^2/s)**	α	***IM***
14380.00	3,67	0.001	80	0.0007	15
$S_{2, max}$ **(‰)**	$S_{4, max}$ **(‰)**	ρ_2 **(kg/m^3)**	ρ_4 **(kg/m^3)**	Δx **(m)**	Δt **(s)**
1.76	36.3	1000.0	1021.0	1000	100

The finite difference equation allows the examination of different salinity levels (*S*) at various time intervals by increasing the number of time steps (*NM*). Additionally, it provides the opportunity to analyse the velocity at examination points (*U*) and water surface fluctuations (ζ) at different points in time, according to the number of time steps chosen.

Results

The computer-aided analysis of finite difference equations has yielded three distinct findings. The first pertains to the temporal variations in water flow velocities at middle points M (Figure 6a).

and then focuses on the temporal evolution of water surface levels at control points 4 (Figure 6b). The findings concern the temporal changes in salinity ratios and density along the riverbed (Figure 7a, 7b). Finally, contour diagrams of changes in velocity, water surface, salinity and density are given in Figure 8 and 9.

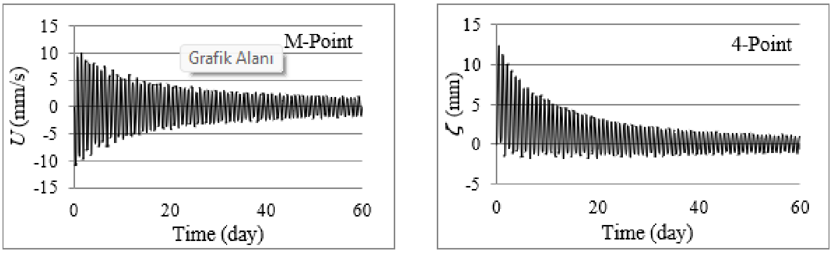

a) Velocity changes in the middle of the river.

b) Surface changes in the boundary of the river.

Figure 6. *Variation of velocity and surface over time at selected points during the analysis.*

According to assumptions, the results of the numerical analyses indicate that the velocity and surface oscillation amplitudes are stabilized within a certain range of progress (Figure 6). The decrease of the amplitude of the velocity also affects the decrease in the spread of salinity.

As shown in Figure 7, at the inception of the temporal axis (0 km, upstream direction of the river), the salinity level converges at zero. Conversely, the sea salinity reaches about 36,3% at approximately 14.38 kilometers downstream. Salinity reached the level of 12‰ within the initial three days and calculated as 23‰ by the 10th day of the analysis. Freshwater salinizes completely by 60th day as seen in Figure 7 The changes in velocity, water surface, salinity and density values over position and time are presented in Figure 8 and 9. These variations of the calculated values are displayed in contour diagrams to enhance comprehensibility.

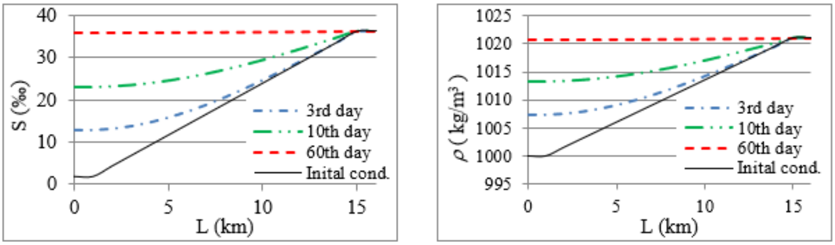

a) Salinity variation.

b) Density variation.

Figure 7*. The changes in salinity and density along the channel throughout the analysis.*

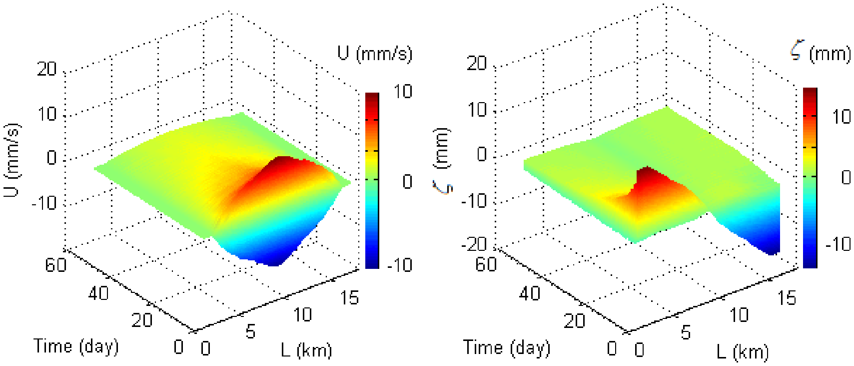

a) Velocity variation

b) Surface variation

Figure 8. *Contour diagrams of changes in velocity and water surface over time during the analysis.*

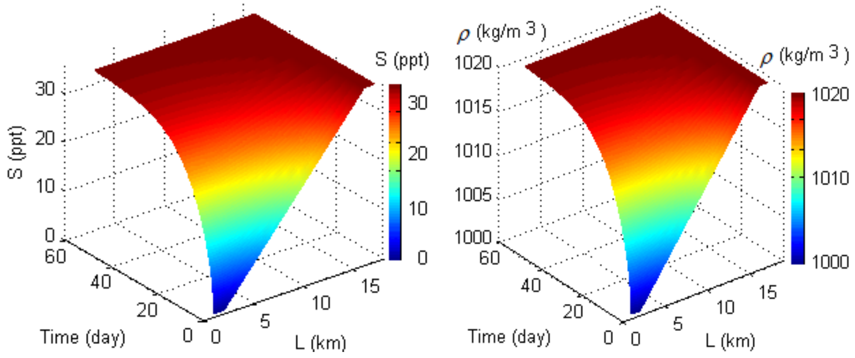

a) Salinity variation b) Density variation

***Figure* 9**. *Contour diagrams of changes in salinity and density over time during the analysis.*

Conclusion

In summation, this study has undertaken a comprehensive investigation into the interaction between river and seawater, yielding a mathematical model that elucidates the salinity fluctuations along the riverbed. Furthermore, meticulous calculations have been performed to delineate water surface fluctuations and flow velocities.

The outcomes have revealed that in rivers characterized by low flow velocities, there is a discernible, time-evolving increase in salinity towards the upstream direction along the riverbed, originating from the point of freshwater discharge into the sea. Notably, this transition exhibits a gradual nature.

In mitigating the inland progression of salinity via river conveyance, it is advisable to contemplate the construction of barriers at the junctures where freshwater is introduced into the sea, particularly in rivers with sluggish flow rates.

As avenues for future inquiry, mathematical models may be employed to investigate the extent of salinity influence in rivers for various flow velocities and to calculate salinity ratios. Additionally, an exploration of the basin-level impacts of reduced river flow velocities during periods of drought on salinity progression is recommended.

References

Ajansı, B. K. (2023). *Batı Karadeniz Turizm Master Planı*. https://batikaradeniz.gov.tr/?p=3105 adresinden alındı

Ajansı, D. H. (2023). *Melet Irmağı'nın Karadeniz'e döküldüğü yere yat limanı inşa edilecek*. Retrieved from https://www.denizhaber.net/melet-irmaginin-karadenize-dokuldugu-yere-yat-limani-insa-edilecek-haber-105481.htm

ARSLAN, H., CEMEK, B., DEMİR, Y., & YILDIRIM, D. (2011). Deniz Suyu Girişiminin Belirlenmesinde Çevresel İzotopların Kullanılması. *Reserach Journal of Agricultural Sciences*.

Berger, E., Frör, O., & Schäfer, R. B. (2019). Salinity impacts on river ecosystem processes: a critical mini-review. *Philosophical Transactions of the Royal Society B*, 374.

Chen, Y., Xiao, C., Zhang, Y., & Lai, Z. (2023). The Mixed Layer Salinity Budget in the Northern South China Sea: A Modeling Study. *Journal of Marine Science and Engineering*, 1693.

ÇETİN, H. C., HARMANCIOĞLU, N., SARIYILDIZ, A., & SİLAY, A. E. (2009). GEDİZ NEHRİ SU KALİTESİ PARAMETRELERİNİN EĞİLİM ANALİZİ. (pp. 603-611). İzmir: TMMOB İzmir Kent Sempozyumu.

Google Earth. (2023). Retrieved from https://earth.google.com/web/search/gediz/@38.60323145,27.57148985,35.66447486a,232540.14683094d,35y,0h,0t,0r/data=CnAaRhJACiUweDE0YjlhMjFjZTJkNDgxZmI6MHhmNzdkMjkxNDVhMmY3MDVjGapeI-5WTkNAIWeyf54GkjtAKgVnZWRpehgCIAEiJgokCUkl1Ii0fENAEV4ODmvisEJAGZ3WIStVlTxA

Han, W., & Jr, J. P. (2001). Modeling salinity distributions in the Indian Ocean. *Journal of Geophysical Research*, 859-877.

Hutchison, D. (2018, October 24). *Quora*. Retrieved from https://www.quora.com/Why-has-the-salty-nature-of-sea-water-not-lessened-even-though-so-many-rivers-flow-into-the-ocean

Kaymakamlığı, T. K. (2023). *Yenimahalle (Sakarya Nehri Ağzı) - Sakarya*. Retrieved from http://www.karasu.gov.tr/yeni-mahalle1

Koutitas, C. G. (1988). Mathematical Models in Coastal Engineering. Pentech.

Lehmann, A., Krauss, W., & Hinrichsen, H. (2002). Effects of remote and local atmospheric forcing on circulation and upwelling in the Baltic Sea. *Dynamic Meteorology and Oceanography*, 299-316.

Li, H., Reed, C. W., & Brown, M. E. (2012). Salinity calculations in the coastal modeling system. *Technical note (Coastal and Hydraulics Engineering (U.S.)) ; IV-80.*

Matsoukis, C., Amoudry, L. O., Bricheno, L., & Leonardi, N. (2021). Investigation of Spatial and Temporal Salinity Distribution in a River Dominated Delta through Idealized Numerical Modelling. *Estuaries and Coasts*, 1-26.

NSW. (2003). Working together to protect river quality and sustain economic development. Sydney: AL.

Nyadjro, E. S., Foli, B. A., Agyekum, K. A., Wiafe, G., & Tsei, S. (2022). Seasonal Variability of Sea Surface Salinity in the NW Gulf of Guinea. *Remote Sensing in Earth Systems Sciences*, 83-94.

Qiao, H., Zhang, M., Jiang, H., Xu, T., & Zhang, H. (2018). Numerical study of hydrodynamic and salinity transport processes in the Pink Beach wetlands of the Liao River estuary, China. *Ocean Science*, 437-451.

Shaha, D. C., Cho, Y.-K., Kwak, M.-T., Kundu, S. R., & Jung, K. T. (2011). Spatial variation of the longitudinal dispersion coefficient in an estuary. *Hydrology and Earth System Sciences*, HESS, 15, 3679–3688, 2011.

SOMAY, M., GEMİCİ, Ü., AKAR, T., & TARCAN, G. (2015). Ildırı (Çeşme-İzmir) Karstik Kaynaklarının Duraylı İzotop Özellikleri. *4. ULUSAL HİDROLOJİDE İZOTOP TEKNİKLERİ SEMPOZYUMU* (s. 351:363). İstanbul: ORMAN VE SU İŞLERİ BAKANLIĞI DEVLET SU İŞLERİ GENEL MÜDÜRLÜĞÜ.

TAŞDEMİR, A., USTAOĞLU, M. R., & BALIK, S. (2009). Gediz Deltası (Menemen-İzmir) chironomidae (Diptera) faunası'na katkılar. *Journal of FisheriesSciences.com*.

Wang, A., Z. W., Liu, J., Xu, N., & Li, H. (2021). The Sr/Ba ratio response to salinity in clastic sediments of the Yangtze River. *Chemical Geology*, 559.

West, J., & Williams, D. (2015). An Evaluation of Mixing in the Tay Estuary. *Coastal Engineering*.

Wonder. (2023). *Gediz Deltası*. https://pin.it/6gJWIS2 adresinden alındı

CHAPTER III

Development of Empirical Equations to Predict the Strength Properties of Rocks with Non-Destructive Test Techniques

Mehmet Can BALCI[1]
İsmail İNCE[2]
Ali BOZDAĞ[3]

Introduction

For determination of uniaxial compression strength (UCS), the main input parameter for engineering projects and rock mechanics studies, standard methods recommended by different institutions and organizations (ISRM, ASTM, EN, etc.) are used. In situations where it is not possible to take samples with the dimensions and features

---

[1] Assistant Professor, Batman University, Faculty of Engineering and Architecture, Department of Civil Engineering, Batman, Turkey

[2] Associate Professor, Konya Technical University, Faculty of Engineering and Natural Sciences, Department of Geological Engineering, Konya, Turkey

[3] Associate Professor, Konya Technical University, Faculty of Engineering and Natural Sciences, Department of Geological Engineering, Konya, Turkey

stated in the standards, the indirect method commonly used to determine UCS is the point load test (PLT). This method provides the advantage of being able to be used in the field (on site) and in the laboratory, but has an important disadvantage considering the difficulties in preparing samples suitable for the standards. This situation has led researchers to perform studies related to prediction of strength parameters (Tugrul and Zarif 1999; Palchik 1999; Kahraman 2001, 2014; Kahraman et al 2005, 2016; Tsiambaos and Sabatakaki 2004; Yasar and Erdoğan 2004; Zorlu et al 2008; Yagiz 2011; Heidari et al 2018; Matin et al 2018; Çelik 2019). In these studies, simple and multiple regression analyses are used for strength parameters based on one or more rock group index and strength properties (Table 1).

Table 1. Parameters Used in Simple and Multiple Regression Equations Developed by Some Researchers to Predict Strength Values

Rock type	Variables	References
Granite	n	Tugrul and Zarif 1999
Sandstone	n	Palchick 1999
Dolomite, sandstone, limestone, marl, tuff	ISI	Kahraman 2001
Limestone, sandstone, marl	PLT	Tsiambaos and Sabatakaki 2004
Dolomite, marble, limestone	Vp	Yasar and Erdoğan 2004
Pyroclastic rock	TS	Kahraman et al 2005
sandstone	GS, PQ, TPC	Zorlu et al 2008
Limestone, sandstone, marble	SD	Yagiz 2011
Sedimanter kayaçlar	BPI, PLT, Vp, SHR	Heidari et al 2018
travertine	PLT, Vp	Matin et al 2018
Marble, dolomite, limestone, travertine	SHR, Vp, UW	Çelik 2019
Pyroclastic rock	PLT	Kahraman 2014
Basalt, limestone	SD	Kahraman et al 2016

BPI: Block Punch Index, GS: Grain size, ISI: Impact strength index, n: Porosity, PLT: Point load strength, PQ: Percent quartz, SD: Slake durability index, SHR: Schmidt hammer rebound, TPC: Total percent cement, TS: Tensile strenght, UW: Unit weight, Vp: P-wave velocity

As seen in Table 1, strength properties and values were predicted using petrography (grain size, percent quartz, total percent cement), index (porosity, unit weight, P-wave velocity), strength (impact strength index, point load strength, tensile strength, block punch index, Schmidt hammer rebound) and abrasion (slake durability index) properties of rocks. As stated in previous studies, strength values were researched using different rock properties and non-destructive test (NDT) values (Schmidt hammer rebound, P-wave velocity). In this study, the aim was to detect strength parameters (UCS and PLT) using practical and cheap non-destructive test techniques that can be used both in the field and in the laboratory. With this aim, strength values of magmatic rocks were predicted with simple regression using two different surface hardness methods with different application energies and P-wave velocity.

Material and Method

In the experimental stage of this study, 25 magmatic rock samples (igneous, volcanic and pyroclastic) were collected from quarries operating in different regions of Anatolia. Homogeneous rock blocks from the quarries with 20 × 30 × 30 cm were used to prepare NX-diameter (54 mm) core samples for use in the experimental stage. The locations and rock types for the samples are given in Table 2.

Table 2. Location and Lithology of Samples Used in The Study

Sample No.	Location	Rock lithology	Sample No.	Location	Rock lithology
1	Antalya	Diabase	13	Gölbaşı-2/Ankara	Andesite
2	Yaylak/Aksaray	Granite	14	Sivrihisar-1/Eskişehir	Andesite
3	Kaman-1/Kırşehir	Granite	15	Sivrihisar-2/Eskişehir	Andesite
4	Ortaköy/Aksaray	Granite	16	Hisar /Konya	Andesite
5	Kaman-2/Kırşehir	Granite	17	Aksaray	Pyroclastic
6	Kayseri	Andesite	18	Karayazı-1/Nevşehir	Pyroclastic
7	İscehisar-1/Afyonkarahisar	Andesite	19	Başakpınar/Kayseri,	Pyroclastic
8	İscehisar-2/Afyonkarahisar	Andesite	20	Karayazı-2/Nevşehir	Pyroclastic
9	Kulu/Konya	Andesite	21	Karayazı-3/Nevşehir	Pyroclastic
10	Sincan/Ankara	Andesite	22	Başakpınar/Kayseri,	Pyroclastic
11	Çayırlı/Ankara	Andesite	23	Karayazı-4/Nevşehir	Pyroclastic
12	Gölbaşı-1/Ankara	Andesite	24	Kızılören/Konya	Pyroclastic

The UCS and PLT values, among strength values, for the samples were determined according to the ASTM D7012 (2014) and ASTM D5731 (2008) standards, respectively. Samples prepared for the experiments had the NDT of P-wave velocity (Vp), Schimdt hammer rebound (SHR) and Leeb hardness (HL) tests performed. Determination of the P-wave velocity of samples met the standards stated in ASTM E494 (2010). For each rock, P-wave velocity (Vp) measurement was repeated three times and the average of these measurements was taken as P-wave velocity. The SHR value for samples was determined using an L-type hammer according to the method recommended in ASTM D5873 (2014). When determining the SHR value for each sample, 10 measurements were performed at different points on the rock sample. Firstly, the average of these measurements was taken and the values deviating more than seven units from the average were removed. Later the average of the remaining values was taken and the SHR value was calculated.

Though the HL test has a universal standard for metals, there is still no standard for rocks for this test. However, some researchers stated that the length to diameter (L/D) ratio for Leeb hardness measurements in core samples should be ≥1.5 (Ghorbani et al, 2023; Çelik et al, 2023). In this study, the L/D ratio was noted in Leeb hardness measurements. For Leeb hardness measurements, an Insize ISH-PHB brand device and D-probe were used. The test was performed perpendicular to the base and top surfaces of the core samples. Measurements were performed at 20 different points evenly distributed on the surface of the samples and the HL value was defined as the arithmetic mean of these values.

Results and Discussion

Some Indexes-Strength Properties of Stones

While the P-wave velocity, SHR and HL values were determined with non-destructive tests, the strength properties of the rocks used in the study were identified with UCS and PLT values (Table 3). For the surface hardness tests of the rocks, the SHR values varied from 16.70-64.20, while the HL values varied from 195.10 to 892.30 over a broad interval. The highest Vp value for the rocks was 5.30 km/s, with lowest Vp value of 2.04 km/s. The PLT values for the samples varied from 11.22 MPa to 1.04 MPa. According to the PLT classification in ASTM D5731 (2008), sample number 1 was in the extremely high category, samples 2-16, 18, 21 and 24 were in the very high category and samples 17, 19, 20, 22 and 23 were in the high category. The UCS values for samples used in the study varied from 6.87 MPa to 144.10 MPa

Table 3. Index Properties of Rocks Used in The Study

Rock Properties	Minimum	Maximum	Mean	Std. Deviation
Vp- km/s	2.04	5.30	3.70	0.97
SHR	16.70	64.20	37.44	11.62
HL	195.10	892.30	601.05	242.54
PLT-MPa	1.04	11.22	5.49	2.76
UCS-MPa	6.87	144.10	65.07	42.49

Prediction of Strength Properties of Rocks

For determination of the strength properties (UCS and PLT) of rocks in the study, the non-destructive tests of P-wave velocity and surface hardness tests of HL and SHR were used. Correlations between the values obtained from non-destructive tests with strength values of rock samples were investigated with simple regression analyses (linear, exponent, exponential, logarithmic and polynomial). To assess the suitability of the developed equations, reliability at 5% significance level ($\alpha=0.05$) and p values less than 0.05 were noted. To identify the equations that met these criteria and were most significant among the developed equations, the equation with highest correlation coefficient (R^2) was chosen. The developed equations are given in Table 4. The correlations between strength values of rock samples and non-destructive test properties are presented in Figure 1.

With the increase in surface hardness values of rocks (HL and SHR), the UCS values were identified to increase (Figure 1.a-b). The R^2 values between UCS with SHR and HL were 0.809 and 0.843, respectively. The correlation between Vp and UCS values of rocks was polynomial with R^2 value of 0.826 (Figure 1.c).

Between the SHR values and PLT values of rocks, there was a polynomial relationship with R^2 value of 0.674 (Figure 4.d). There was an exponential relationship between the HL values and PLT values of rocks with R^2 of 0.744. Between P-wave velocity and PLT values, there was an exponential relationship with R^2 value of 0.854

(Figure 4.f). For magmatic rock samples, as the PLT value increased, the NDT (Vp, SHR and HL) values increased (Figure 4.d-f).

Table 4. Equations Developed for Prediction of Strength Parameters

Strength parameter	Equation No.	Developed equation	R^2
UCS	1	UCS=3.291SHR-58.137	0.809
	2	$UCS=5.4686e^{0.003HL}$	0.843
	3	$UCS=6.0446Vp^2-3.486Vp-10.437$	0.826
PLT	4	$PLT=0.0036SHR^2+0.4817SHR-7.0074$	0.674
	5	$PLT=0.0038HL^{1.1324}$	0.744
	6	$PLT=0.309Vp^{2.1297}$	0.854

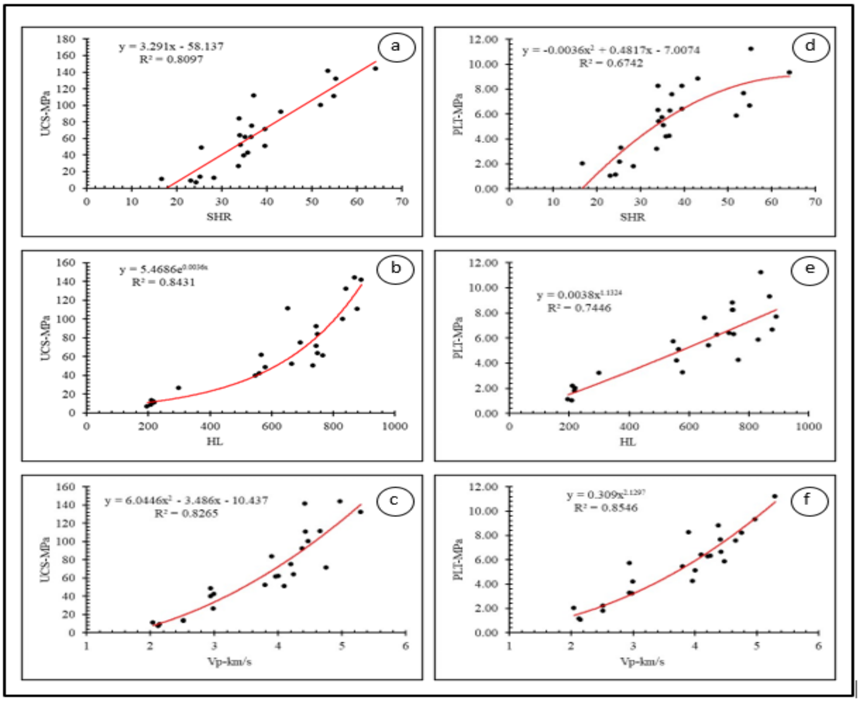

Figure 1. Correlations Between Strength Values and NDT Values a) UCS and SHR, b) UCS and HL, c) UCS and Vp, d) PLT and SHR, e) PLT and HL, f) PLT and Vp

Additionally, the fit of the developed equations was checked with variance investigations and results are given in Table 5. The statistical models were concluded to be able to be used reliably for prediction of UCS and PLT features of magmatic rocks.

Table 5. The Analysis of Variance of Regression Model for Strength

Equation No.	F	p
1	93.617	0.000
2	268.389	0.000
3	49.957	0.000
4	21.729	0.000
5	128.865	0.000
6	148.162	0.000

Conclusion

Using the values obtained from non-destructive test techniques for rocks, the following results related to prediction of strength features (UCS and PLT) are presented.

- As the strength values for rocks (UCS and PLT) increased, the chosen NDT values (Vp, SHR and HL) were observed to increase.

- The correlation coefficients between the Vp value with UCS and PLT were 0.826 and 0.854, respectively.

- Among the surface hardness test methods, high correlations were identified between SHR (R^2: 0.809) and HL (R^2: 0.843) with UCS. A similar relationship was found for PLT with surface hardness values.

For engineers, NDT methods are simple, rapid, economic and repeatable methods. These methods are thought to provide positive contribution in terms of time-consuming studies, in addition to practical prediction of engineering features of rocks. Additionally, in engineering and rock mechanics studies, the use of these empirical equations, developed and presented in this study, was revealed by analyses of their usability to practically predict strength values of magmatic rocks. The results obtained from this study are only valid for the rock samples used here. For these types of empirical equations to reach universal levels, it is recommended to support the hypothesis of the study with experiments involving rock samples with physical features varying over a broad interval, different genesis and higher numbers of samples.

REFERENCES

ASTM D5731. (2008). Standard Test Method for Determination of the Point Load Strength Index of Rock and Application to Rock Strength Classifications, American Society for Testing and Materials, West Conshohocken

ASTM E494. (2010). Standard Practice for Measuring Ultrasonic Velocity in Materials. ASTM International, West Conshohocken

ASTM D5873. (2014). Standard test method for determination of rock hardness by rebound Hammer method. Annual book of ASTM standards. American Society for Testing and Materials, West Conshohocken, pp 1–6

ASTM D7012. (2014). Standard Test Methods for Compressive Strength and Elastic Moduli of Intact Rock Core Specimens under Varying States of Stress and Temperatures, American Society for Testing and Materials, West Conshohocken

Çelik, S. B. (2019). Prediction of uniaxial compressive strength of carbonate rocks from nondestructive tests using multivariate regression and LS-SVM methods. *Arabian Journal of Geosciences*, *12*(6), 193.

Çelik, S. B., Çobanoğlu, İ., Koralay, T., & Gireson, K. (2023). Investigation of the Leeb hardness test in rapid characterisation of rock cores with particular emphasis on the effect of length to diameter ratio. *International Journal of Mining, Reclamation and Environment*, 1-20.

Ghorbani, S., Hoseinie, S. H., Ghasemi, E., & Sherizadeh, T. (2023). Adoption of ASTM A956-06 Leeb hardness testing standard to rock engineering applications. *Construction and Building Materials*, *364*, 129886.

Heidari, M., Mohseni, H., & Jalali, S. H. (2018). Prediction of uniaxial compressive strength of some sedimentary rocks by fuzzy and regression models. *Geotechnical and Geological Engineering*, *36*, 401-412.

Kahraman, S. (2001). Evaluation of simple methods for assessing the uniaxial compressive strength of rock. *International Journal of Rock Mechanics and Mining Sciences*, *38*(7), 981-994.

Kahraman, S., Gunaydin, O., & Fener, M. (2005). The effect of porosity on the relation between uniaxial compressive strength and point load index. *International Journal of Rock Mechanics and Mining Sciences*, *42*(4), 584-589.

Kahraman, S. (2014). The determination of uniaxial compressive strength from point load strength for pyroclastic rocks. *Engineering Geology*, *170*, 33-42.

Kahraman, S., Fener, M., & Gunaydin, O. (2017). Estimating the uniaxial compressive strength of pyroclastic rocks from the slake durability index. *Bulletin of Engineering Geology and the Environment*, *76*, 1107-1115.

Matin, S. S., Farahzadi, L., Makaremi, S., Chelgani, S. C., & Sattari, G. H. (2018). Variable selection and prediction of uniaxial compressive strength and modulus of elasticity by random forest. *Applied Soft Computing*, *70*, 980-987.

Palchik, V. (1999). Influence of porosity and elastic modulus on uniaxial compressive strength in soft brittle porous sandstones. *Rock Mechanics and Rock Engineering*, *32*(4), 303-309.

Tsiambaos, G., & Sabatakakis, N. (2004). Considerations on strength of intact sedimentary rocks. *Engineering Geology*, *72*(3-4), 261-273.

Tuğrul, A., & Zarif, I. H. (1999). Correlation of mineralogical and textural characteristics with engineering properties of selected granitic rocks from Turkey. *Engineering geology*, *51*(4), 303-317.

Yagiz, S. (2011). Correlation between slake durability and rock properties for some carbonate rocks. *Bulletin of Engineering Geology and the Environment*, *70*, 377-383.

Yasar, E., & Erdogan, Y. (2004). Correlating sound velocity with the density, compressive strength and Young's modulus of carbonate rocks. *International Journal of Rock Mechanics and Mining Sciences*, *41*(5), 871-875.

Zorlu, K., Gokceoglu, C., Ocakoglu, F., Nefeslioglu, H. A., & Acikalin, S. J. E. G. (2008). Prediction of uniaxial compressive strength of sandstones using petrography-based models. *Engineering Geology*, *96*(3-4), 141-158.

CHAPTER IV

Evaluation of Oak and Pine Wood Ashes in Gypsum-Based Mixtures

Serdar Aydoğan[1]
Ahmet Hayrullah Sevinç [2]
Yusuf Uras [3]

1. Introduction

Wood and plant-derived biomass fuels are widely used around the world as an alternative to fossil fuels. Energy obtained from biomass is considered carbon-free because the total carbon dioxide (CO_2) released during its combustion is equal to the total amount of

---

[1] Student, Kahramanmaras Sütçü İmam University, Graduate School of Natural and Applied Sciences, Department of Geological Engineering, ORCID: 0000-0002-5552-9249

[2] Assoc. Prof., Kahramanmaraş İstiklal University, Elbistan Vocational School of Higher Education, Construction Program,
ORCID: 0000-0003-3338-8366

[3] Prof.Dr., Kahramanmaras Sütçü İmam University, Department of Geological Engineering, ORCID: 0000-0001-5561-3275

CO_2 absorbed during the biomass growth. This makes biomass a sustainable source of energy with zero net CO_2 emissions (Munawar et al., 2021). In response to the global warming crisis, there has been a growing demand for bioenergy as an alternative to energy derived from fossil fuels. This has led to extensive research being conducted worldwide to develop the use of biomass fuel for energy conversion, which has many advantages over fossil fuels (Vassilev et al., 2013a). If a complete transition from fossil fuels to biomass-fueled energy production is achieved, CO2 emissions could be reduced by up to 95% (Wang et al., 2012). In addition, biomass is readily available and has a large reserve, making it an attractive option for sustainable energy production (Munawar et al., 2021). It is estimated that the world's biomass reserves are approximately 110 to 220 billion tons per year and the annual amount of forest residues to be used in energy production is approximately 3 billion tons (Heinimö & Junginger, 2009; Vassilev et al., 2013; Williams et al., 2012). The contribution of biomass fuels to energy production in the world is around 8% to 15%. It is thought that the contribution of these fuels will be between 33-50% in 2050 (Andrea Jordan & Akay, 2012; Vassilev et al., 2013; Williams et al., 2012). The amount of ash formed in these fuels is approximately 480 million tons per year (Munawar et al., 2021). Currently, ash is often stored in landfills or randomly thrown into the environment, causing serious harmful effects on the aesthetics of the region as well as on the environment as the largest source of inert pollution (Munawar et al., 2021; Voshell et al., 2018).

Sakhare and Ralegaonkar (2016) investigated the use of biomass ash in cement-based bricks in their study. This ash replaced sand at a rate of 5-55%. Mechanical, physical, durability, and thermal tests were applied to the produced samples. As a result of the study, it was stated that ash-added cement-based bricks have better mechanical and thermal properties and are more economical products (Sakhare & Ralegaonkar, 2016). At the same time, cement mortars are produced by substituting part of the cement with woody biomass ash (Rajamma et al., 2015), in some studies, cement mortars have been produced by using woody biomass ash totally or partially instead of aggregate (da Costa et al., 2019; Ukrainczyk et al., 2016). In different studies, the use of this ash in ground stabilization, subgrade base material, bitumen coating additive, and mineral filler material has been examined (da Costa et al., 2020; Melotti et al., 2013; Pasandín et al., 2016; Yoshitake et al., 2016).

Gypsum plaster is a commonly used construction material that has been used for centuries to build historical buildings, temples, and monuments. (Durgun, 2020). In recent times, the use of plaster as a building material has increased because it is environmentally friendly and has good thermal and acoustic properties (Durgun, 2021). Unlike cement, gypsum does not shrink at normal temperatures, making it a versatile material that can be used for many applications just by mixing it with water (Karni & Karni~, 1995). Furthermore, the hemihydrate gypsum binder is produced at a lower temperature than other binders such as cement or air lime, which makes gypsum plasters a sustainable solution with low energy consumption (Ranesi et al., 2022).

The economic efficiency of construction products can be increased by adding waste and replacing raw materials (Farinha et al., 2019; Santos et al., 2021). Among the various types of waste, researchers have found that agro-industrial waste can be utilized to create economical construction products. This can help improve the physical and chemical properties of these products, such as their density and thermal conductivity behavior. In addition, this approach can also create useful applications for various biomass, as mentioned in a recent study by Ranesi et al. (2022).

In this study, the usability of ashes obtained from the burning of oak and pine wood used as fuel in bakery ovens in gypsum-based composites was investigated. Oak and pine ash were sieved with a 0.25 mm square mesh sieve and replaced with gypsum at the rates of 10, 20 and 30% by weight. Physical and mechanical tests such as unit volume weight, water absorption, apparent porosity, capillary water absorption, ultrasonic pulse velocity, thermal conductivity coefficient, compressive strength, and bending strength were applied to the produced samples.

2. Materials and Methods

The plaster provided in this study complies with TS EN 13297-1 standard, and its density is 0.71 g/cm^3. Oak and pine ashes were obtained from pita bakeries in the Kahramanmaraş region. These ashes were sieved with a 0.25 mm mesh sieve. The sieved state of the ashes and the residue on the sieve are given in Figure 1.

Figure 1. Ashes used in the study

7 different plaster mixtures were obtained by substituting 10%, 20%, and 30% pine and oak ashes by weight instead of plaster. The plaster mixtures were prepared with a water/dry material ratio of 0.55, and additional water was added to achieve the same consistency as the reference. The mixture design of these mixtures is given in Table 1.

Table 1. Mixture design of plaster composites (in g)

Sample	**Gypsum**	**Water**	**Oak Ash**	**Pine Ash**	**Extra Water**	**Water/Dry material ratio**
R	1200	660	-	-	0	0.55
O10	1080	594	120	120	60	0.55
O20	960	528	240	240	120	0.54
O30	840	462	360	360	180	0.54
P10	1080	594	-	-	80	0.56
P20	960	528	-	-	140	0.56
P30	840	462	-	-	220	0.57

During the production process of the mixtures, ash, and gypsum were first mixed dry to ensure they were evenly distributed. Then, water was added and mixed in. The fresh mixture was then placed in molds of size 4*4*16 cm and 12*12*2 cm. The products were exposed to short-term vibration. After 24 hours, the samples were taken out of the mold and kept in an environment with 65% humidity and a temperature of 22±2 ^{o}C for 1 week. Before beginning the experiment, the samples were dried in an oven at 65 ^{o}C for 24 hours. The experiments were carried out according to the standards in Table 2, and pictures of the experimental studies are shown in Figure 2.

Table 2. Tests performed and the standards

Tests	Standard
Thermal conductivity	ASTM C 1113
Compressive strength	TS EN 196-1
Bending strength	TS EN 196-1
Unit weight	ASTC C 138
Thermal conductivity	ASTM C 1113
Capillary water absorption	TS EN 480-5
Water absorption	ASTM C 20
Ultrasonic pulse velocity (UPV)	ASTM C 597
Apparent porosity	ASTM C 20

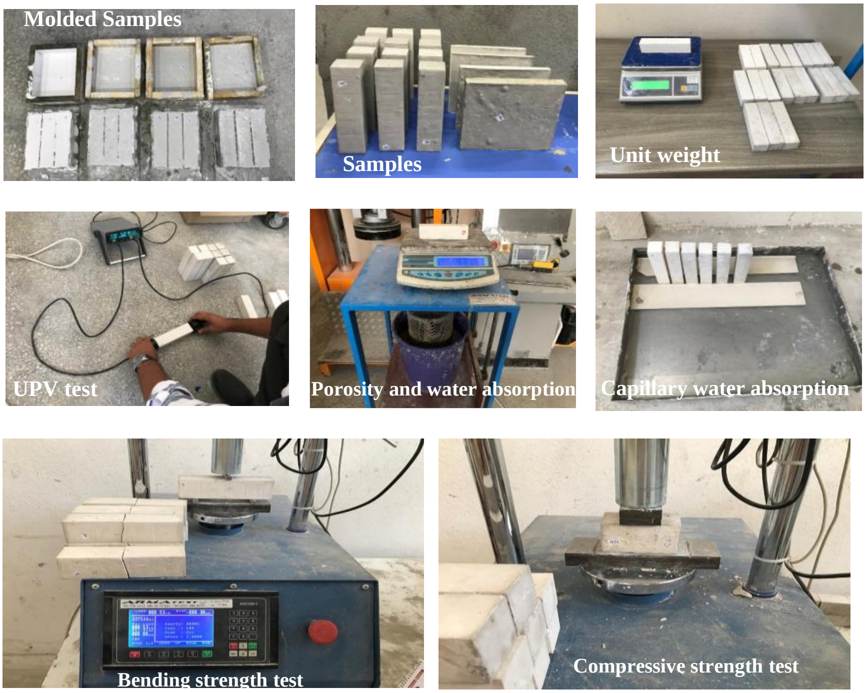

Figure 2. Photos of experimental procedure

3. Results and Discussion

The unit weights of plaster composite samples are provided in Figure 3.

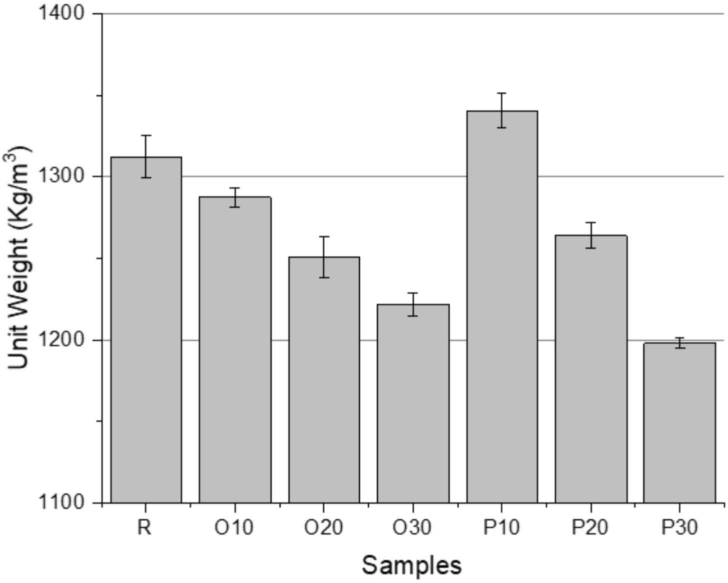

Figure 3. Unit weight values of plaster composite samples

Upon examining the unit weights of the samples, it was observed that they varied between 1197.9 and 1340.5 kg/m3. The P10 sample had the highest value, while the P30 sample had the lowest. As the additive ratio increased, the unit volume weight value generally decreased. Compared to the reference sample, the samples O10, O20, O30, P20, and P30 were lighter by 1.9%, 4.7%, 6.9%, 3.7%, and 8.7%, respectively. The P10 sample was 2% heavier. To minimize the dead weight of a structure, it is essential to decrease the weight of its elements. This reduction leads to smaller cross-sections of the elements and can also enhance their thermal insulation properties (Durgun, 2020).

The ultrasonic velocities values of plaster composite samples are provided in Figure 4.

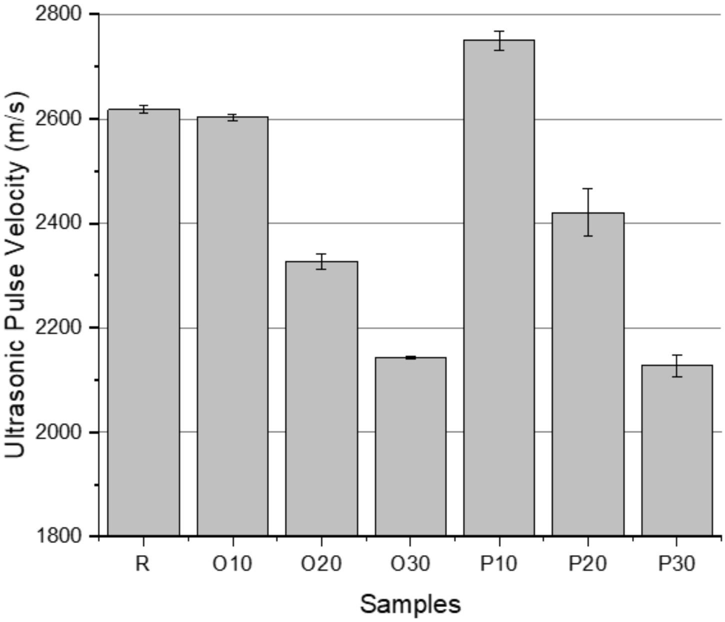

Figure 4. Ultrasonic velocity pulse values of plaster composite samples

After analyzing the sound speeds of the samples, it was found that the values ranged between 2128 and 2750 m/s. Sample P10 exhibited the highest speed value, while sample P30 had the lowest. As the additive ratio increased, sound speeds generally decreased. Compared to the reference sample, samples O10, O20, O30, P20, and P30 showed a decrease of 0.6%, 11.1%, 18.1%, 7.5%, and 18.7%, respectively in sound velocity value. 5% increase in sound velocity was observed in the P10 sample. It is well-known that the ultrasonic pulse velocity results are highly dependent on the pore structure of the material. As the number of pores or cracks in the matrix increases, the ultrasonic pulse velocity results decrease (Benaicha et al., 2015).

The thermal conductivity coefficients of plaster composite samples are provided in Figure 5.

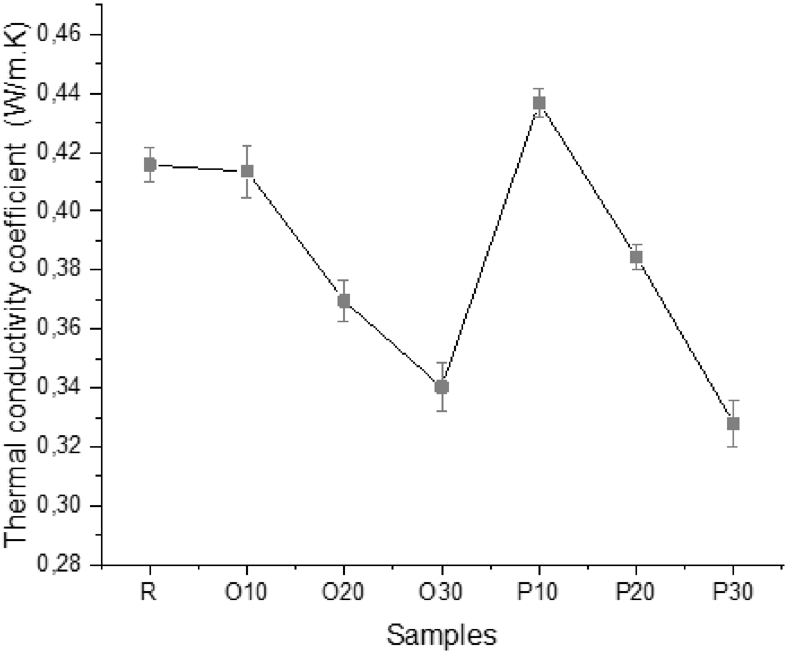

Figure 5. Thermal conductivity coefficients of plaster composite samples

The thermal conductivity coefficients vary between 0.328 and 0.437 W/mK. While the P10 sample gave the highest thermal conductivity coefficient value, the P30 sample gave the lowest value. 21.2% lower thermal conductivity coefficient value was obtained for the P30 sample compared to the reference sample. It showed a similar trend between UPV values and thermal conductivity coefficient value.

The capillary water absorptions of plaster composite samples are provided in Figure 6.

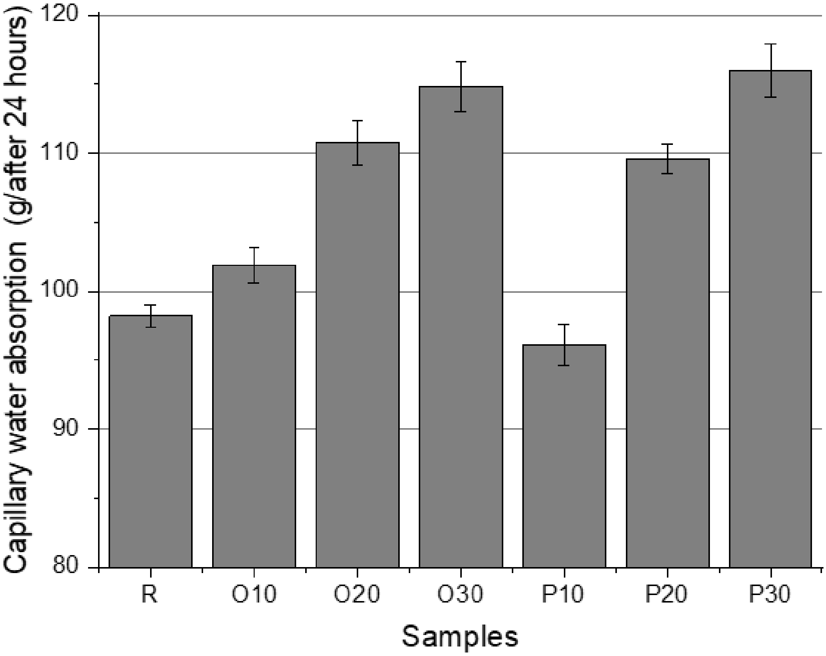

Figure 6. Capillary water absorptions of plaster composite samples

It is seen that the amount of water absorbed by capillary route after 24 hours varies between 96 - 116 g/day. While the highest water absorption amount was observed in the P30 sample, the least water absorption was observed in the P10 sample. These results show the same trend as UPV, unit weight, thermal conductivity coefficient experiments. Compared to the reference sample, O10, O20, O30, P20 and P30 samples absorbed 3.8%, 12.8%, 16.9%, 11.6% and 18.13% more water capillary. The P10 sample absorbed 2.1% less water. It can also be concluded that the use of oak and pine ash affects the micropore structure as well as macropores.

The water absorptions and apparent porosity values of plaster composite samples are provided in Figure 7.

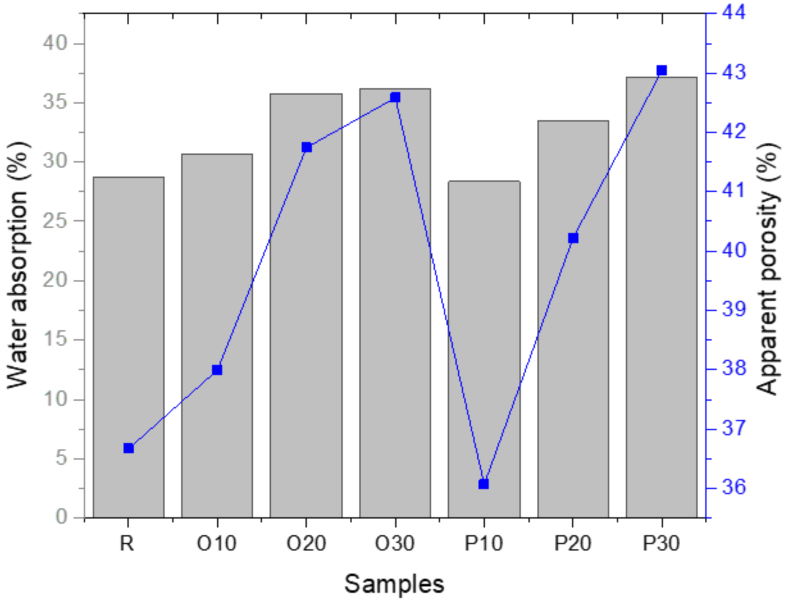

Figure 7. Water absorptions and apparent porosity values of plaster composite samples

Water absorption and apparent porosity of materials are related to their void structure. The size and interconnection of gaps within a material can affect both properties. Ultrasonic Pulse Velocity test can provide information about the cavity structure of a material before conducting experiments. The water absorption and porosity values of the tested samples varied between 28.37% - 37.12% and 36.07% - 43.05% respectively. In general, the results of both experiments were found to be consistent with each other. The P30 sample had the highest values while the P10 sample had the lowest. Both test results showed that the porosity of the samples increased as the amount of additive increased.

The bending and compressive strength values of plaster composite samples are provided in Figure 8.

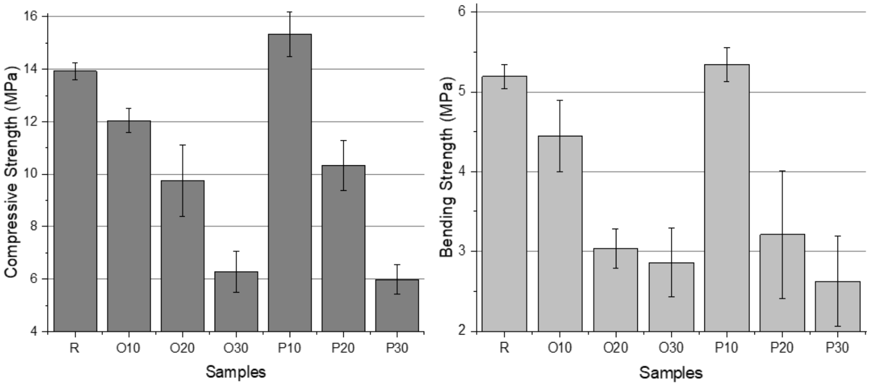

Figure 8. The bending and compressive strength values of plaster composite samples

It was observed that the compressive and bending strengths of the samples varied between 5.99 - 15.34 MPa and 2.63 - 5.34 MPa, respectively. Based on the Turkish TS EN 13729 - 1 standard, which is in line with the European standard for structural gypsum plasters, it is required that the minimum compressive strength of the plaster should be between 2 and 6 MPa. Additionally, after 7 days, the minimum bending strength of fiber-reinforced structural gypsum plaster should be at least 3 MPa. According to both strength results, the highest load data was given by the P10 sample, while the lowest data was given by the P30 sample. Although all samples met the specified compressive strength, both O30 and P30 samples failed to meet the specified bending strength.

3. Conclusions

In this study, the authors experimentally investigated the use of waste oak and pine ashes in gypsum-based mixtures. Based on the experimental results, the following conclusions can be drawn:

- As the ash usage rate increased, the unit weights of the plaster samples decreased. Only the P10 sample is 2% heavier than the reference sample.

- As the UPV values additive rate increases, lower speed values are given. The P10 sample gave 5% better results. These findings are consistent with the apparent porosity, capillary water absorption and water absorption measurements.
- O30 and P30 samples have 18.2% and 21.2% lower thermal conductivity coefficient values, respectively, when compared to the reference sample. The thermal conductivity coefficient values for O30 and P30 are 0.340 and 0.328 W/mK, respectively.
- All samples, except for sample P10, showed a significant reduction in mechanical effects when additives were added.
- These gypsum-based samples with oak and pine ashes can be evaluated as non-load bearing partition elements, such as walls. Additionally, these materials may aid in energy conservation due to their low thermal conductivity coefficients

KAYNAKÇA

Andrea Jordan, C., & Akay, G. (2012). Speciation and distribution of alkali, alkali earth metals and major ash forming elements during gasification of fuel cane bagasse. *Fuel*, *91*(1), 253–263. https://doi.org/10.1016/j.fuel.2011.05.031

Benaicha, M., Jalbaud, O., Hafidi Alaoui, A., & Burtschell, Y. (2015). Correlation between the mechanical behavior and the ultrasonic velocity of fiber-reinforced concrete. Construction and Building Materials, 101, 702–709. https://doi.org/10.1016/j.conbuildmat.2015.10.047

da Costa, T. P., Quinteiro, P., Tarelho, L. A. C., Arroja, L., & Dias, A. C. (2019). Environmental assessment of valorisation alternatives for woody biomass ash in construction materials. *Resources, Conservation and Recycling*, *148*, 67–79. https://doi.org/10.1016/j.resconrec.2019.04.022

da Costa, T. P., Quinteiro, P., Tarelho, L. A. C., Arroja, L., & Dias, A. C. (2020). Life cycle assessment of woody biomass ash for soil amelioration. *Waste Management*, *101*, 126–140. https://doi.org/10.1016/j.wasman.2019.10.006

Durgun, M. Y. (2020). Effect of wetting-drying cycles on gypsum plasters containing ground basaltic pumice and polypropylene fibers. *Journal of Building Engineering*, *32*. https://doi.org/10.1016/j.jobe.2020.101801

Durgun, M. Y. (2021). Experimental research on gypsum-based mixtures containing recycled roofing tile powder at ambient and high temperatures. *Construction and Building Materials*, *285*. https://doi.org/10.1016/j.conbuildmat.2021.122956

Farinha, C. B., Silvestre, J. D., de Brito, J., & Veiga, M. do R. (2019). Life cycle assessment of mortars with incorporation of industrial wastes. *Fibers*, *7*(7). https://doi.org/10.3390/FIB7070059

Heinimö, J., & Junginger, M. (2009). Production and trading of biomass for energy - An overview of the global status. *Biomass* *and Bioenergy*, *33*(9), 1310–1320. https://doi.org/10.1016/j.biombioe.2009.05.017

Karni, J., & Karni~, Y. (1995). Gypsum in construction: origin and properties. In *Materials and Structures* (Vol. 28).

Melotti, R., Santagata, E., Bassani, M., Salvo, M., & Rizzo, S. (2013). A preliminary investigation into the physical and chemical properties of biomass ashes used as aggregate fillers for bituminous mixtures. *Waste Management*, *33*(9), 1906–1917. https://doi.org/10.1016/j.wasman.2013.05.015

Munawar, M. A., Khoja, A. H., Naqvi, S. R., Mehran, M. T., Hassan, M., Liaquat, R., & Dawood, U. F. (2021). Challenges and opportunities in biomass ash management and its utilization in novel applications. In *Renewable and Sustainable Energy Reviews* (Vol. 150). Elsevier Ltd. https://doi.org/10.1016/j.rser.2021.111451

Pasandín, A. R., Pérez, I., Ramírez, A., & Cano, M. M. (2016). Moisture damage resistance of hot-mix asphalt made with paper industry wastes as filler. *Journal of Cleaner Production*, *112*, 853–862. https://doi.org/10.1016/j.jclepro.2015.06.016

Rajamma, R., Senff, L., Ribeiro, M. J., Labrincha, J. A., Ball, R. J., Allen, G. C., & Ferreira, V. M. (2015). Biomass fly ash effect on fresh and hardened state properties of cement based materials. *Composites Part B: Engineering*, *77*, 1–9. https://doi.org/10.1016/j.compositesb.2015.03.019

Ranesi, A., Faria, P., Correia, R., Freire, M. T., Veiga, R., & Gonçalves, M. (2022). Gypsum Mortars with Acacia dealbata Biomass Waste Additions: Effect of Different Fractions and Contents. *Buildings*, *12*(3). https://doi.org/10.3390/buildings12030339

Sakhare, V. V., & Ralegaonkar, R. V. (2016). Use of bio-briquette ash for the development of bricks. *Journal of Cleaner Production*, *112*, 684–689. https://doi.org/10.1016/j.jclepro.2015.07.088

Santos, T., Almeida, J., Silvestre, J. D., & Faria, P. (2021). Life cycle assessment of mortars: A review on technical potential and drawbacks. In *Construction and Building Materials* (Vol. 288). Elsevier Ltd. https://doi.org/10.1016/j.conbuildmat.2021.123069

Ukrainczyk, N., Vrbos, N., & Koenders, E. A. B. (2016). Reuse of woody biomass ash waste in cementitious materials. *Chemical and Biochemical Engineering Quarterly*, *30*(2), 137–148. https://doi.org/10.15255/CABEQ.2015.2231

Vassilev, S. V., Baxter, D., Andersen, L. K., & Vassileva, C. G. (2010). An overview of the chemical composition of biomass. In *Fuel* (Vol. 89, Issue 5, pp. 913–933). https://doi.org/10.1016/j.fuel.2009.10.022

Vassilev, S. V., Baxter, D., Andersen, L. K., & Vassileva, C. G. (2013). An overview of the composition and application of biomass ash. Part 1. Phase-mineral and chemical composition and classification. In *Fuel* (Vol. 105, pp. 40–76). https://doi.org/10.1016/j.fuel.2012.09.041

Vassilev, S. V., Baxter, D., Andersen, L. K., Vassileva, C. G., & Morgan, T. J. (2012). An overview of the organic and inorganic phase composition of biomass. In *Fuel* (Vol. 94, pp. 1–33). https://doi.org/10.1016/j.fuel.2011.09.030

Voshell, S., Mäkelä, M., & Dahl, O. (2018). A review of biomass ash properties towards treatment and recycling. In *Renewable and Sustainable Energy Reviews* (Vol. 96, pp. 479–486). Elsevier Ltd. https://doi.org/10.1016/j.rser.2018.07.025

Williams, A., Jones, J. M., Ma, L., & Pourkashanian, M. (2012). Pollutants from the combustion of solid biomass fuels. In *Progress in Energy and Combustion Science* (Vol. 38, Issue 2, pp. 113–137). https://doi.org/10.1016/j.pecs.2011.10.001

Yoshitake, I., Ueno, S., Ushio, Y., Arano, H., & Fukumoto, S. (2016). Abrasion and skid resistance of recyclable fly ash concrete pavement made with limestone aggregate. *Construction and*

Building Materials, *112*, 440–446. https://doi.org/10.1016/j.conbuildmat.2016.02.185

CHAPTER V

Influence of Drill-Holes on Moulded Column-Like Test Samples' Surface Displacements: Digital Image Correlation Analyses

Mehmet UZBAS[1]
Mehmet Kemal GOKAY[2]

Introduction

Solid materials, natural, casted or moulded by men can be in different compositions. Metal casts and solid organic&inorganic compounds have been produced for their specific purposes in factories. One example of these solid materials is concrete which is moulded by using mixtures of different inorganic (sand, cement, aggregate) and additive materials (quartz sand, metal fibres, fly ashes, organic fibres, inorganic chemicals, etc.). Mechanical behaviours of load-bearing moulded columnar & standard test samples (with/without reinforcement) have been evaluated in

---

[1] Research Assistant, Konya Technical University, Mining Engineering Department, Konya, Turkey.

[2] Prof. Dr., Konya Technical University, Mining Engineering Department, Konya, Turkey.

different researchers to present their fracture initiation and propagation stages. Column-like or disk-shaped test samples have also been put under analyses in fracture mechanics research works (with purposely included modelled cracks). Fracture initiation and propagation have then been evaluated through geometry of the fractures at the moulded, (or massive: metals, rock, composite) intact test samples at those studies.

Similarly, solid column-like small scale tests samples which were moulded by using special gypsum powder and tap-water were studied here. Holes in different diameters were drilled through the samples to understand their influences on the stress-strain behaviours of the test samples under vertical loading conditions. Test samples’ surface displacements (in micro-level) have also been determined here through Digital Image Correlation, DIC, technique. In DIC analysis, position differentiation of image dots on the test samples’ surface were used to realise the micro-level position differentiations. Software programs in computer technology have their digital colour recognition capacities, which is over 16 million colour differences in RGB colour palette for instance. Solid test samples (with/without drill-hole) were analysed here for their stress-strain differentiation behaviours through DIC procedures. DIC graphics obtained in the tests presented that fracture initiation and propagation localities were influenced by drill-holes. Besides, drill-holes in the test samples caused detrimental impacts on tests samples’ vertical load-bearing capacities and their toughness characteristics.

Toughness characteristics of materials

Strength of materials for applied 3D-stress states are usually taught in engineering education after lecturing static states’ (equilibrium of applied forces on solids) related contexts. Strength is resistance of solid materials to applied forces according to their physical, chemical and mechanical characteristics. Main mechanical properties are related to compressive, tensile, shear, bending, impacts, etc. types of forces. When the applied 3D force levels are too low with respect to solid material strength levels, the displacements could not be realised without micro-level measurements. Humans can differentiate the bending behaviour differences of hard and soft wood beams *(if the thickness of them is around 5cm in 5x20x350cm beam dimension)* while walking over them. Similarly, displacement behaviours of different types/sizes of springs are closely observable also without any measuring equipment. However micro displacements of materials which have high strength values cannot be recognisable without special measuring apparatus/methods. Elasticity is the main parameter in the consideration of solid materials' mechanical behaviours and can be defined through stress-strain graphics obtained from 2D or 3D compressive/tensile loading tests. Elastic modulus of solid materials including rocks and concrete are defined through their stress-strain graphics (Fig.1 and Fig.2b). Curve angles in these graphic (at linear region, up to yielding strength, Y value, levels) are named as Elastic (Young) modulus; *(E=σ/ϵ, where E: Elastic modulus of solid material, σ: Applied stress level, and ϵ: Strain, displacement level).* The curves in the stress-strain graphs present also the mechanical behaviours of solids besides their; yield, (Y values); ultimate, (U values), and failure (F values) strength values beside their elastic modulus values. The area occupied under the stress-strain curve is related to energy stored in the solid materials. In the elastic regions of stress-strain curves, energy stored in the solid materials during applied loadings is released back while the load is being eliminated. If the strains are totally discharged and there are no permanent shape/size differentiations in the solid test samples, energy storage procedure for the selected solid materials could then be named as "operation in elastic state". If there are micro/nano level shape differences, or micro/nano level strain is detected in solid materials after all the stresses are removed from the solid materials, then the mechanical behaviour of the solid materials cannot be considered anymore as "elastic". The amount of area stayed under the stress-strain curves before the solid materials' total fracturing (strength level defined with F values; Fig.1), represents also the amount of energy they store. These energy levels could also be considered as the level of resistance, *toughness,* for applied loading conditions before total fracturing. The types of stress-strain curves could be similar or different in shape for solid materials like their E values. The shapes of curves and stress levels of yielding (Y values), ultimate (U values), and failure (F values) are illustrations of solid materials mechanical behaviour differences. Solid materials' mechanical behaviour differences in ductile or brittle behaviours are then described as they are illustrated in Fig.1. Yield, ultimate, and fracture strength levels at stress-strain curves, and their positions with respect to each other are defining the characteristics of ductility and brittle properties of solid materials. Differences of stored energy levels during; elastic, strain-hardening, and strain softening (necking) regions are used to differentiate solid materials. Figure 1a illustrates the necking region which is absent for brittle materials due to the same stress level for U and F values. Ductile materials, on the other hand, supply different stored-energy area shapes due to the different levels of Y, U, and F values on their stress-strain curves (Fig.1b). These area differentiations originated due to solid materials' mechanical behaviour characteristics. Stored energy area differences (mechanical behaviour differentiations) is also defined as the modulus of toughness which is described as; *"the amount of strain energy per unit volume (strain energy density) that a material can absorb just before it fractures",* (MechaniCalc, 2023). Since the amount of the area is a governing factor in toughness; the areas illustrated in Fig.1b represent two different solid materials. Tested solid materials might have higher (Solid-1) or lower (Solid-2) yield, (Y), and ultimate, (U), strength values. However, the amounts of the areas

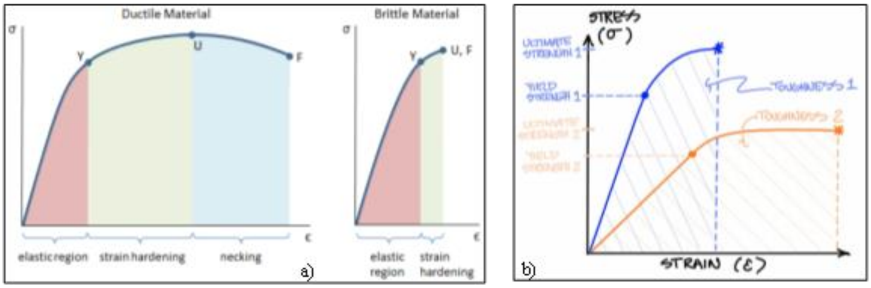

Figure 1. a) Stress-strain curves samples of solid materials. Ductile and brittle material properties influence the energy stored just before the failure strength (F value) level, (MechaniCalc, 2023); b) Schematic presentation of two different toughness characteristics of solid materials, (SEN, 2023).

under their curves could be different which is directly related to toughness characteristics of the solids. If the solid material resists to applied stress level up to its F value, (after supplying relatively long resistances; giving strain but sustain resistance to the applied stress), they might have higher toughness values with respect to the solids supplying high Y and U values but low stored-energy areas under their stress-strain curves. Sketch illustrated in Fig.1b supplies an example that solid material named as “Solid-1” has higher Y and U values but less amount of area under its stress-strain curve when it is compared to the values obtained for the “Solid-2” material. *“Thus, Material 2 has higher toughness characteristics than Material 1. In other words; Material 2 may have a lower strength than Material 1 but it is able to absorb more total energy before failure”,* (SEN, 2023). It should be borne in mind that the sketch in Fig.1b reflects two hypothetical materials’ curves. Many other types of stress-strain curve profiles could be possible according to materials’ toughness differences. When toughness is under concern, there are different stress-strain curve profiles which might represent the same toughness value as well. Then characteristics of the total areas under stress-strain curves are taken into consideration. The amount of areas under; “elastic-region”, “strain hardening”, and “strain softening” regions are governing factors to define the material property differentiations. The toughness values described here are related to whole material solid properties, but there are also other toughness characteristics of solid materials like; impact toughness, notch toughness, and fracture toughness. When the crack is initiated in the rock and concrete masses (or any other types of solid materials), fracture propagation is governed mainly through; applied 3D stress stages, material strength properties, fracture geometries, and material/fracture toughness properties. Brittle materials have U and F strength values almost similar, so fracturing after their yield strength, (Y values) up to their ultimate strength, (U values) levels is important. After U values, brittle materials are fractured apart without showing any resistance to the applied stresses. However, ductile materials show their resistances to the applied stresses after their U strength values are achieved. Ductile materials usually require more time *(they supply displacements through their formed cracks while still resisting applied stresses)* to reach their F strength values. Therefore, fracture propagations controlled through material fracture toughness characteristics of rock materials is also a discrimination property for those solid materials like rocks and concrete masses. Some solid materials like polymers, rocks, woods, ceramics, metals, metal-alloys, steels, etc. have their fracture toughness properties. Fracture toughness values were plotted against elastic modulus properties of common solid materials including Bulk Metallic Glasses, (BMG), in Fig.2a, (Greer, 2009). Yu etal., (2018) wrote that,

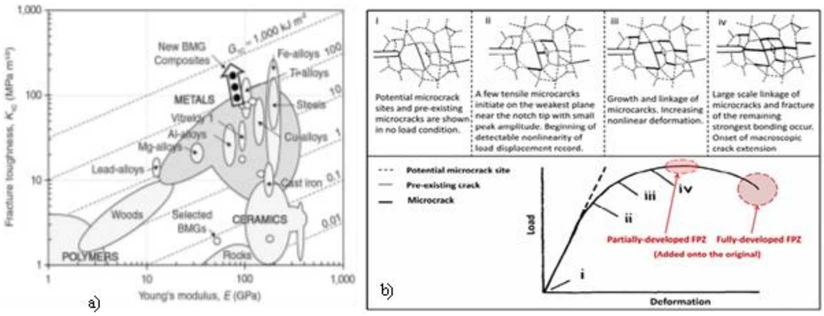

Figure 2. a) Fracture toughness differences between common materials and rocks (Greer, 2009), b) Schematic load deformation curve representation of 3-point-bending test of granite rock sample, including 4 progressive fracture stages, covering fracture initiation & propagation, (Yu, etal., 2018, after Hashida&Takahashi, 1993).

"prior to the peak stress under quasi-static loads, the tip of notched crack can appear (as) an inelastic zone, which is defined (as) the fracture process zone (FPZ)", Fig.2b. These researchers also pointed out that; this area of study (fracture mechanics) in materials' mechanical behaviour context has a special focus after "*Hillerborg, etal., (1976) proposed the fictitious crack model (or cohesive crack model) to describe the FPZ"*. In order to explain fracture development, *"the cohesive stresses are used to explain the crack-bridging mechanism due to zig-zag cracking and frictional sliding and pull-out of grains",* (Hillerborg, 1991; Yu, etal., 2018). Then, Yu, etal., (2018) wrote that FPZ is formed in phase (ii) stage in Fig.2b. In this stage there are *"large numbers of micro cracks aggregation and interaction in a local region"*.

Solid materials' mechanical behaviours have been tested through several research based laboratory tests mainly for; compressive, tensile, shear, and bending strength properties. The failure of concrete specimens (and/or man-made rock-like solid materials) could also be tested in a similar manner. Rock fracture initiation and their propagations in the test specimens (through the naturally existing rocks and/or newly prepared ones) are governing issues of their mechanical behaviours. Fracture behaviours at these specimens are controlled mainly by; applied 3D stress conditions, fracture related parameters, and rock material properties. Rock types and their mineralogical & petrographic features, naturally existing crack densities, newly formed cracks and their density values, crack geometries and their main orientations, localisation of high/low crack density areas are also influencing the fracture rupture conditions, (thus the toughness of rock materials). Natural rock materials and artificially cemented man-made rock-like materials (i.e: bricks, concrete) have been used mainly as load-bearing solid materials during urbanisation history. Their mechanical properties have recently been researched more comprehensively for stable working and living places. In order to form urban spaces in/on earth crust, load-bearing columns and beams have to be designed to transfer overburden loads in stable conditions. The strength of these structural elements (columns, beams) are a vital issue during their modelling in engineering design efforts. Good practices and adequate engineering knowledge are required for stable surface/underground space designs. Keeping the natural rock mass structural conditions as it is found before the engineering activities, moulding concrete columns/beams with minimum internal micro-voids are two important key-factors influencing the results of engineered designs (including load-bearing structural elements). While imposing the significance in the intactness of rock and concrete materials at load-bearing structural elements of engineering projects, any defects adding them purposely (like drilling a hole) should be evaluated more comprehensively for their outcomes. Any positive/negative impacts influencing load-bearing resistance (toughness) of the structural columns are then vital subjects to be considered comprehensively.

Column-like surface/underground load-bearing structural elements

Load carrying structural elements at surface/underground constructions have important concerns due to their stabilities. Pillars (at underground mining operations) and reinforced concrete columns

(RC-columns) at surface/underground constructions (Fig.3) are main features to be designed prudently to carry overburden loads. Therefore, they have to be designed for their long-term stability circumstances. Engineers have estimated loads over pillars & RC-columns to provide 3D plans describing their positions and sizes in the planned engineered structures.

When the load-bearing capacity of solid materials are under consideration, laboratory compressive tests are performed in 2D and 3D loading conditions. Actual size RC-columns have also been tested in civil engineering laboratories for their load-carrying performances by introducing different design and raw material mixture configurations. Testing mine pillars & construction RC-columns at in-situ positions could be possible for detailed research activities but crushing one of these load-bearing structural elements might definitely cause further stability problems. Therefore, their strength characteristics are evaluated through their "material strength" properties determined in laboratories. Engineers working in rock mechanics context have well informed that, size-effect differences among "*actual sizes of mine pillars"* and "*sizes of samples*

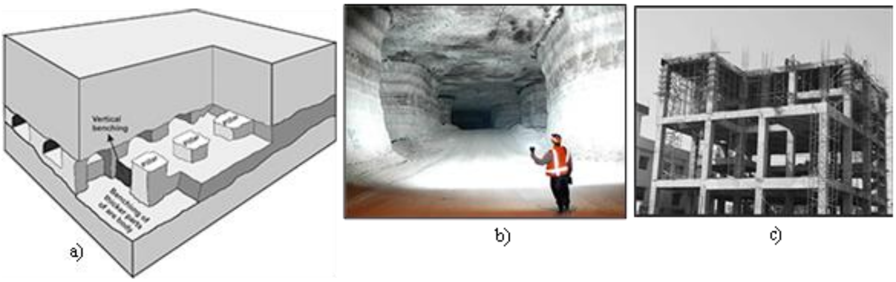

Figure 3. Column like load-bearing structural elements; a) Pillar configuration for room & pillar mining method (3D schematic illustration), (Hamrin, 1980), b) Underground pillars in limestone mine, (depth:275m), (Esterhuizen, etal., 2011), c) Reinforced concrete columns and frameworks under construction, (Obinna, 2020).

tested in laboratories” for their strength values need adequate estimations of in-situ strength values of pillars. These estimations always have their decision risks in engineering concerns. As the size of the mine pillars are designed larger in dimensions, the number of discontinuities they included are increased as well. The locations of pillars in 3D mine plans and the strength values of rocks/ores surrounding pillars are influencing parameters on pillars’ load-bearing properties. When the fractures *(illustrated in Fig.4a, 4b, 4c, (mine pillars), and 4g, (rock column))*, are under consideration, engineers have to think about the stresses and rock structural features which have

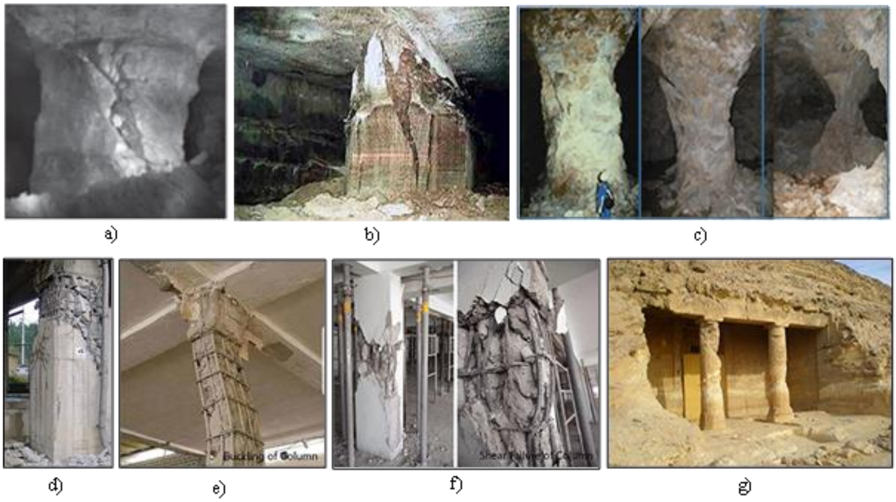

Figure 4. Failures at column-like load carrying structural elements; a) Fractured underground mine pillar (Esterhuizen, etal., 2011), b) Pillar failure, Cleveland ,US, (Photo by Franks, A.M. & information by Coleman, T.) (ECIA, 2023), c) Progressive spalling of a gypsum mine pillar (Photos from 1996, 2000, 2004), (Sorgi & Gennaro, 2011; Sorgi & Watelet, 2007), d) Failure due to compressive stress at a reinforced building column (Structural guide, 2023), e) Buckling failure at reinforced building column (Structural guide, 2023), f) Shear failure at reinforced building

column (Structural guide, (2023), g) Fractures and alterations in rock columns, El Minya archaeological site, Egypt, (FTS, 2019).

caused them to form. The fractures in these rock pillars & RC-columns have influenced their mechanical behaviours (especially their load-bearing capacity). During mechanical behaviour estimation for rock pillars, physical & mechanical properties of rock materials *(including; average strength values at yielding, ultimate, and failure stages, elastic modulus, material & fracture toughness, etc.)* are important design decision parameters which engineers should think about. Material differences in rock pillars' bodies (rock/ore strata differentiation in the pillar bodies, damage zones, discontinuities and their structural features in pillars, etc.) directly affects the mechanical behaviours of these pillars. Mine engineers who are educated purposely on rock engineering are graduated to be ready to think about further precautions to be taken for stable and safe working environments.

When strength considerations have been under evaluation for reinforced concrete columns, the raw materials, cements, additives, water and their mixing proportions have provided different types of concrete researched in civil engineering context in detail. Influences of different types of aggregate, aggregate-strengths, cement types, water qualities, additive types & their properties, steel-rod types (their size & quality differences) in RC-columns' performance have formed wide research areas in civil engineering. Influences of time and human-activities (during construction or later periods) on RC-columns' strength properties (compressive & tensile strength, elastic modulus, toughness, for instance) have supplied complex circumstances to be thought about. As the mechanical property differentiation (deteriorated) progressed in time for a selected RC-column, drilling a hole in this column purposely for different purposes put additional catastrophic strength circumstances for that RC-column's mechanical behaviours. RC-columns have their failure types (Fig.4d, 4e, 4f) according to induced stress types. Progressive spalling failure types observed for mine pillars (Fig.4c) might not be one of the expected failure forms for RC-columns but, mechanical property deterioration and micro-fracturing (fracture initiations and propagations) are two significant factors influencing RC-columns' load-bearing capacities in time. Therefore, toughness characteristics of concrete *(or any other solid materials used in construction industry)* together with their fracture toughness properties have been important to be studied in detail.

Likewise, influencing the mechanical behaviours of RC-columns by any manners (i.e; drill-hole) is also vital consideration for the stabilities of constructions. Adequate design procedures have covered all the necessary construction steps in consideration according to the available technology before the construction operation is started. Therefore, in any application circumstances appeared in time; drilling a hole through load-carrying RC-columns is out of question for all surface and underground man-made structures. However, unauthorised human-acts might be the reasons for such holes at certain structures. There are always different; technological, social, cultural, or human-acts driven reasons for these holes which should be difficult to control. However, when an unauthorised hole drilling is recognised at loadbearing RC-column anywhere in the world, it should be officially recorded and legal issues should be followed according to rules & acts. In some cases, RC-column strength properties are asked to be determined (through drill-hole core samplings) after the completion of construction works for legal disputes. Similarly, (In some other cases), legal documentation might be asked for the mechanical properties of RC-columns of public buildings (hospital buildings especially) after their constructions (as a safety&control action) to analyse their earthquake resistance features. These human influences on load-bearing RC-columns at surface/underground constructions are needed to be considered in detail for the stability concern of the buildings.

Distractions in load-bearing characteristics of columns due to drilled-holes

Urbanisation in the modern world has extended its limits in all parts of the world. Constructions in/on earth crust have occupied one of the main activities of human societies. When the living spaces are planned for surface/underground structures, it is needed to have load-bearing pillars, columns and beams to support designed spaces for their overburden loads. Mining and civil engineering field of applications cover the design procedures of those load-bearing pillars and columns especially. Mine pillars are rock/ore parts left unexcavated (untouched, undisturbed) at underground mine operation layers to support mine openings' roof layers. They are main mine supports transferring overburden (hanging wall) loads to footwall layers in certain underground mining methods. Mine engineers know that any natural and/or man-made damages affecting the intactness of the mine pillars influences the strength of them and consequently safety of mines.

Similarly, column-like dimensioned stones were used in ancient surface structures (especially at monumental buildings), until RC-columns have become one of the main load-bearing structural elements in modern constructions, buildings. Engineers are well aware of the column design precautions, their defects, and harmful post-construction activities influencing the strength of the RC-columns. However, there can still be some circumstances in the world which influence the load-carrying strength of the building columns. Drilling a hole through the RC-column is one of the defects observed. Lack of knowledge about the strength of materials (concrete), deficit in the stability controls of constructions might be the causes of examples illustrated in Fig.5a and 5b. Catching awkward circumstances of holed RC-columns are possible in the world. In some cases; steel tubes, casing, left purposely during moulding of the RC-columns to form ready-to-use holes could also be seen. In other cases, these holes are drilled through the RC-columns in post-construction times. In these cases, there are possibilities of cutting several steel-rods of RC-columns used for their reinforcements. Cutting a few of them directly decreases total reinforcement efforts of the designed steel-bar configuration in the RC-columns. In some other cases, in order to detect official concrete quality, sometimes core testing samples are decided to be taken from RC-columns of surface structures. Kurklu (2005) and Akdag (2015) presented examples of RC-column hole drilling operations and their analyses.

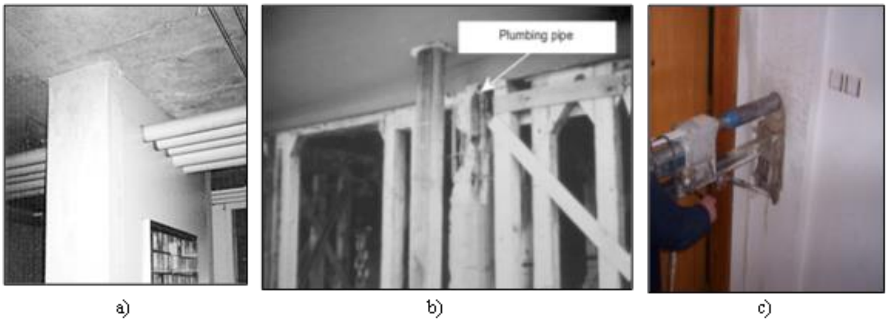

Figure 5. RC-Column which have hole(s); a) Horizontal holes drilled for building services (Son, etal., 2006), b) Vertical hole in RC-column as a plumbing pipe, "earthquake damage sustained by columns containing plumbing pipe", (Son, etal., 2006), c) Core drilling at RC-column of a building by a portable drilling machine, (after Kurtulus&Bozkurt, 2011).

There are procedures described in different standards for core drilling and testing procedures for existing concrete structures as mentioned by Alwash (2017) together with non-destructive testing methods and their evaluations. Son, etal., (2006) focused on holes drilled through RC-columns and they mentioned some drill-hole applications *"to install additional services or equipment"*. According to their evaluation these acts *"can lead to loss of strength and possible structural failure"*. They added also that little study had been performed on drill-holes on columns up to 2006. In order to analyse the effects of drill-holes on RC-column strength capacities, they performed laboratory column tests with 200x300x1600mm lab-scale RC-column samples. They tested the lab-scale RC-column samples with/without drill-holes. They positioned the circular drill-hole(s) (in different diameters) at the vertical and horizontal centres of the prepared test samples. They had lab-scale RC-columns' vertical loading test results for single and multiple drill holes. In these tests, Son, etal., (2006) configured the hole positions (vertically/horizontally) with different clearance, (aperture, between them). Their results illustrated that drill-holes influence the vertical compressive strength of the samples and the fracture patterns developed on the tested samples (Fig.6). Fracture traces illustrated in Fig.6b presented the influences of the drill-hole. The fracture traces *(on the test samples' surfaces which had 50mm drilled-hole)* showed that fracture propagation and their orientations were influenced by existing drill-hole in a negative manner. The fractures which have connection with the existing drilled hole in Fig.6b is obviously the diversion of these two figures (Fig.6a and 6b). In order to understand fractures' initiations and their propagations around a circular hole in a solid material, induced stresses formed in the RC-column test samples, (with/without drill-

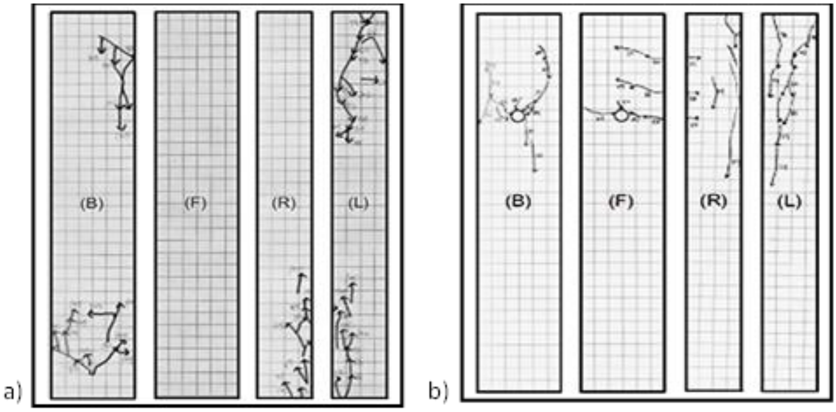

Figure 6. Lab-scale RC-column samples (200x300x1600mm in dimensions) tested for their strength capacities, (image taken from the faces; F: front, B: back, R: right, L; left), a) Crack traces on the intact, massive, sample, b) Crack traces on the sample which have drill-hole (50mm in diameter), (after Son, etal., 2006).

hole) are the key factors besides RC-column samples' strength values. Forwarded 2D stress-strain solutions provided by Kirsch (Fig. 7a) is one of the manners to estimate influences (induced stress-strain differentiations) of a circular hole in homogeneous solids loaded by uniform 2D field stresses (P and q in Fig.7a), (Kirsch, 1898; Li, etal., 2017). Kirsch's

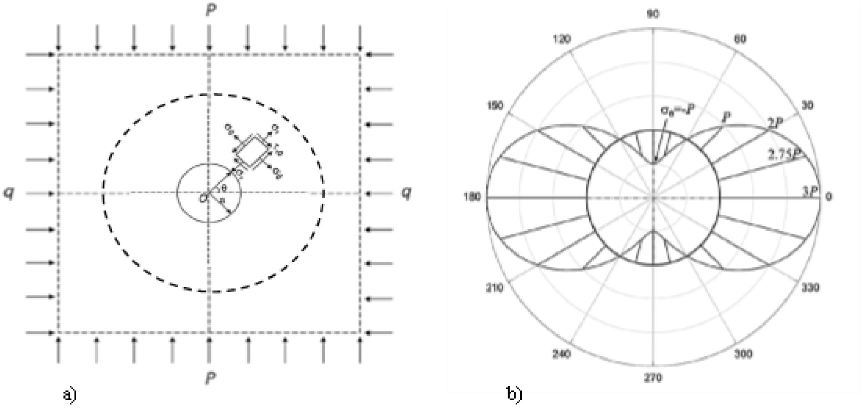

Figure 7. a) Kirsch solution, (induced stress configuration in an influenced circular zone, area in dotted circle) surrounding a hole in homogeneous material (after Kirsch, 1898; Li, etal., 2017), b) Tangential stress differentiation surrounding a circular hole under uniaxial compression level, (P). (Li, etal., 2017).

approach supplied for homogeneous solid materials, may be used in the first hand by rock engineers to evaluate if the induced (secondary) stress distributions around the tunnels are overcome the strength capacities of the rock materials at the selected country rock locations (surrounding the tunnels) by assuming the circular tunnel is opened in homogeneous rock materials. In reality this assumption is not the case in real-world rock conditions around the tunnels. But, it opens opportunities to understand the induced stress levels if the tunnel cases are realised in homogeneous rock masses.

As Kirsch's solution demonstrated, induced tangential stress levels are decreasing as the distance is increased starting from the perimeter of the circular hole. The levels of tangential stresses around the hole are also different when the 2D field loading conditions (P and q) are considered. Induced stress levels are getting decreased as the distance increases away from the perimeter of the opened hole. These levels generally are accepted to be effective in a circular zone around the hole which has a 3 times bigger radius than the opened hole in a solid material, (Kirsch, 1898). Induced stresses are accepted to have influences outside of this hypothetical "influence zone" but their levels are also assumed to be in very low to be considered in stress-strain analyses. Evaluation provided by Li, etal., (2017) could also be considered during analyses of fractures around the drill-holes in RC-columns. The graph (Fig.7b) which was presented by them includes induced tensile and compressive stresses around a circular hole, (opened in a homogeneous solid; it is under uniaxial compressive stress, P). They wrote that "*the tensile stress zone is formed in the top and bottom of the circular hole with a maximum magnitude of -P, and correspondingly, the compressive stress zone is formed at the left and right walls of the hole with a maximum magnitude of 3P* " levels. If there are more than one drill-hole and the distance among them are close enough, their induced stress-strain influence zones are overlapped. That means the effectiveness of the resultant induced stress-strain levels might be more dangerous for the solid material strength capacities (it may cause fracturing). Thus, fractures observed around the drill-hole in any RC-columns could also be evaluated in a similar manner to comprehend fracture localisations (initiations and propagations) by considering RC-columns' toughness characteristics as well.

When the studies performed for drill-hole effects on RC-columns strength characteristics through laboratory based research are under consideration, the work of Campione, etal., (2015) is considered as well. As a main starting point of researches, reasons for drill-hole occurrences in the load-bearing RC-columns are summarised by them as all the other researchers. They wrote also that, "c*ore-drilling technique is nowadays always more frequently performed in existing reinforced concrete (RC) structures in order* *to investigate on the mechanical properties of concrete and for structural health monitoring purposes. Even if the engineering practice discourages to drill columns, this can be often unavoidable".* Since any voids, defect zones, cracks, spaces and purposely drilled holes in rock blocks, rock pillars, concrete materials and RC-columns influence their strength properties and their mechanical behaviours in uniaxial, biaxial, or 3D loading conditions, drill-hole influence analyses have to be evaluated by considering related information as well. In order to examine stress-strain differentiation cases for RC-columns (with/without drill-holes), Campione, etal., (2015) prepared two sets of lab-size RC-columns moulded through two different concrete compositions to have two different uniaxial compressive strength values for A-series and B-series samples. Tested lab-size RC-columns had size in 150x300x750mm, and they prepared 4 types of RC-columns for A and B-series of concrete compositions. These 4 types of RC-columns are differentiated according to whether they have drill-holes or not. If the samples included drill-holes, hole diameters driving the types of test samples. These 4 types of lab-size RC-columns are classified according to drill-hole diameter as; i) normal specimens (no hole), ii) 60mm, iii) 90 mm, and iv) 120 mm. Drill-holes were positioned at the centre of the test samples and they were drilled through the faces (width=300mm) of the samples. During the tests, strains formed due to applied vertical compressive stresses were measured through LVDT apparatuses positioned on the tested samples. Fractures appearing on the

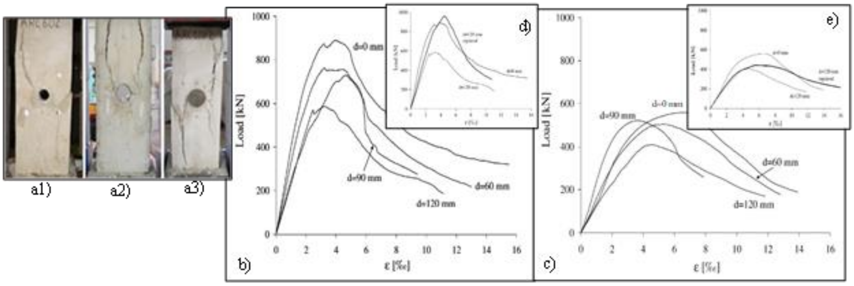

Figure 8. a) Lab-size RC-column test samples' images after the tests; a1:ARC60 (A-series sample with a hole d=60mm), a2: BRC90 (B-series sample with a hole d=90mm) and a3:ARC120 (A series sample with a hole d=120mm) samples' fracture patterns (Campione, etal., 2015), b) Uniaxial stress-strain curves for the lab-size RC-column tests with different drill-hole diameters of A-series samples, c) Similar curves for B-series samples, d)Similar curves for repaired drill-hole in A-series samples, e) Similar curves for repaired drill-hole in B-series samples, (after Campione, etal., 2015).

face of RC-columns tested were usually vertical in directions (Fig.8a). Fractures around the drill-holes implies clear influences of these holes on mechanical behaviours of the tested RC-columns. Maximum compressive stress concentration areas at both horizontal sides of drill-holes (Fig. 8a) seem to influence the fracturing procedures of test samples. Fractures observed in these localities around the holes (instead of top and bottom sides of the drill-holes) imply these observations. Uniaxial stress-strain graphics illustrated in Fig.8b, 8c, 8d, 8e presented influences of drill-holes on the strength and toughness characteristics of the tested lab-size RC-columns *(moulded with A-series and B-series concrete compositions),* (Campione, etal., 2015). In these graphs, curves labelled with d=0mm were obtained from the test samples which have no drill-holes. Decreasing the peak stress (U) values in these graphs can be seen as the diameters of the drill-holes are increased. The areas under these stress-strain curves, (material toughness values of the tested lab-size RC-columns), are comparably decreasing as the diameters of the drill-holes are increased (Fig.8b and 8c). Campione, etal., (2015) performed repair activities also for the selected drilled-holes to test their influences on lab-size RC-column strength characteristics. They use special composition to prepare repair-mortar for the selected holes drilled at A-series and B-series test samples. The axial stress-strain curves obtained during vertical loading tests for lab-size RC-column samples which have repaired drill-holes are given in Fig.8d and 8e. Since A-series samples have higher strength values than B-series ones, the stress-strain curves presented in Fig.8 should be evaluated accordingly. Campione, etal., (2015) wrote that; they prepared concrete composition mixtures for A-series and B-series concrete and they tested them for their uniaxial compressive strengths measurements after 28 days of utilizing; (through cylindrical and cubic concrete test samples). Average compressive strengths were determined for the cylindrical samples for A-series: 33.32 MPa and B-series:14.01 MPa. Similar compressive strength test results for cubic concrete test samples were determined for A-series: 23.02 MPa and B-series:11.49 MPa. For the drill-hole repairing activity (filling the drill-hole with concrete mortar mixture) the authors wrote that; "*Material used for the hole repairing was a high strength tixotropic cement-based mortar. The admixtures were reinforced with polymeric micro-fibers. The 7-days compressive strength was 51 MPa"*. Since the repairing admixture mortar had higher compressive strength than A-series and B-series concretes, repaired RC-columns' behaviours under vertical loading conditions were observed in different stress-strain characteristics as illustrated in Fig.8d and 8e. These researchers wrote that, tested B-series lab-size RC-column samples which had repaired drill-holes with the prepared admixture mortar supply lower strength characteristics. The researchers' words in this matter were; "*the behaviour of column type B* (B-series concrete composition) *repaired (with a material which has a comparable strength to type A* (A-series concrete composition) *is governed by the resistance of the weaker material"*. The effects of drill-hole influences on lab-size RC-column strength (including drill-hole location) was also researched by Zhu, etal., (2010). They reported compressive strength variations due to drill-hole position differences and different reinforcement arrangements by 3 groups of lab-size RC-column test samples. Their dimensions were 300x300x1200mm, 400x400x1200mm, and 400x600x1200mm. Test samples were prepared by using a specific raw materials proportions (in concrete composition) to obtain solid concrete which had compressive strength around 19.5 MPa. They reported also that they used repairing concrete mortar which had special raw material proportions to produce "slight-expansion, high-strength" concrete, (which had average compressive strength values of 58.6 MPa). Their results implied that drill-holes decreased the load-bearing capacity of the lab-size RC-columns in 5.63% to 22.14% according to their test configurations. After they reinforced the drill-holes with a prepared repairing concrete mortar, they wrote that the average load-bearing capacity decreased in the impaired lab-size RC-columns was around 3.76%.

When the stress-strain curves illustrated in Fig.8d and Fig.8e are under consideration where these figures have curves obtained from the repaired lab-size RC-column test samples, influences of concrete mortar used for drill-hole repair activity could be seen. As it is supplied before, Campione, etal., (2015) explained the differences of peak compressive strength, (U), values of A-series and B-series of lab-size RC-columns which have repaired drill-holes with 120mm in diameters. Beside the analyses and explanation provided through these researchers' work, following situations should also be thought of for more comprehensive strength failure circumstances. There are 3 different mechanical behaviour differences which might be formed after the repair processes of drill-hole openings for RC-columns. In order to explain these cases, it was assumed that, a RC-column test sample like one illustrated in Fig.8a (a1) has elastic modulus, Es, uniaxial compressive strength, σcs, and uniaxial tensile strength, σts, values. Similar strength values were assumed to be determined for the solid fillings of drill-holes (solidified repairing concrete mortar mixture) as Er, σcr, and σtr values. When the filling mortar is applied for their repairing duties into the drill-holes in RC-columns, the following three cases should be considered in detail; a) *Es=Er*, b) *Es<Er*, and c) *Es>Er*. Contact surface conditions between repairing mortar types *(prepared as a mould-slurry mortar mixture through different raw materials compositions, and then let it to be solidified)* and inner peripheries of the drill-holes in RC-columns should also be taken into evaluations. Any voids, micro/nano spaces, micro-scale apertures formed in *the drill-hole filled mortar mass* and/or at *the contact surfaces of mortar-hole peripheries* during these solidifications processes of filled mortars, they will then ready to influence the strength and toughness characteristics of the RC-columns. These apertures/voids even in micro/nano scale affect the areas of the contact surfaces. Any decrease in these contact surface areas causes stress concentrations in certain positions of the hole peripheries which might cause further strength failure problems. Therefore, negative effects of these voids/apertures are also important aspects to be researched.

In the first case (case-1) which can be defined by *Es=Er* condition (Fig.9a), load carrying features of repaired RC-columns are expected to be near a uniformly coupled state. The periphery of drill-holes might influence the vertical load distributions in RC-columns due to its periphery traces. If the fillings of the holes are performed; a) by suitable moulding & pressurising filling equipment, b) avoiding any voids in the repaired holes and apertures at the periphery traces, c) filling the holes with the repairing mortars (materials) which are ready to provide similar uniaxial compressive strength and toughness characteristics, (stronger adhesion capacity is also required for good attachment of repairing mortars to the periphery of the drill-holes), after solidifications. Successful drill-holes repairing works may provide repaired drill-holes (filled with solidified mortar concrete material) which mechanically behave similar (similar uniaxial compressive strength and toughness characteristics) to RC-column mass, (Case-1 in Fig.9b). However, there

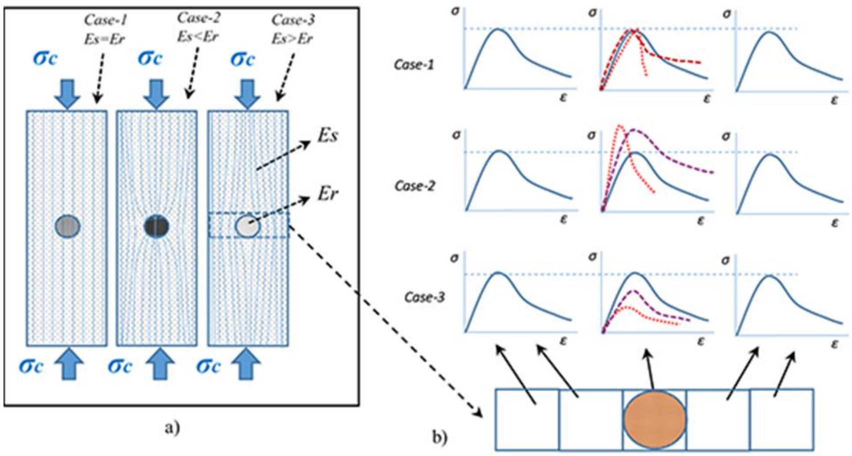

Figure 9. a) Stress projection lines expected during uniaxial loading conditions for the repaired RC-columns which could be analysed in different "case" conditions; (Es=Er, Es<Er, and *Es>Er), b) Repairing material uniaxial compressive strength and toughness differences with respect to RC-columns' uniaxial compressive strength and toughness characteristics. Engineers must remember that all these mechanical characteristics are dynamic and they have been changed in time due to a variety of influences.*

are some other possibilities which the repairing activities might end up. Dotted stress-strain curves (Fig.9b) defining uniaxial compressive strength features of the repairing materials are similar uniaxial compressive strength but they have different toughness characteristics. These differences are ready to supply diverse mechanical behaviours of repairing materials in the hole to create further strength property changes of whole repaired RC-columns' load-bearing capacities. Engineers, who decided to have a drill-hole in the load-bearing RC-column for concrete quality checking for example, should then be very careful about this application. Since it is very difficult to obtain "*theoretical Es=Er conditions*" (Case-1 in Fig.9), therefore, engineers must avoid drilling load-bearing RC-columns. Engineers should also be aware of the mechanical behaviour differentiations of concrete used in RC-columns of surface/underground structures which have mechanical characteristics differentiating dynamically in time. Thus, these features have deteriorated in time. Actual uniaxial compressive strength and toughness values of RC-columns at available surface and underground constructions could be different when the values are compared to the new similar constructions (built in exactly the same plans and constructions procedures). Therefore, engineers must be careful about their reports implying they managed to provide Es=Er conditions in their RC-columns' drill-hole repair projects. Because supplying this *"theoretical condition"* is almost impossible.

The second condition (Case-2) described for repairing material behaviours in repaired RC-columns (Case-2 in Fig.9) covers the elastic modulus condition of Es<Er. When the repaired drill-holes are assumed as an enclosed volume under uniaxial compressive stress in a load-bearing RC-columns, mechanical behaviours of solidified mortars used for drill-hole repair fillings should be analysed with the volumes including RC-column's concrete body parts at the left & right hand side of the repaired drill-holes (Fig.9b). Elastic modulus differences in Es and Er (as provided in Case-2: Es<Er) brings extra differentiation of mechanical properties like the differences in toughness characteristics. Their influences on repaired RC-columns should be considered and evaluated accordingly. In Case 2; solidified repairing mortars' higher Er values are supplied to RC-columns' drill-holes with their characteristic brittle/ductile behaviours. Higher yielding, ultimate, and fracturing strength levels and different toughness behaviours of these solidified mortars (in the drill-holes) influence their resistance to applied vertical loads. They might have higher stress-strain energy storage capacity, (higher toughness), as well. Fig.9b illustrates that; *(in an example of a normal stress-strain conditions defined for the working conditions of a repaired RC-columns in Case 2);* as the load over the RC-column is increased, the first yielding strength (Y value) level reached is the one related to RC-columns' material (this level is lower than the yielding (Y value) strength level of the solidified

filled mortars in Case 2). This was the result obtained also by *Campione, etal., (2015).*

The third condition (Case-3) described the elastic modulus conditions, Es>Er, in repaired RC-columns (Case-3 in Fig.9). In these cases, solidified repairing mortars provide lower elastic modulus (Er) than the RC-column materials (Es). That means, under the load carrying circumstances of a RC-column (which have a repaired drill-hole), due to elastic modulus differences between RC-column material and solidified filling mortar in the repaired drill-hole, solidified mortar is squeezed in the drill-hole (due to its softer material properties, lower Er values). Solidified repairing mortars' mechanical properties (i.e; uniaxial compressive strength and toughness characteristics) could be different (lower) as it is illustrated in Fig.9b. When the repaired RC-column under increasing overburden load, (Fig.9b, Case-3), yielding strength (Y values) of repairing material is reached before the RC-column material. Toughness of mortars' is then the governing factor for further load transferring and fracturing procedures of the solidified drill-hole fillings. Since the overburden loads are gradually transferred through the surrounding RC-column materials then, (due to strength losing behaviour of the solidified fillings) fracture initiations and their propagation characteristics in RC-column materials become important factors here.

Influences of drill-holes on RC-columns have been evaluated through numerical analyses as well. In these works; drill-hole diameters, drill-hole positions, and the number of drill-holes in RC-columns have been analysed in detail to understand their effects on RC-columns health (strength & toughness characteristics). Negassa, (2020) was one of the researchers who used finite element method, (through ANSYS software), to evaluate stress-strain distributions in RC-columns with/without drill-holes. RC-columns with 300x300x3000mm in dimensions were modelled with different drill-hole configurations in that numerical study. Diameters of drill-hole(s) (single, double or triple), and positions in the test samples were differentiated to understand their influences by using digital analyses. Negassa (2020) provided results also for square shaped hole to examine shape differences on RC-column mechanical behaviours. Stress-strain differentiation curves which are presented for different drill-hole configurations also have their toughness characteristics. The curves obtained to analyse the influences of shapes (which have similar displaced volume in RC-columns) were presented by Negassa (2020) in Fig.10a. When these curves are examined; it can be seen that; curve obtained from RC-column without drill-hole (CC1: solid control column) has higher U and F values with respect to the values obtained from RC-column samples which had square hole, SS1 (width=length=88.60mm, displaced volume=2354.99mm^3) and circular, SC3 (diameter=100mm, displaced volume= 2355mm^3) drill-holes. The curves supplied in Fig.10b show the effects of drill-hole diameters on the stress-strain behaviours of the RC-columns. The curves in this graph illustrate the ultimate strength level decreased as the diameters of the drill-hole were increased. Effects of horizontal positions of drill-holes were also given by Negassa (2020) through plotted digital analyses results (stress-strain curves) for the intact sample (CC1), and the samples with circular drill-hole in different horizontal positions. The researcher was also pointed out that the number of drill-holes had influences on the strength and toughness characteristics of RC-columns. Negassa’s (2020) evaluations in digital analyses have similarities with the laboratory test studies performed by Zhu, etal., (2010) and Campione, etal., (2015). These researches revealed clearly that drilling a hole into a load-bearing RC-column causes complicated, undesirable, results.

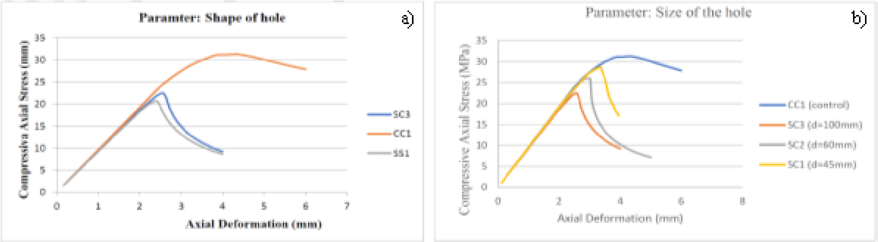

Figure 10. Numerical analysis results for vertical compressive stress-strain differentiation graphs for RC-columns. Effects of different drill-hole configurations were handled to compare; a) shape of drill-holes, b) size of drill-holes, (Negassa, 2020).

The influences of drill-holes are more complicated (and increased) as the numbers of drill-holes, and the displaced volumes are increased. Additionally, influences formed due to drill-holes in RC-columns cannot be retrieved. That means; repairing of the drill-holes by filling special concrete mortars or any other admixtures could not totally eliminate the loss of load-bearing capacity of the RC-columns.

Digital image correlation method to capture fracture movements

Computer technology and software development in different computer operating systems provide new environments for engineers to facilitate. Defining colours in computer screens through 24-bit colour definition of Red, Green, Blue (RGB) colours, *($2^{(8)}$ bit for each colour to produce "true colour")*, 256x256x256 matrix formats provides opportunities to the computer users to manage around 16.777 million colour tone differences in their computer graphic applications. Taking sequential photos and defining the colour differences among them is one of the image processing applications for aerial/satellite photographing to define; sessional agricultural land uses, forest borders, extension of urban areas, new urban developments, new roads, flooding areas in wet seasons, desertification areas, etc. Sequential photographs used here can also be taken in different light-frequencies to improve the analyses required. Taking as many digital images as possible in a second (i.e. 60, 360, 6000, 750K, etc., image frame per sec.) push the image capturing computer technology & analyses into the upper level of opportunities. Differentiating the colour differences in the sequential frames which have been taken in a certain time *(very small time interval in a second)* provides a new image processing method which is called digital image correlation, DIC. There are researches including DIC applications in different engineering fields. Likewise, Cheng, etal., (2023) supplied a brief description of DIC for strain measurements as; "*DIC technology is a non-destructive measurement method that can obtain the full-field strain information of a specimen surface".* They mentioned that, in DIC methodology images are divided into *"many small blocks*" and they are compared with the image obtained for one step earlier. The pixel position differences led to understanding very small displacements which could not be possible to measure in mechanical measuring apparatus. Cheng, etal., (2023) presented their fracture recognition studies for uniaxial compressive strength of high-strength, self-compacting, C80 coded concrete (CO samples in their tests). Their studies included a uniaxial compressive strength determination test with 100x100x100mm samples through DIC strain measurements. They used specially arranged raw materials added to C80 raw material configuration to obtain CAR coded samples (adding extra: rubber particles and polymer latex powders), and CARF coded samples (adding extra: rubber particles, polymer latex powders, and polyethylene fibres). The DIC analysis result presented in Fig.11a was obtained from one of the uniaxial compressive tests performed for CARF sample by Cheng, etal., (2023).

Similarly works performed by Kozicki&Tejchman, (2007) included applicability of DIC analyses for notched concrete samples. Micro-level displacement recognitions were aimed to analyse the cracks, (micro fractures), at "*notched concrete samples"* tested through "three-point bending" procedures. The researchers noted here that; *"during experiments, load-deflection curves and evolution of fracture process zones were determined*". Like this study, fracture initiation and propagations concepts have been the main research area in the characteristics of solid materials. Especially industry branches, using metal alloys for ships, planes and automobile manufacturing industries, force the researchers to analyse cracks in detail. Likewise, edges of discontinuities (cracks, voids etc.) in rock and concrete masses are starting points of propagated fractures in these masses. In rock mechanics context, engineers have knowledge that the possibility of finding massive rock masses (they do not have discontinuity) is very low, (rare case). Discontinuities, cracks, in rock masses and concrete are ready to be connected if the rock or concrete materials (bridges) among them have been collapsed due to applied external stresses. RC-columns have their load in uniaxial manners, (in vertical directions), and they have to bear this vertical stress along their life-span. Gokay, etal. (2004) worked for existing discontinuity edge influences on further fracture propagations in massive rock masses. Fracture propagation in massive marble plates (20x100x150mm) including 20mm notches across each vertical side of the massive marble samples were tested by them to observe propagated fracture traces. Traces of fractures are recorded and analysed to evaluate their propagation behaviours due to configured vertical loading conditions.

Failure of RC-columns including drill-holes or repaired drill-holes under uniaxial compressive stress have supplied their characteristic stress-strain distributions and toughness values. Fractures have propagated in particular directions which are governed by 3D induced stress conditions in these concrete structural elements. Micro-fractures in concrete columns/beams are usually found to extend far further than their visible traces. Invisible parts of the fracture elongations have also been study subjects in several works like it was targeted in the electrical resistivity measurement test through modelled mesh-net on the fractured concrete column sample performed by Gokay, (2016). Combinations of fracture determination methods, (acoustic emissions, electrical resistivity, electro magnetic resonance imaging techniques, etc.), and DIC analyses have provided a more comprehensive understanding of the stress-strain distributions in the test samples together with their fracture trace recognition opportunities on the samples' surfaces. Fractures initiated and propagated in the RC-columns have to be recognised by engineers to supply stability related precautions and safety procedures. In order to determine the fracture initiation locations and expected fracture propagation directions, DIC analyses supply suitable prospects in practical engineering operations. Engineers usually would like to examine (evaluate) the fractures inside the tested laboratory/field samples (like in the research studies in; oil & geothermal resource explorations, RC-column defects, etc.). DIC and acoustic emission analyses, (through several sensors attached on the test samples), are coupled evaluations employed, for instance, by Alam, etal., (2014). They analysed fracture initiations and propagations in detail by taking into consideration the samples' inner body parts through acoustic emission data. In addition to these research examples, the works performed by Li, etal., (2017) should be mentioned as well. They worked about the fractures formed surrounding the circular and elliptical holes in the marble samples. They applied DIC test procedures and analyses to identify micro-level displacements (cracks' initiation & widening stages, Fig.11b). DIC graphics presented by them illustrated the fracture initiations stages and fracture traces through their studied test samples *[totally 21 samples: 3 intact plate samples, 6 plate samples with circular holes (A&B types, according to their diameter differences), 15 plate samples with elliptical holes (A,B,C,D and E types according to their positioning configuration in the tested plates].* The marble plates prepared for the tests had dimensions slightly differentiating due to marble cutting procedures and these dimensions were changing in the values of: (59.90-60.22)x(99.35-100.15)x(14.89-15.10) mm. Circular holes 10mm and 15mm in diameters in this study drilled at the centre of the marble plate samples. Marble plate

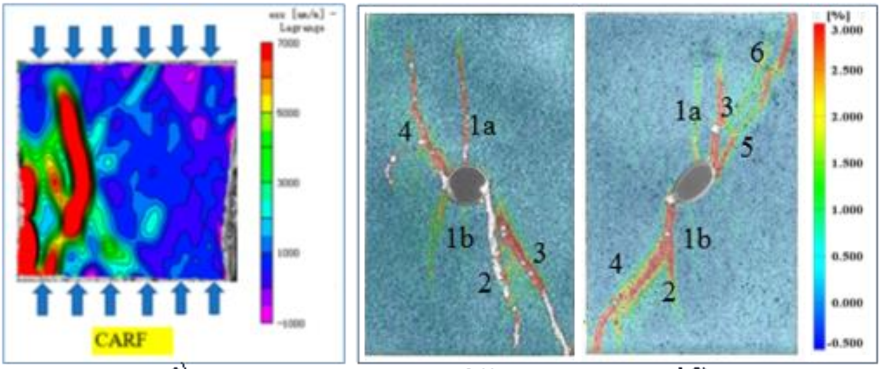

a) b1) b2)

Figure 11. a) Strain distributions under vertical uniaxial compressive stress in the specially prepared CARF samples (after Cheng, etal., 2023). b) Major principal strain distributions in different types of hole in tested marble samples, b1) Circle-10-1; (Circular hole with 10mm diameter), b2) Ellipse-D-2. (Elliptical hole with; (length of long axis=12mm, length of short axis=6mm, inclination angle=45^o). Fractures occurred on the test samples were numbered according to their sequences, (after Li, etal., 2017).

samples with elliptical holes had been arranged with their long axis (12mm) and short axis (10 and 6 mm) in length. Elliptical holes are positioned differently according to their long axis elongation angle (0^o, 45^o, 90^o degrees) to horizontal direction (passing from the test samples' centroids). The fracturing analyses of the test samples supplied through DIC procedures were reported (Li, etal., 2017) accordingly and two of them presented here to illustrate the fracture positioning around the drill-holes (Fig.11b).

DIC analyses for column-like gypsum based test samples

In order to understand toughness differentiation in solid material fracturing, special test samples were prepared by using a special gypsum powder mixture. Laboratory test samples were prepared in this study in 5 test groups according to their drill-hole diameters, “d”; *[i) Intact, massive, samples, (d=0mm); b) S-d8 samples (d=8mm); c) S-d10 samples (d=10mm); d) S-d15 samples (d-15mm); e) S-d20mm samples (d=20mm)]*. Drill-hole centres were arranged in a way that they were at the centre positions of the samples vertically and horizontally. All the samples prepared in 50x50x150mm in dimensions by using gypsum mortar, (prepared through special “hrn-α” gypsum powder mixture (YYM, 2023) was used *(75% in weight amount)* together with tap water *(25% in weight)*) to mould the test samples. There is no reinforcement in the test sample bodies, and on the surfaces of them. When they solidified in their moulding cases, they assumed to be massive, intact, and homogeneous, gypsum samples which were square prisms in geometric volume (square cross-sectioned, column-like samples). After the handling of the samples from their mould cases, (which were whitish in colour), they were kept at room temperature to stabilize their moisture contents. Then one longitudinal face of each sample was spray painted to get black-dotted patterns for DIC analyses. These faces were used in image capturing and micro-displacement recognition procedures of DIC analyses. Vertical loading tests were performed at a hydraulic laboratory press (at Mining Engineering Department, Tech. University of Konya, (Turkey) which was purposely controlled to supply very low stress increments per second (0.1 kNewton/sec.). Test samples in the study were coded with; *int, S-d8, S-d10, S-d15, and S-d20,* representing; intact samples (Fig.12a, 12b, and 13a); samples with d=8mm drill-holes (Fig. 12c, 12d, and 13b); samples with d=10mm drill-holes (Fig.12e, 12f, and 13c); samples with d=15mm drill-holes (Fig.13d), and samples with d=20mm drill-holes (Fig.13e) respectively.

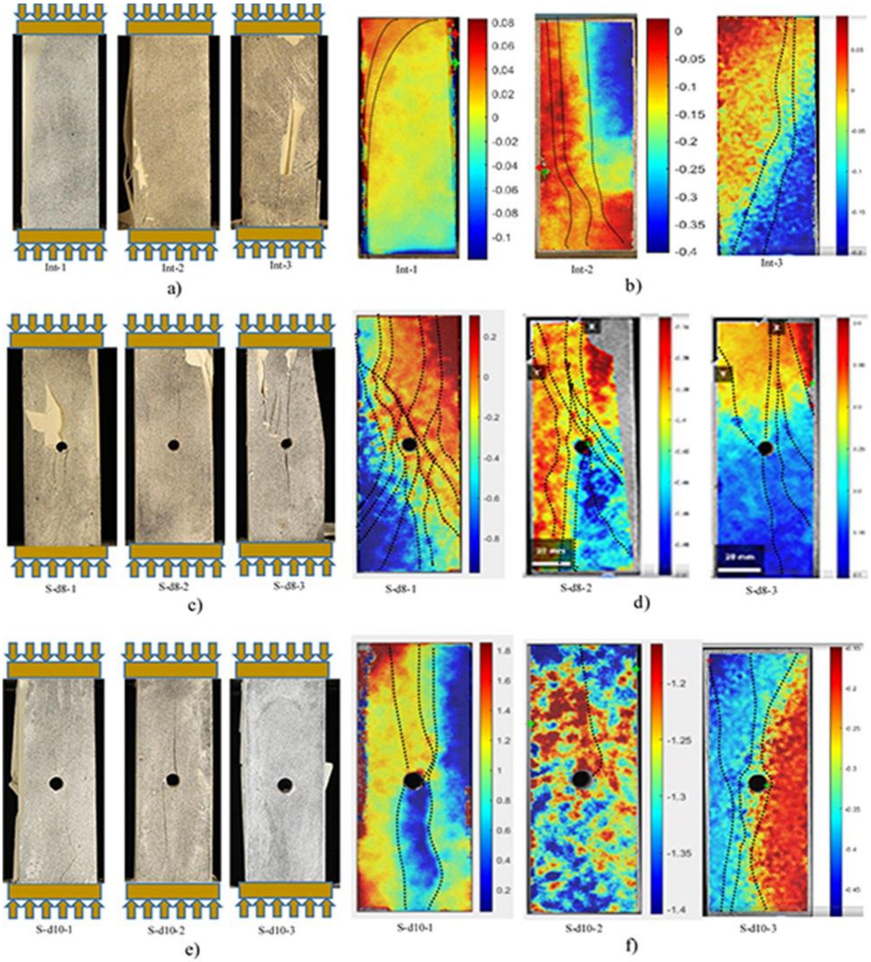

Figure 12. Fracture observation through DIC analyses at vertical compressive stress-strain conditions for the prepared gypsum based test samples. Vertical displacement had been determined continuously during the tests. The DIC analysis plots given for the tested samples here represent the last-stages of the vertical displacements just before their fragmentation. The values in the scales near to the DIC graphs show the vertical displacement differentiation in mm; a) Intact, solid, samples, b) vertical displacements on the front faces of intact samples. c) Test samples

with d=8mm drill-hole, d) vertical displacements on the front faces of the samples with d=8mm drill-hole. e) Test samples with d=10mm drill-hole, f) vertical displacements on the front faces of the samples with d=10mm drill-hole.

Test sample images for intact, S-d8 and S-d10 are illustrated in Fig.12, these images were captured just before their fragmentations, (fracturing, F value level) stages during their vertical loading test procedures. During the experiments, the strains (micro-displacements) were recorded frame by frame by DIC camera (Full HD, 120 frame per second) while vertical loadings on the test samples were increased at a very slow rate. Like many other uniaxial compressive test results, induced fractures observed on the test samples' surfaces are either vertical or angular extensions. When the micro-cracks have been initiated and related deformations have already influenced the inner body of the test samples, material toughness and strength characteristics of the samples have been main

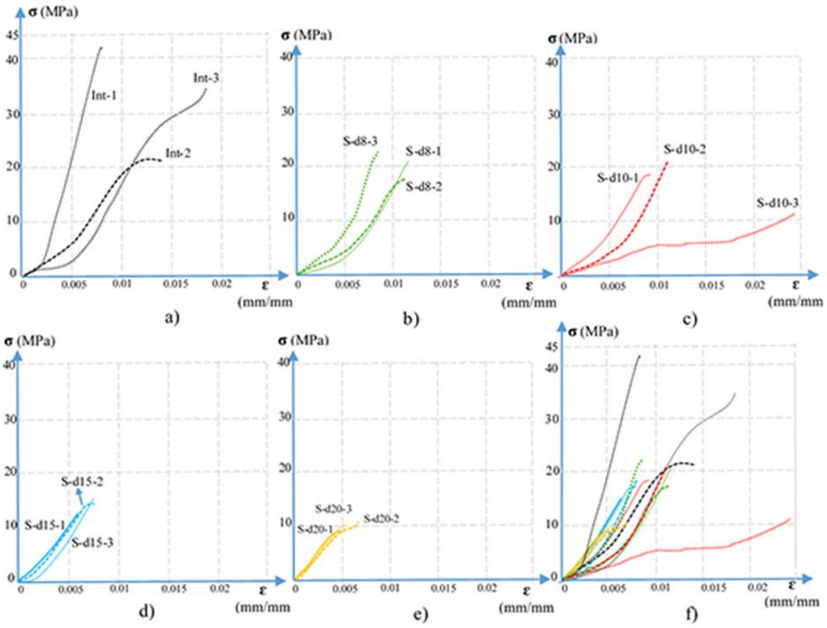

Figure 13. Vertical stress-strain distributions for tested column-like test samples a) Intact samples (int-1, int-2 and int-3), b) Samples with drill-holes 8mm in diameter (S-d8-1, S-d8-2, and S-d8-3), c) Samples with drill-holes 10mm in diameter (S-d10-1, S-d10-2, and S-d10-3), d) Samples with drill-holes 15mm in diameter (S-d15-1, S-d15-2, and S-d15-3) e) Samples with drill-holes 20mm in diameter (S-d20-1, S-d20-2, and S-d20-3), f) Uniaxial stress-strain curves of all the test samples (intact, S-d8, S-d10, S-d15, and S-d20).

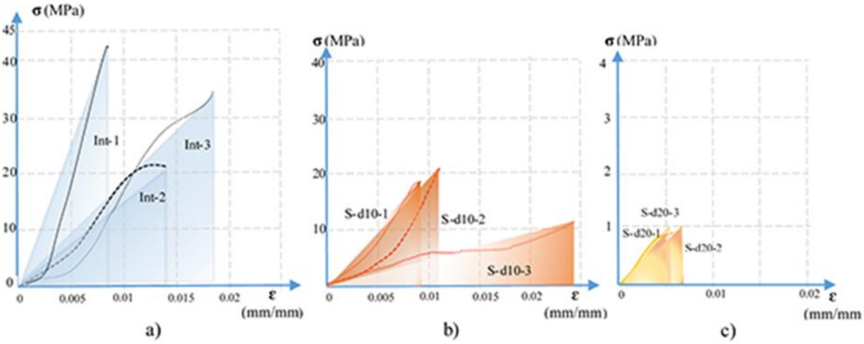

Figure 14. Strain energy stored under vertical stress-strain distribution curves of the column-like test samples; a) Intact samples, b) S-d10 samples, and c) S-d20 samples.

governing factors on their fragmentation (total fracturing) levels. The fracturing of the test samples illustrated in Fig.12 have already supplied influences of drill-holes by presenting deviations in fracture orientations due to drill-holes. It was also observed that induced fractures had mostly been directed to the left and right hand sides of the drill-holes where higher induced stress concentrations were expected (Fig.7). Fractures seemed to be arched over immediate top/bottom sections of the drill-holes. Energy accumulated in the test samples under vertical loading conditions is differentiated due to the test samples' mechanical properties. Toughness values representing the stored energy levels define also the resistance levels provided by the tested samples to the applied vertical stresses. The values of toughness actually are not enough alone to visualise, evaluate, the test samples' resistance progresses during the tests. Stress-strain variation graphs (Fig.13) plotted by continuous stress-strain measurements play an important part in these considerations to understand toughness characteristics presented in Fig.14. Uniaxial compressive strength of the test material (prepared through special gypsum mixture in this study) was also determined as 18.58 MPa (average value) by testing the cubic (50x50x50mm) test samples. These tests were performed under standard vertical loading rate which is applied for rock material testing conditions. When the strength values of ultimate, (U values), and failure, (F values), levels are under consideration for the column-like test samples, averaged uniaxial compressive strength value was also taken into account for their evaluations. Thus, Fig.15 implies that there is a certainly negative influence of drill-hole on the strength values of the column-like tested samples. Increasing the drill-hole diameters decrease the effective cross-sectional area where the applied vertical stress is concentrated. These area decreases were formed due to drill-holes which were passing through the samples bodies. If the intact samples cross-sectional area accepted as full area, (25 cm^2, 100%), then effective areas and (the decrease in the cross-sectional-areas with their %) were calculated as follows; S-d8: 21cm^2, (4cm^2, 16%), S-d10: 20cm^2, (5cm^2, 20%), S-d15: 17.5cm^2, (7.5cm^2, 30%), and S-d20: 15cm^2, (10cm^2, 40%). Micro fractures appearing on the samples' surfaces were expected to be developed inside the samples' bodies as well. Therefore, material toughness differentiations are also examined together with the strength limits (Y, U, and F values) of the tested samples. Material toughness properties for the tested samples have been analysed by calculating stored energy amount in two categorised areas. In the first category, toughness values (area under the stress-strain curves) of the samples were calculated by limiting the areas with ultimate strength, (U values) levels by triangulation like in Fig. 14. The second category included the resistive energy amount representing the areas limited with ultimate (U values) and failure (F values) strength levels. Total stress energy amount accumulated under the stress-strain curves of each tested sample is then determined by adding the energy amount estimated for these two categories, (Fig.16).

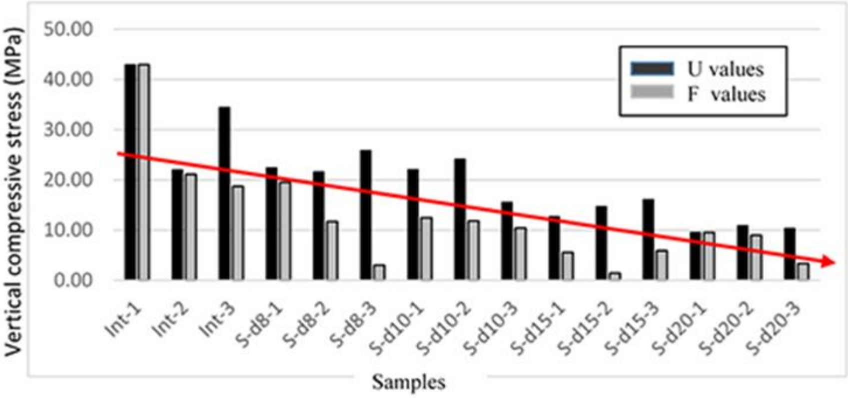

Figure 15. Vertical compressive strength test results obtained through column-like (50x50x150mm) samples moulded from special gypsum powder. (Vertical loads affecting through full ($25cm^2$) cross-sectional area for the intact test samples were decreased to "Effective cross-sectional area", at the centre levels of the drill-holes according to their diameters).

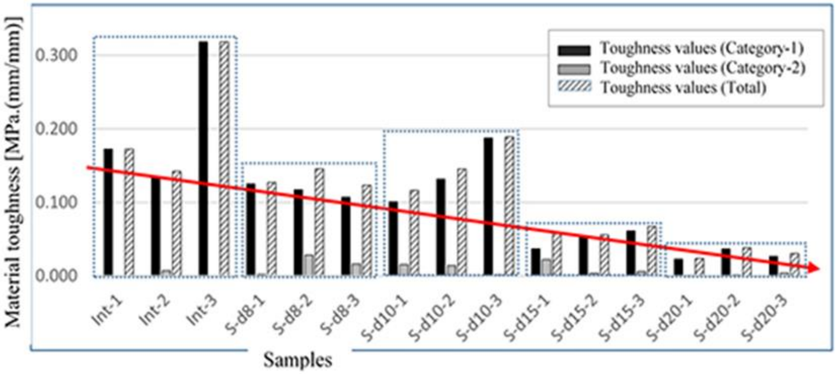

Figure 16. Graphical presentation of the material toughness differences of the tested samples,

Actually, the toughness values which cover the energies accumulated during the category-2 stages of the tests (post-failure region, the necking region described in Fig.1), could be analysed in a more comprehensive manner if the vertical compressive strength test is performed by a special stiff testing system, *(equipped with servo-hydraulic closed-loop electronic and hydraulic systems)*. Researchers concentrating on the post-failure properties of solid materials (rock materials) specially have focused on the characteristics of stress-strain curves after the ultimate stress (U values) levels (Crowder, etal., 2004; Jianxin, etal., 2012; Oge, 2013).

Fracture traces developed in the test samples illustrated the importance of fracture toughness properties of the samples. Beside the effects of influencing design parameters; *[i) vertical stress distribution in the tested samples, ii) drill-hole diameters, iii) drill-hole locations, iv) drill-hole shapes, v) number of drill-holes, vi) if there is repaired drill-hole, mechanical characteristics of fillings (strength (Y, U, and F) values, elastic modulus, and toughness values)]* on induced fractures' trace orientations, material properties of the test samples (solidified special gypsum powder mortars) have also important influences on induced fracture characteristics. Toughness values related with fracture propagations in the column-like test samples have then also been influencing factors to be researched to evaluate further mechanical behaviours in engineering decisions. Similar tests could also be performed with concrete test samples (column-like prismatic samples, lab-size RC-columns, actual-size RC-columns) to understand the fracturing circumstances of load-bearing RC-columns (with/without drill-holes).

Conclusions

Strength of solid column-like, (cylindrical or prismatic), structural load-bearing elements are sensitive to their; material properties, geometric shape & size factors, defects zones, micro-fractures, voids & aperture contents, induced stress-strain distributions, temperature variations, etc. Solid materials engineered to provide resistivity for induced stresses in 3D environments could be seen at different engineering works, projects. RC-columns and mine pillars are two of them and they have similar load-bearing characteristics for surface/underground engineered spaces. They resist vertical loads according to their individual material properties. RC-columns are designed for particular construction projects by arranging their moulding procedures and mortar contents. Concrete types or any other solid substances obtained through solidification of moulded mortars have their own strength characteristics which are sensitive to any differentiation of their raw-material types and their proportions. Mine engineers always put maximum care for the mine supports for the stability of mine galleries, stopes, and other underground openings. That means, mine pillars have their important care and protection in mining operations. Similarly, RC-columns at surface/underground constructions have their importance to be protected as in their original design shape & size. Mining environments including pillars and all the other mine supports are controlled every man-shift for their stability cases by shift engineers. Mining related work&work-places safety rules and legislative acts require these compulsory controls for mine safety cases. Controlling health of surface/underground structures (including load-bearing RC-columns) on the other hand have different procedures in civil engineering activities. Engineering check/control procedures for civil purpose constructions are usually defined mainly for their design and construction stages. During their usage periods, these activities have performed mainly for dams, bridges, ports, airports, etc. Civil engineering structures have been providing services for almost all human kinds since early times. Therefore, some of them have their problematic cases related to their design & construction complications, and post-construction activities (without getting engineered permissions). Drilling hole(s) through surface/underground structures' walls, RC-columns and beams (for instance) is one of those deficits which influences the stability cases of them. Supplying service lines/pipes, and concrete quality control activities of buildings, are two main reasons for those drilling operations. The effects of drill-hole on the strength of RC-columns have been researched through lab-size samples. The work performed in our study here presents the results obtained through column-like (without reinforcement) laboratory samples by handling digital image correlation, DIC, analyses. Stress-strain distribution curves which supply ultimate and failure strength levels of the tested samples were used here to estimate material toughness values of them as well. The test samples were moulded by using special gypsum powders and they prepared with/without drill-holes (in different diameters). The results presented that having a drill-hole in the test sample forms negative influences on their ultimate and toughness value levels. It was observed that these values were decreased as the diameters of the drill-holes were increased. Fracture patterns observed on the surface of the tested samples illustrated also that fracture orientations were affected by drill-holes.

REFERENCES

Akdag, E. (2015) Experimental investigation of concrete strength of the personal and public structures in Bilecik province, *MSc Thesis*, (in Turkish), Seyh Edebali University, Civil Engineering Dept., Institute of Applied Science, Bilecik, Turkey, p97.

Alam, S.Y., Saliba, J. and Loukili, A. (2014) Fracture examination in concrete through combined digital image correlation and acoustic emission techniques, *Construction and building materials*, 69, pp232–242.

Alwash, M.F.A, (2017) Assessment of concrete strength in existing structures using non- destructive tests and cores : analysis of current methodology and recommendations for more reliable assessment. *PhD Thesis*, School of physics and engineering sciences, Mechanics-physics, Université de Bordeaux, 2017. English, NNT 2017BORD0587, Hal open science id; tel-01531241, https://theses.hal.science/tel-01531241.

Campione, G., Cucchiara, C., and Minafo`, G. (2015) Effects of circular openings on the compressive behaviour of R.C. columns, *Materials and structures*, 48, pp1995–2008.

Cheng, Z., Zhao, H., Long, G., Yang, K., Chen, M. and Wu, Z. (2023) The mechanical characteristics of high-strength self-compacting concrete with toughening materials based on digital image correlation technology, *Materials*, 16, 1695. https://doi.org/ 10.3390/ma16041695.

Crowder, J.J. and William F. Bawden, W.F. (2004) Review of post-peak parameters and behaviour of rock masses: Current trends and research, https://api.semanticscholar.org/CorpusID: 162177712, and *https://www.researchgate.net/publication/253116156*, p14.

ECIA, (2023) *East Cleveland image archive visit the past through photographs*, Pillar crush, (Photo by Franks, A.M. &

information by Coleman, T.), Webpage; www. image-archive.org.uk/?cat=32, Retrieved in Nov. 2023.

Esterhuizen, G.S., Dolinar, D.R., Ellenberger, J.L. and Prosser, L.J. (2011) *Pillar and roof span design guidelines for underground stone mines,* U.S. Department of Health and Human Services, Public Health Service, Centers for Disease Control and Prevention, National Institute for Occupational Safety and Health, Pittsburgh, PA, DHHS (NIOSH) Publication No: 2011-171, IC 9526, May 2011, pp1-64.

FTS, (2019) *El Minya day trip from Cairo by private car*, FTS Travels, Webpage, www.fts-travels.com/egypt-excursions/cairo-excursions/day-trip-from-cairo-to-el-minya, Retrieved in Nov. 2023.

Gokay, M.K., Ozkan, I., Dogan, K. (2004) Mermerlerde birlesmeye zorlanan catlakların davranısı, (in Turkish), *7th Regional rock mechanics symposium*, Oct. 21-22, 2004, pp151-156, Sivas-Turkey.

Gokay M.K. (2016) Determination of potential electric values to verify micro fractures in concrete, *International conference on civil, architectural and structural engineering*, (ICCASE-2016), ISBN 978- 93-84468-90-3, V2, pp125-129, Dubai-UAE.

Greer, A.L. (2009) Metallic glasses, on the threshold, *Materials today*, 12, 1-2, pp14-22. Doi: 10.1016/S1369-7021(09)70037-9, ISSN:1369 7021.

Hamrin, H. (1980) *Guide to underground mining methods and applications,* Atlas Copco, Stockholm, Sweden.

Hashida, T. and Takahashi, H. (1993) Significance of AE crack monitoring in fracture toughness evaluation and non-linear rock fracture mechanics, *Int. J. Rock Mech. Min. Sci. & Geomech. Abstr*act, 30, 1, pp47-60.

Hillerborg, A., ModeÂer, M. and Petersson, P.E. (1976) Analysis of crack formation and crack growth in concrete by means of fracture mechanics and finite elements, *Cement and concrete research*, 6, pp773-782.

Hillerborg. A. (1991) Application of the fictitious crack model to different types of materials, *International journal of fracture*, 51, pp95-102.

Jianxin, H., Shucai, L., Shuchen, L. and Lei, E. (2012) Post-peak stress-strain relationship of rock mass based on Hoek-Brown strength criterion, Int. conference on structural computation and geomechanical mechanics, *Procedia earth and planetary science*, 5, pp289-293.

Kirsch, E.G., (1898|) Die Theorie der Elastizität und die Bedürfnisse der Festigkeitslehre. Zeitschrift des Vereines deutscher Ingenieure, 42, pp797–807.

Kozicki, J. and Tejchman, J. (2007) Experimental investigations of strain localization in concrete using digital image correlation (DIC) technique. *Archives of hydro-engineering and environmental mechanics*, 54, 1, pp3–24.

Kurklu, G. (2005) Mevcut betonarme yapilarin deprem guvenliginin incelenmesindeki teknikler ve beton dayaniminin belirlenmesi, MSc Thesis, (in Turkish), Afyon Kacatepe University, Civil Engineering Dept., Institute of Applied Science, Afyon, Turkey, p143.

Kurtulus, C. and Bozkurt, A. (2011) Determination of concrete compressive strength of the structures in Istanbul and Izmit Cities (Turkey) by combination of destructive and non-destructive methods, *International journal of the physical sciences*, 6, 16, pp4044-4047.

Li, D., Zhu, Q., Zhou, Z., Li, X. and Ranjith, P.G. (2017) Fracture analysis of marble specimens with a hole under uniaxial compression by digital image correlation. *Engineering fracture mechanics*, http://dx.doi.org/10.1016/j.engfracmech.2017.05.035.

MechaniCalc, (2023) *Mechanical properties of materials*, MechaniCalc. Inc., Website, https:// mechanicalc.com/reference/mechanical-properties-of-materials, Retrieved in Nov. 2023.

Negassa, F. (2020) Numerical investigation of reinforced concrete columns with transverse holes, *MSc Thesis*, Addis Ababa Science and Technology University, Department of Civil Engineering, Addis Ababa, Ethiopia. P46.

Obinna, U. (2020) *Bracing systems in a high-rise building, Construction*, Structville integrated services Ltd., Webpage; www.structville.com/2020/10/bracing-systems-in-a-high-rise-building.html, Retrieved in Nov. 2023.

Oge, I.F. (2013) A prediction method on the post-failure properties of rock and its application to tunnels, *PhD Thesis,* The Graduate School of Applied and Natural Sciences, Middle East Technical University, Ankara, Turkey, p114.

SEN, (2023) *Strength vs. Hardness vs. Toughness*, Engineering, Stack Exchange Network, Webpage; htpps://engineering.stackexchange.com/questions/25943/strength-vs-hardness-vs-toughness, Retrieved in Nov. 2023.

Structural guide, (2023) *Eight types of column failure methods*, Structural guide, Civil and structural engineering knowledge base, Webpage, www.structuralguide.com/types-of-column-failures/, Retrieved in Nov.2023.

Son, K.S., Pilakoutas, K. and Neocleous, K. (2006) Behaviour of concrete columns with drilled Holes, *Magazine of concrete research*, 58, 7, pp411-419.

Sorgi, C. and Watelet, J. (2007). *Fenomeni di degrade e rischio di crollo nelle cave di gesso abbandonate: l'esperienza francese*. Proceedings Dissesti indotti dall'alterazione di rocce evaporitiche, Patron Editore, Bergamo, Italy, Sep.2007, pp41-59.

Sorgi, C. and Gennaro, V.D. (2011) *Water-Rock Interaction Mechanisms and Ageing Processes in Chalk,* Book Chapter, Advances in Data, Methods, Models and Their Applications in Geoscience, doi: 10.5772/26928.

YYM, (2023) Yanmaz yapi malzemeleri Ltd. Co. (Yanmaz construction materials), Konya, Turkey.

Yu, M., Wei, C., Niu, L., Li, S. and Yu, Y. (2018) Calculation for tensile strength and fracture toughness of granite with three kinds of grain sizes using three-point-bending test. *PLoS ONE*, 13, 3, e0180880. Doi: 10.1371/journal.pone.0180880.

Zhu, L., Xu, Q., Li, X. and Zhu, C. (2010) Experimental studies of reinforced concrete column capacity affected by core drilling, *Advanced materials research*, 133-134, pp1195-1200.